INAUGURAL-DISSERTATION

zur

Erlangung der Doktorwürde

der

Naturwissenschaftlich-Mathematischen Gesamtfakultät

der

RUPRECHT-KARLS-UNIVERSITÄT

HEIDELBERG

vorgelegt von

Dipl. Math. Anna Marciniak-Czochra

aus Lublin, Polen

Tag der mündlichen Prüfung: 12.01.2004

Developmental models with cell surface receptor densities defining morphological position

Gutachter: Prof. Dr. Dr.h.c.mult. Willi Jäger

Priv. Doz. Dr. Steffen Heinze

To My Parents

Abstract

New receptor-based models for pattern formation and regulation in multicellular biological systems are proposed. The test organism for the mathematical modelling is a fresh-water polyp, hydra. Another model is applied to describe the growth of tumour along linear or tubular structure.

Models are defined in the form of reaction-diffusion equations with zero flux boundary conditions coupled with ordinary differential equations. Two mechanisms of pattern formation: diffusion driven instability and hysteresis-driven mechanism are studied and their possibilities and constraints in explanation of different aspects of pattern formation and regulation are demonstrated.

Three-variable (describing the dynamics of ligands, free and bound receptors) and four-variable models (including also an enzyme cleaving the ligand) are analysed and compared. It is shown under which conditions they can involve diffusion driven instability mechanism for pattern formation. It is shown that gradient in the density of bound receptors occurs if there is also a second diffusible substance, an enzyme, which degrades ligands. The four-variable model is able to capture results from cutting experiments and reflects *de novo* pattern formation from dissociated cells.

To explain the grafting experiments a new model including memory-based relation is proposed. Production of the diffusible biochemical molecules has a hysteretic dependence on the density of these molecules and is modelled by additional ordinary differential equations. The stationary and oscillatory patterns, resulting from multiple steady states and switches in the production rates, are found.

Finally, a receptor-based approach is applied to a model of the growth of a tumour. Mathematical model describing the population of cells distributed over a linear or tubular structure and the diffusing growth factor which regulates the proliferation is derived and analysed.

Contents

1

Introduction

This work is devoted to *mathematical modelling* of *pattern formation*. Spatial and spatio-temporal patterns occur widely in physics, chemistry and biology. In many cases, they seem to be generated spontaneously. These phenomena have motivated a great deal of mathematical modelling and the analysis of the resultant systems has led to a greater understanding of the underlying mechanisms.

Partial differential equations of diffusion type have long served as models for regulatory feedbacks and pattern formation in aggregates of living cells. In this work, we consider new mathematical problems arising in models of this type. In particular, the systems describing our models are composed of both diffusion-type and ordinary differential equations. Such systems cause some difficulty, since both existence and behaviour of solutions are more difficult to establish. Many aspects of qualitative behaviour have to be investigated numerically. We found qualitatively new patterns of behaviour of solutions of our equations, including, in some cases, a strong dependence of the emerging pattern on initial conditions, and quasi-stability followed by rapid growth of solutions.

In this work we propose new *receptor-based models* for pattern formation and regulation in multicellular biological systems. We develop the idea that patterns are controlled by the specific cell-surface receptors, which transmit to the cells signals responsible for their differentiation. The main aim of the work is to check which aspects of *self-organisation* and *regeneration* can be explained within such framework.

The test organism for the mathematical models is a fresh-water polyp, *hydra*. We try to answer the question what is the mechanism of formation of new structures and regeneration of missing ones. We show also how model of a similar structure can be applied to describe the *growth* and *morphogenesis* of a *tumour*.

1.1 Morphogenesis: mathematical models and biological systems

Understanding the evolution of spatial patterns and the mechanisms which create them are among the most crucial issues in developmental biology. Recent advances made in genetic and molecular biology have led to detailed descriptions of a number of events in embryological development. Although genes control pattern formation, genetics alone will not be sufficient to understand which physiochemical interactions of embryonic material produce the complex spatio-temporal signalling cues which ultimately determine the cell's fate. Model mechanisms can suggest to the embryologists possible scenarios as to how, and sometimes when, a pattern is laid down and how the embryonic form might be created.

The role of mathematical modelling is to verify what processes are sufficient to produce the patterning. It does not prove that this is the mechanism, it only says that this is a candidate mechanism. Modelling also allows to make experimentally testable predictions. Another use of mathematical models is to provide alternative explanations for the observed phenomena.

In other areas of biology, such as neurophysiology or ecology, mathematical modelling has led to many discoveries and insights through a process of synthesis and integration of experimental data. Also in developmental biology many different morphologies have been the subject of mathematical modelling. Some of the biological systems have attained the status of a paradigm in theoretical work.

One such example which shows how the study of model mechanisms can suggest real scenarios for the process of pattern formation is the *limb* development, Murray [61]. Mechanochemical model describes the diffusion, haptotaxis and advection of mesenchymal cells which evolve in a developing limb bud and which eventually become cartilage.

The other developmental process for studying pattern formation and different aspects of embryogenesis is the segmentation of the *insect embryo* modelled by Schnell et al. [68] and Kauffman [32].

The models based on chemotaxis and the response of cells to gradients in the chemoattractant were applied to study the life cycle of the slime mould *Dictyostelium discoideum*. The amoebae move towards regions of high concentrations of a chemical attractant, cyclic-AMP secreted by the amoebae themselves. The chemotaxis equations as a model to describe the aggregation of *Dictyostelium discoideum* were introduced by Keller and Segel [33, 34] and rigorously derived from an interacting stochastic many

particle system by Stevens [73]. The kinetics involved have been modelled by several authors e.g. Monk and Othmer [52] and all the results were recently summarized by Horstmann [27].

Recently, models of morphogenesis have been applied to understand the *growth of tumours*. They involve a wide range of biological phenomena such as cell-adhesion and cell traction, angiogenesis, pattern formation in cancer and macrophage dynamics, see e.g. Chaplain [9], and Murray [61]. There are even examples of applying the theoretical results to cancer treatment by Jackson et al. [28], [29], [30].

All these models, although based on different biological hypotheses, have many common mathematical features and are mostly based on a few views of pattern generation. One is the chemical prepattern approach involving hypothetical chemicals (morphogens) which diffuse and react in such a way that spatial heterogeneous patterns can evolve from the uniform steady states. Second is the mechanochemical approach which takes into account mechanical forces and properties of cells and tissues. Another class of models rely on chemotaxis and the response of cells to gradients in a chemoatractant.

In some applications there arise systems of reaction-diffusion equations coupled with ordinary differential equations, e.g. Hodgking-Huxley models of *nerve-pulse propagation* [60] or models of *bacterial growth* proposed by Hoppensteadt and Jäger [25], and Hoppensteadt, Jäger and Pöppe [26]. Such systems give rise to a number of interesting phenomena like e.g a treshold behavior and hysteresis. Pattern formation in these models is caused by the initial instability of the ordinary differential equations. Systems of reaction-diffusion equations coupled with the ordinary differential equations, which lead to the spatio-temporal patterns were also applied to model *heterogeneous catalysis* by Krömker in [40].

Different models are able to produce similar patterns. The question is how to distinguish between them so as to determine which may be the relevant mechanism. Of course the first necessary condition is that the model must produce observed patterns. But then it is important how consistent are predictions of the model with the results of the different experiments.

In conclusion, growth and pattern formation provide a great source of interesting and novel mathematical problems, while mathematics can be used as a tool to explore different mechanisms and processes underlying these phenomena. The use of realistic models can help to understand many complex processes.

1.2 Outline of the thesis

This thesis is focused on systems of reaction-diffusion equations coupled with ordinary differential equations applied to the modelling of pattern formation in biological systems. We address important issues of developmental biology such as self-organisation and regeneration.

In **Chapter 2**, we introduce the model of hydra. We show the variety of questions arising in the experimental research and motivate the usage of mathematical modelling to understand the process of pattern formation in hydra. Hydra is an example where theoretical models had much influence on experimental design, starting from the activator-inhibitor model of Gierer and Meinhardt [19]. We discuss the differences between our approach and existing approaches.

The model is based on the idea that both head and foot formation are controlled by receptor-ligand binding. Positional value is determined by the density of bound receptors. Use of receptor-based framework is motivated by the ideas presented by Müller in [56] and refinement of receptor-based model for hydra by Sherrat, Maini, Jäger and Müller in [70]. It is emphasised in [56] that many external signals in animal cells are received by specific cell surface receptors. Since the theoretical activator-inhibitor model for pattern formation in hydra was proposed by Gierer and Meinhardt, [19], there were many efforts to identify signal molecules but they have not yet succeed.

The model is defined in the form of reaction-diffusion equations coupled with ordinary differential equations. Most results on pattern formation in developmental biology have been derived for reaction-diffusion systems [60], [61] and [45] and since the famous paper of Turing [77] the mechanism of diffusion-driven instability has been applied to variety of pattern formation problems in biology.

Thus our first objective is to check what minimal systems are sufficient to produce patterns in the framework of a diffusion-driven (e.g. Turing-type) instability assuming that some of the considered substances do not diffuse and which experimental results can be explained by such approach.

Chapter 3 concerns mathematical formulations of the receptor-based models of hydra. We discuss the analytic techniques for reaction-diffusion systems which can be applied to the models containing ordinary differential equations. We outline the idea of bounded invariant rectangles, which is used to prove the existence of global solutions of the receptor-based models of hydra in Section 4.2.1 as well as of the model of tumour

growth presented in Section 6.2.6. We discuss also results on linearised stability which justify the formal use of the linearisation techniques later on.

In **Chapter 4** we analyse and compare three-variable models, describing the dynamics of ligands, free and bound receptors and four-variable models, including also an enzyme cleaving the ligand. Using linear stability analysis we find conditions for the kinetic system under which the diffusion-driven instability appears. The minimal three-variable model takes into consideration the density of free receptors, bound receptors and ligands. In such model patterns can evolve only if self-enhancement of free receptors, i.e. a positive feedback loop between the production of new free receptors and their present density, is assumed. The final pattern strongly depends on initial conditions.

Introduction of the second diffusing biochemical species improves the performance of the model. In the four-variable model a diffusion-driven instability occurs without the assumption that free receptors stimulate their own synthesis. Numerical simulations are performed to investigate the long-time behaviour oft solutions. We compare the behaviour of solutions for the three- and four-variable systems and find out that, in the case of only one diffusion equation, the final pattern strongly depends on the initial condition while patterns evolving in models with two diffusion equations are more robust.

The proposed four-variable model with diffusion-driven instability is able to simulate some aspects of self-organisation, such as regeneration of the complete organism from a cut piece and from randomly distributed cells. In this way we demonstrate that a receptor-based model can explain exactly the same experiments as the activator-inhibitor model for hydra which assumes existence of diffusing morphogens.

Our investigations suggest that the results of grafting experiments, which result in the animals with multiple heads or feet, cannot be predicted by the models with Turing-type mechanism of pattern formation.

To explain them it is necessary to seek a new mechanism. We propose to incorporate into our receptor-based model a memory-based relation via a hysteretic dependence of production of new biochemical molecules on the density of these molecules (ligands and enzyme).

In **Chapter 5** we introduce additional ordinary differential equations to model the production of ligands and enzyme and show that the results of grafting experiments can be simulated within such a framework. We assume that the production of the diffusible biochemical molecules has a hysteretic dependence on the density of these

molecules. The hysteresis term is controlled by the process. Patterns in this model do not arise from the stationary homogeneous steady states of the kinetics system. They result from multiple steady states and possible switches between them. We observe patterns stationary in time and also, for some parameters, temporary oscillations. For the simplified model, without equations describing an enzyme and a production of enzyme, we show the existence of a stationary front connecting two stable stationary homogeneous solutions and compare it with the solutions of the complete system.

We introduce a new concept of positional value, which allows for the interpretation of oscillatory solutions. We show how switches in the production rates can result in the formation of spatial patterns. Such mechanism is able to reproduce the results of grafting experiments since it allows the coexistence of different spatially inhomogeneous solutions evolving from different initial conditions.

Finally, we show how a model of similar structure can be applied to different biological system. In **Chapter 6**, we apply the formalism of receptor-based models to study the growth and morphogenesis of tumour. We examine a mathematical model of a population of cells distributed over a linear or tubular structure. Growth of cells is regulated by a growth factor, which can diffuse over the structure. Aside from this, production of cells and of the growth factor is governed by a pair of ordinary differential equations. The model is derived from a description in the form of a discrete stochastic process. Using the theory of bounded invariant rectangles and a priori estimates we show the existence of solutions.

Using linear stability analysis we find conditions under which diffusion causes destabilisation of the spatially homogeneous steady state, leading to exponential growth and apparently chaotic spatial patterns, following a period of almost constant state. This phenomenon may serve as a mathematical explanation of the "unexpected" rapid growth and invasion of temporarily stable structures composed of cancer cells. We solve the model equations numerically and demonstrate the strong dependence of the final spatial pattern on the initial conditions as well as on the scaling parameter.

In **Chapter 7** we conclude the thesis with further discussion of the challenges and restrictions of different possible mechanisms of reaction-diffusion models for pattern formation in hydra. Also, we stress special aspects of modelling the phenomenon of tumour growth, which by its nature is unstable.

To improve the readability of the text we present in **Appendix A** the mathematical formulation of existing models for pattern formation in hydra. In **Appendix B** we describe the different experimental settings in the language of proposed receptor-

based models. Finally **Appendices C** and **D** provide details concerning numerical investigations.

Acknowledgements:

I express my sincere thanks to Prof. Willi Jäger for supervising the research leading to this thesis and encouraging me to try new approaches. I thank Prof. Werner Müller for suggesting the problem of hydra pattern formation and through discussions of biological background of this work. I am grateful to Prof. Marek Kimmel for his interest in my research, his ideas and collaboration on the development of the model of tumour growth. I thank Dr. Markus Kirkilionis for fruitful discussions on hydra modelling and Dr. Steffen Heinze for his valuable comments on the analytical aspects of this work.

This work was financed from the grant of Graduiertenkolleg 484 "Signalling systems and gene expression in model systems of developmental biology" and from the grant of Interdisciplinary Centre for Scientific Computing, University of Heidelberg.

2

Motivating application: pattern control in hydra

2.1 Hydra as a model organism

Hydra has been one of the most frequently discussed organisms in theoretical papers on biological patterns formation.

What is peculiar about hydra?

Hydra, a fresh-water polyp, is one of the oldest and simplest multi-cellular organisms equipped with typically animal cells such as sensory cells, nerve cells and muscle cells and it plays an important role as a prototype organism for morphogenetic patterning [56], [57], [58], [59], [80].

The body architecture is relatively simple. Polyp has a tube-like body about 5 mm long with a whorl of tentacles surrounding the mouth at the upper end and a disk-shaped organ for adhesis at the lower end. The longitudinal pattern is subdivided into: a head, a gastric region, a budding zone (where new animals are generated by a process of natural cloning), a stalk and a foot.

The function of cells is determined by their location. This can be shown by a simple cutting experiment (Fig. 2.2): after a transverse cut cells of the gastric region of the animal are located at the upper end of the lower fragment, with their former neighbours at the lower end of the upper fragment. Within 2-3 days they form the head and the foot, respectively. Moreover, overlapping cut levels show that the same cells can form either the gastric region, or the head, or the foot, according to their position along the body axis. Experiments of this kind suggest that the cells respond to local positional cues that are dynamically regulated. The hypothesis is that cells differentiate according to positional information (compare Fig. 2.3). The question is how this information is supplied to the cells.

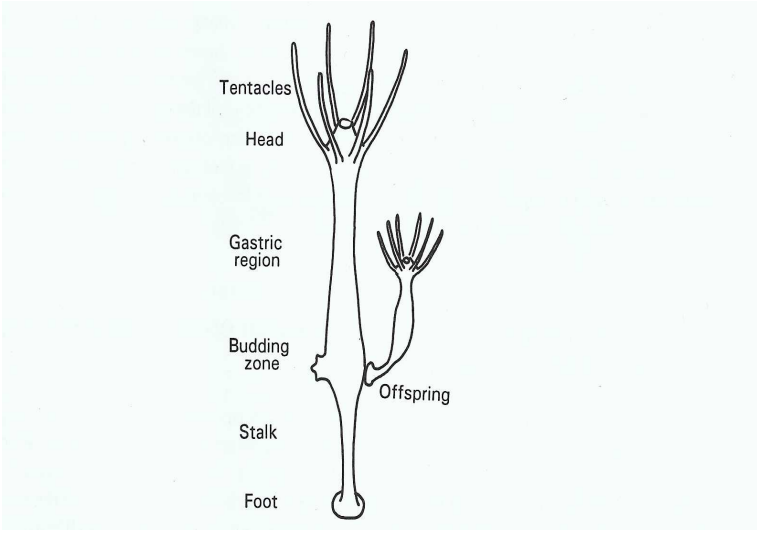

Figure 2.1. Hydra

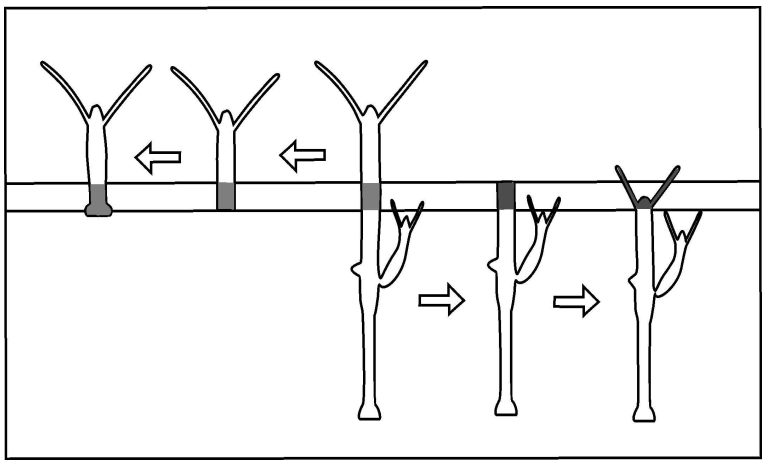

Figure 2.2. Cutting experiment. Hydra regenerates after a transverse cut of cells of the gastric region (from both upper and lower half of the body column). The experiment shows the availability of positional cues. A hydra, as shown in the middle, is cut in two ways. In one experiment (left hand-side) the lower body column is removed, in the second experiment (right hand-side) the upper part is removed. The cut levels are not identical but somewhat different to show that one and the same group of cells (marked in grey) can form a foot (left hand-side), or a head (right hand-side) or a gastric segment (original state in the middle). The function of the cells depends on the position along the body column. [Courtesy of W. Müller]

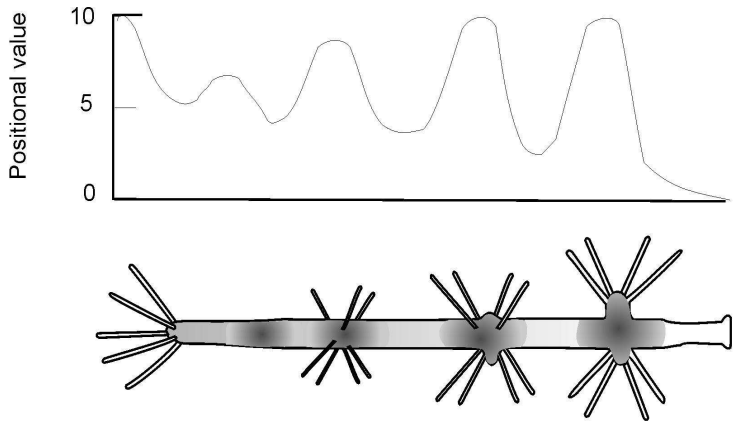

Figure 2.3. The illustration of the idea of "positional value", which is supplied to the cells and interpreted by them. The hypothesis is that the formation of the head is determined by the high "positional value" (which is above some threshold). The figure shows the "positional value" for a supernumerary head structure. The animal has been treated with activators of protein-kinase C periodically over about two weeks. This treatment caused a periodic increase in the positional value and eventually the emergence of head structures. [Courtesy of W. Müller]

There exist a number of models, e.g. [60] for pattern formation and regulation based on the idea that positional information is supplied to the cells by a diffusible biochemical morphogen. For example, the Gierer-Meinhardt model for hydra is based on this hypothesis [19], [49].

The other idea [56] is that positional value of the cell can be determined by the density of bound receptors, which do not diffuse. Regulatory and signalling molecules (ligands) in biology act by binding and activating receptor molecules which are located in the cell membrane (or, with lipophilic ligands, in the cytoplasm) [59], [56]. The main aim of this work is to show under which conditions a receptor-based model can produce and regulate patterns. Our models do not describe cells differentiation and the process of creating new structures. We concentrate on the dynamics of receptors and diffusing biochemical molecules which lead to the pattern formation in the density of bound receptors.

A classical genetic approach is very tedious [59]. Although genetic crossing is not currently possible in hydra [59], the use of reverse genetic and molecular screening techniques have resulted in the identification of many genes involved in the control of body pattern development, such as homeobox genes.

2.2 Connection to experiments

The exact molecular mechanism of pattern formation in hydra is unknown and the proposed models are hypothetical. Experiments performed on hydra provide an opportunity to test the abilities and limits of the models. We investigate what kind of mechanisms regulating the dynamics of the cell surface receptors and diffusing biochemical molecules can explain the observed results of experiments.

Our research attempts to answer the following questions which are closely related to the experiments:

- What minimal processes are sufficient to produce patterns?

We try to build a model for *de novo* pattern formation. It was shown [18], [62] that normal hydra can regenerate from random cellular aggregates. Reorganisation is not the result of a spatial rearrangement, but of concerted changes in the functional state of the cells. The cells do not sort with respect to the positional origin along the body axis [67], [76]. There have to exist mechanisms which define new centres of head or foot organising activity within an initially chaotic mass of cells.

- Which models are able to capture the results of cutting and grafting experiments?

Hydra has a high capacity to regenerate any lost body part and is a subject of many regeneration studies. Regeneration is the ability of the fully developed organism to replace lost parts by growth or remodelling of somatic tissue. In hydra regeneration occurs mainly by the repatterning of existing tissues. Thus the regeneration in hydra is an example of morphallaxis and is connected with little new growth while the epimorphosis in e.g. newt limb is connected with a growth of new correctly patterned structure [80].

The lack of growth requirements for regeneration is shown in heavily irradiated hydra, no cell divisions occur in these animals, but they can still regenerate normally [80]. Thus the mechanism of pattern formation in hydra seems to be independent on growth.

The cutting experiments show that the polarity is maintained even in small pieces of the body. A tissue piece containing 150-300 epithelial cells, i.e. about 1 percent of normal polyp, regenerate a complete hydra. However, below this size regeneration does not take place [71], [6]. There are also observation connected with the influence of size

of the animal on the time of pattern formation, showing that the time required for the regeneration decreases with the increase of the tissue size [71].

These observations can suggest the diffusion-driven mechanism for pattern formation.

The same cells can produce different structures depending on their relative position along the body column. Experiments show (Fig. 2.2) that the head and foot regenerate when they are cut off [78], [6]. If we cut at various levels, we will see that the entire body column between the existing head and the foot has the potential to form both the head and the foot. An upper half of a transversally cut hydra will regenerate a foot at its lower end, the lower half will form a head at its upper end. By slightly varying the cut levels, as shown in the Fig. 2.2, it can be demonstrated that one and the same group of cells forms a head, a gastric region or a foot, depending on their position in the body column.

Grafting experiments show how cells change their functions according to the local cues. Pieces of tissued are grafted from one animal to another and the outcome of such experiments depends on the change of position along the body axes. Transplantation of tissue from parts of the body column near to the head induces head formation while transplantation of tissue from the position near to the foot results in the foot formation [78], [43], [44], [55] (see Figure 2.4). If the position of the tissue in host and donor organism is similar then the piece of tissue is integrated and nothing is observed. Grafting experiments show how the disparities between the positional value of the transplant and the surrounding host tissue result in the head formation or the foot formation and new organisms with multiple heads or feet.

2.3 Models proposed in this work, versus previous models of hydra

Three theoretical models for pattern formation in hydra have previously been proposed. Wolpert [79] suggested a gradient model to account for head (but not foot) formation, in which at the head end a morphogen S is emitted. The morphogen spreads by diffusion and is distributed down the body. This diffusible chemical induces formation of the head.

A different model type, proposed by Meinhardt and Gierer [19], is based on local activation and long-range inhibition (for details see Appendix A.1). In this approach the positional value is interpreted as the density gradient of morphogen. Gradients of morphogens are formed by reaction-diffusion mechanism. Each of the various body

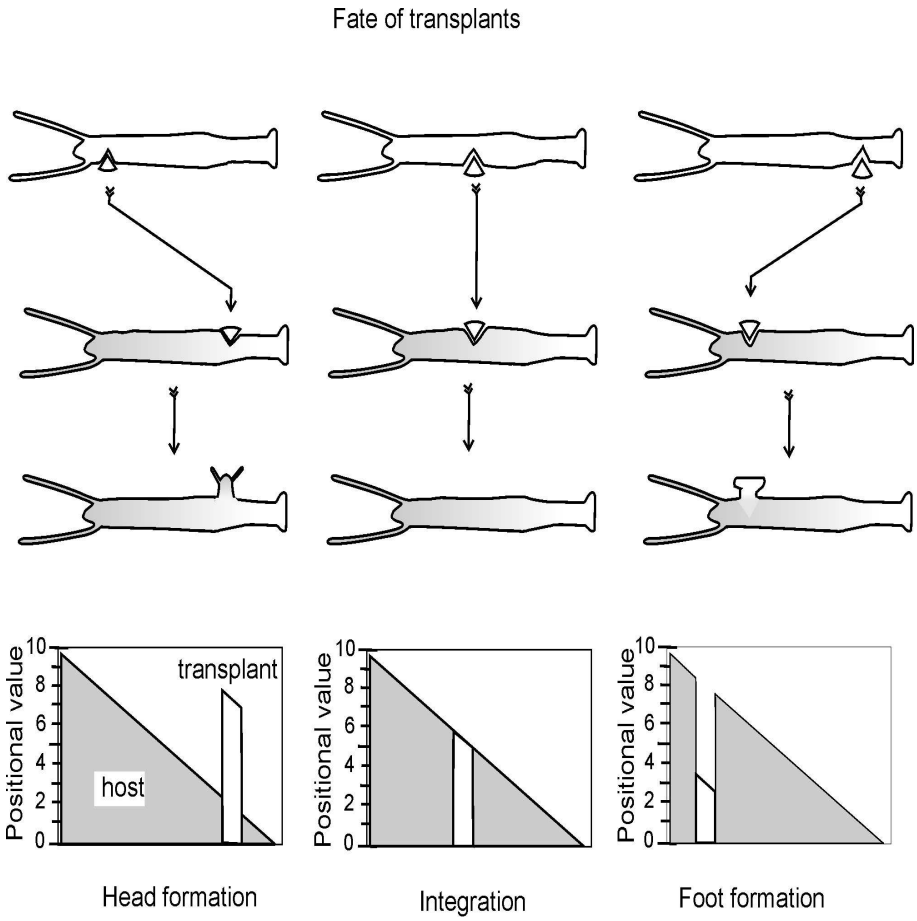

Figure 2.4. Grafting experiment. Determination of relative positional values by transplantation. Pieces of tissue are grafted from one animal to another and one of three outcomes is observed. (1) If the tissue is transplanted from the upper position along the body column to the lower position then a new head is formed. (2) If the former and new position is the same then the piece is integrated and nothing is observed. (3) If the tissue is grafted to the upper position a new foot is formed. We can see that the disparities between the positional value of the transplant and the surrounding host tissue result in the head formation or the foot formation respectively. [Courtesy of W. Müller]

parts is assumed to be under control of a separate activator-inhibitor system (for details see [49]).

Both models mentioned above operate with long-range morphogens. The proposed morphogens are still purely hypothetical. The recent approach proposed by Sherrat, Maini, Jäger and Müller (the SMJM model) [70] is based on the idea that both head and foot formation could be controlled by a receptor-ligand binding. We discuss the basic assumptions of this model later on (for details see Appendix A.2).

The models we study, are motivated by the SMJM model and its receptor-based approach. The objective is to build a receptor-based model without imposing an initial gradient as it is done in the model of Sherrat *et al.*

Following Müller [56] we assume that the positional value is determined by the density of bound receptors (Fig. 2.5). We assume, similarly as in the SMJM model, that a single positional value dictates both head and foot formation. This is one of the major differences between our approach and the Gierer-Meinhardt model. Such assumption is in keeping with experimental evidence for the interactions between the mechanisms of the head and the foot formation. For instance, the head assists in the foot formation, which is considerably delayed in the absence of the head. On the other hand, additional heads can evoke the occurrence of additional, ectopic feet [54], [57]. Our models are based on the idea that epithelial cells secrete ligands (a regulatory biochemical), which diffuse locally within the interstitial space and bind to free receptors on the cell surface.

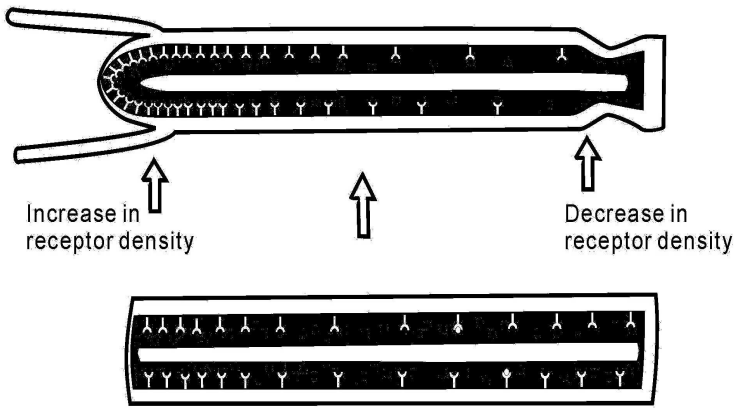

Figure 2.5. Bound receptors density determining "positional value". The hypothesis is that a single "positional value" controls the formation of both the head and the foot: the head is formed if the density of bound receptors is high (above some threshold) and the foot is formed if it is low (below another threshold). Consequently, in normal development we expect a gradient-like distribution of bound receptors. [Courtesy of W. Müller]

We consider the systems of reaction-diffusion equations coupled with the ordinary differential equations and study what kind of phenomena rising from such systems (i.e. diffusion-driven instabilities, travelling waves, hysteresis and threshold behaviour) can explain the results observed in experiments.

A number of different receptor-based models for the evolution of spatial pattern has already been proposed, e.g. for the formation of cAMP patterns in *Dictyostelium* slime mold cells [48] and [52]. The models considered here are rather simple compared with these detailed and complicated schemes. This is due to the absence of detailed biochemical knowledge about pattern control in hydra. Using these simple and general models we try to clarify the ideas of receptor-based mechanism of pattern control and explore their implications.

In the first approach we consider a model without enzyme, because it is in fact the simplest receptor-based scenario and the need for an enzyme is not so obvious for biologists (Müller, *personal communication*). Our second model includes a hypothetic enzyme which actively degrades ligands as it is known, for instance, for the cleavage of the morphogen chordin by the metalloprotease tolloid in the vertebrate embryo [64]. We show that in the case when the enzyme is absent the final pattern strongly depends on initial conditions.

The SMJM model is also represented by reaction-diffusion equations. The major difference between our model and that one is that in the SMJM model the terms describing *de novo* production of free receptors, ligands and enzyme depend on the position of the tissue along the body axes. In order to achieve the required local competition phenomenon, it is assumed in the SMJM model that kinetic functions are explicit functions of x, where x is a position along the body axis. The functions describing the production of new receptors and production of enzyme are linearly decreasing in x. The production of ligands is assumed to be constant on $4/5$ th of the domain and then decrease linearly to zero. The combination of these two parallel gradients enables the model to capture some results of grafting and cutting experiments. Thus, the SMJM model functions not because of nonlinear interactions between receptors and ligands but because of the assumption that cells produce new molecules depending on the position they had in the donor organism. In conclusion, the SMJM model is not a model for *de novo* pattern formation.

In this work, we verify under which conditions our receptor-based model can predict head and foot formation in hydra. The question is what is the form of the reaction

system operating in each cell that can produce the patterns, which are observed in experiments.

Mathematical details of the Meinhardt-Gierer and SMJM models are provided in the Appendix A.

2.4 Mathematical development of receptor-based models

The simplest model describing receptor-ligand binding is given in the form of three equations. It takes into consideration the density of free receptors, of the bound receptors and of the ligands. We use a representation of ligand-receptor binding that is as generic as possible and based on the scheme shown in Fig. 2.6.

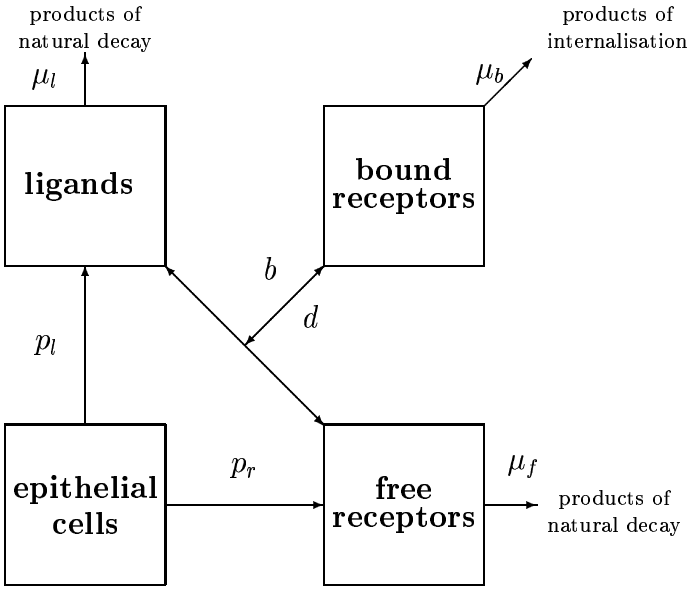

Figure 2.6. General scheme of the simplest receptor-based model. Cells produce new receptors and ligands which diffuse along the body axis and bind to the receptors. Bound receptors dissociate back to free receptors and ligands. All the consider molecules undergo natural decay.

We assume that new ligands and new free receptors are produced on cell surface through a combination of recycling (dissociation of bound receptors) and *de novo* production within the cell. Then a ligand binds to a free receptor reversibly, which results in a bound receptor that is internalised into the cell. Bound receptors also dissociate. Both ligands and free receptors undergo natural decay.

We consider one-dimensional epithelial sheet of length L. We denote the concentration of ligands by $l(x,t)$, where x and t are space and time coordinates, with x increasing

from 0 to L along the body column. The bound and free receptors densities are denoted by $r_b(x,t)$ and $r_f(x,t)$ respectively. For simplicity we assume that all binding processes are governed by the law of mass action without saturation effects.

Our mathematical model consists of the following equations

$$\begin{aligned} \frac{\partial}{\partial t} r_f &= -\mu_f(r_f) + p_r(r_f, r_b) - b(r_f, l) + d(r_b), \\ \frac{\partial}{\partial t} r_b &= -\mu_b(r_b) + b(r_f, l) - d(r_b), \\ \frac{\partial}{\partial t} l &= d_l \frac{\partial^2}{\partial x^2} l - \mu_l(l) - b(r_f, l) + p_l(r_f, r_b) + d(r_b), \end{aligned} \tag{2.1}$$

where

r_f - density of free receptors,

r_b - density of bound receptors,

l - density of ligands,

μ_f - rate of decay of free receptors,

μ_b - rate of decay of bound receptors,

μ_l - rate of decay of ligands,

p_r - rate of production of new free receptors,

p_l - rate of production of ligands,

d - rate of dissociation of bound receptors,

b - rate of binding of ligands and free receptors,

d_l - diffusion coefficient for ligands.

Since the seminal paper of Turing [77] the study of patterns arising through bifurcation has been prevalent in the modelling literature, especially regarding morphogenesis [60], [20], [45]. Again, we restrict our attention here to bifurcating solutions. Diffusion-driven instability is also a mechanism of pattern formation in the activator-inhibitor model for hydra proposed by Meinhardt and Gierer. We aim now to check whether a receptor-based model can include such mechanism and what are the constrains regarding kinetics.

The results of *de novo* pattern formation from the dissociated cells and of the cutting experiments (compare section 2.2) suggest that there exists an organising centre which creates a global structure of the set of solutions. Thus a natural approach is to study at first the diffusion-driven instabilities.

We will show in section 4.1.2 that in model (2.1) patterns can evolve due to a diffusion-driven instability (Turing-type instability) only when the production of free receptors is a nonlinear, growing function of free receptors. It means that a three-variable receptor-based model can produce diffusion-driven patterns only under assumption that the number of free receptors increases nonlinearly by some kind of positive feedback (autocatalysis). Also production of ligands must depend on free receptors.

The present literature does not provide examples of such positive feedback loops in which receptors not occupied by a ligand would stimulate their own synthesis (W. Müller, *personal communication*). It is known from the number of other biological contexts that there can exist a positive feedback loop between the density of bound receptors on the cell surface and the subsequent expression of new receptors [35], [74]. It convinced us to take under consideration a second diffusible substance, functioning as an enzyme as in SMJM model [70]. This enzyme is secreted by cells, diffuses along the body column and degrades the ligands. We introduce to the model a new variable describing the density of an enzyme. The role of the enzyme is to remove the biological regulator, i.e. ligand, before it binds to the receptors on the cell surface. It is important to stress that this model cannot be simplified to an activator-inhibitor system. Our model consists of two subsystems. The reaction-diffusion subsystem describing ligand and enzyme dynamics is not of the activator-inhibitor type and cannot produce diffusion-driven patterns itself. Pattern formation in this model is caused by the coupling with the subsystem of two ordinary differential equations.

The model has the following form

$$
\begin{aligned}
\frac{\partial}{\partial t} r_f &= -\mu_f(r_f) + p_r(r_f, r_b) - b(r_f, l) + d(r_b), \\
\frac{\partial}{\partial t} r_b &= -\mu_b(r_b) + b(r_f, l) - d(r_b), \\
\frac{\partial}{\partial t} l &= d_l \frac{\partial^2}{\partial x^2} l - \mu_l(l) - b(r_f, l) + p_l(r_f, r_b) + d(r_b) - b_e(l, e), \\
\frac{\partial}{\partial t} e &= d_e \frac{\partial^2}{\partial x^2} e - \mu_e(e) + p_e(l, r_b),
\end{aligned}
\tag{2.2}
$$

where

e - density of enzyme,

b_e - rate of binding of ligands and enzyme,

p_e - rate of production of enzyme,

d_e - diffusion coefficient for enzyme,

μ_e - rate of decay of the enzyme

and the rest stays like in the three-variable model.

We will show in section 4.2.2 that in such a model patterns can evolve due to a diffusion-driven instability, even if no self-enhancement of free receptors nor ligands is assumed. p_r is now the function of r_b.

Numerical simulations also show that in the case when the enzyme is absent the final pattern strongly depends on initial conditions (see Fig. 4.5) while the four-variable model (with enzyme) is more robust so that the final pattern does not depend on the spatial profile of the initial small perturbation of the spatially homogeneous state (see Fig. 4.8) but only on the domain size.

On the other hand, grafting experiments suggest that there are a number of locally asymptotically stable patterns depending on the past history (or initial conditions of the system). It encouraged us to built a model with multiple steady states. The kinetics system with hysteresis and two stable steady states allows to explain the coexistence of different patterns for the same parameters but depending on the initial conditions.

In Chapter 5 we consider the following system showing hysteresis,

$$
\begin{aligned}
\frac{\partial}{\partial t} r_f &= -\mu_f(r_f) + p_r(r_f, r_b) - b(r_f, l) + d(r_b), \\
\frac{\partial}{\partial t} r_b &= -\mu_b(r_b) + b(r_f, l) - d(r_b), \\
\frac{\partial}{\partial t} l &= d_l \frac{\partial^2}{\partial x^2} l - \mu_l(l) - b(r_f, l) + p_l + d(r_b) - b_e(l, e), \\
\frac{\partial}{\partial t} e &= d_e \frac{\partial^2}{\partial x^2} e - \mu_e(e) + p_e, \\
\frac{\partial}{\partial t} p_l &= -\delta_l \frac{p_l}{1 + p_l^2} + \frac{m_2 l r_b}{(1 + \sigma_l p_l^2 - \beta_l p_l)(1 + \alpha_l r_b)}, \\
\frac{\partial}{\partial t} p_e &= -\delta_e \frac{p_e}{1 + p_e^2} + \frac{m_3 l e}{(1 + \sigma_e p_e^2 - \beta_e p_e)(1 + \alpha_e r_b)}.
\end{aligned}
\tag{2.3}
$$

Last two equations are proposed to describe the dynamics of production of ligands and enzyme. Numerical simulations show that in this system different dynamic patterns coexist for a specified value of parameters. The final shape of the spatial pattern strongly depends on the initial conditions (on the history).

3

Formulation and analysis of receptor-based models

3.1 Mathematical structure of receptor-based models

Most of the models of morphogenesis are reaction-diffusion models assuming the existence of diffusing substances. Since some of the molecules, which take part in the morphogenetic processes, e.g. receptors or cells, do not diffuse, it is necessary to consider systems of reaction-diffusion equations coupled with ordinary differential equations. In the reaction-diffusion framework, this is equivalent to some of the diffusion coefficients being equal to zero.

The theory of reaction-diffusion equations was developed by many authors, e.g. Britton [7], Smoller [72], Fife [15], Rothe [65], Henry [22] and recently Fiedler and Scheel [14]. Some of the results can also be applied in the case when some of the diffusion coefficients are equal to zero, which is of interest to us.

As it will be seen, different authors made different assumptions on the functional spaces of the solutions, and, in consequence, obtained differing results. However, in the biological context, most of these diverse assumptions are satisfied. Therefore, we include here these results, which could be applicable to the receptor-based models. Many of them are used further on in the thesis.

All considered receptor-based models consist of two subsystems of reaction-diffusion equations and ordinary differential equations coupled via the nonlinear kinetics functions. In general, equations of our models can be represented in the form,

$$
\begin{aligned}
u_t^1 &= f_1(u^1, u^2), \\
u_t^2 &= D_+ \Delta u^2 + f_2(u^1, u^2), \\
\partial_n u^2 &= 0 \ \ in \ \ \partial\Omega, \\
u^1(0,x) &= u_0^1(x), \\
u^2(0,x) &= u_0^2(x),
\end{aligned} \tag{3.1}
$$

where $\Omega \subset \mathbb{R}^N$ is a bounded region and D_+ is a diagonal $(m-r) \times (m-r)$ matrix with positive coefficients. In our models $N = 1$ and $\Omega = [0,1]$.

$u^1 : \Omega \times \mathbb{R}^+ \to \mathbb{R}^r$, $u^2 : \Omega \times \mathbb{R}^+ \to \mathbb{R}^{m-r}$, r is the number of ordinary differential equations and $m-r$ the number of reaction-diffusion equations. f_1 and f_2 are smooth mappings, $f_1 : \mathbb{R}^m \to \mathbb{R}^r$ and $f_2 : \mathbb{R}^m \to \mathbb{R}^{m-r}$.

For convenience we introduce the vector notation which encompasses all of our receptor-based models,

$$
\begin{aligned}
u_t &= D\Delta u + f(u) \ \ in \ \ \Omega \times \mathbb{R}^+, \\
\partial_n u_i &= 0 \ \ for \ \ i = r+1, ..., m \ \ in \ \ \partial\Omega, \\
u(0,x) &= u_0(x),
\end{aligned} \tag{3.2}
$$

where $u = (u^1, u^2)$ and D is a diagonal matrix of nonnegative diffusion coefficients. Let $d_i = 0$ for $i = 1, ..., r$ and $d_i > 0$ for $i = r+1, ..., m$ and $D = diag(d_1, d_2, ..., d_m)$.

The matrix of diffusion coefficients D has the form

$$
D = \begin{pmatrix} 0 & 0 \\ 0 & D_+ \end{pmatrix}. \tag{3.3}
$$

where D_+ is a diagonal $(m-r) \times (m-r)$ matrix with positive coefficients and 0 denotes the zero matrix of the appropriate dimension.

f is a mapping, $f : \mathbb{R}^m \to \mathbb{R}^m$, where m is the number of equations.

In our systems the nonzero diffusion coefficients occur only in one or two equations. However, such system can be treated in the same way as a parabolic system as far as the existence and uniqueness of solutions are concerned [7].

In the following Sections 3.2 and 3.3 we outline the results regarding the existence and uniqueness of different types of solutions of the reaction-diffusion equations.

To show the global existence and uniqueness of the solution to our receptor-based models, in Section 4, we apply the theory of bounded invariant rectangles, i.e. bounded regions, Σ, in a phase space, with the property that if the initial data lie in Σ, then the solution $u(x,t)$ lies in Σ for all $x \in \Omega$ and all $t > 0$. Thus Σ provides an a priori supremum-norm bound on u. We recall elements of the theory, which can be applied to our receptor-based models of hydra. The corresponding theorems and proofs can be found for example in [72]. Theorems about bounded invariant rectangles are applied in Section 4.2.1 to show the existence of global solutions to our receptor-based models of hydra as well as to the model of the tumour growth presented in Section 6.2.6. Also we discuss results on linearised stability (Theorem 3.26), which justify the use of the linearisation techniques later on.

In Section 3.4 we discuss the Turing-type mechanism for pattern formation. We review the standard results for the onset of the instability based on the linearised system.

3.2 Definitions of solutions and theorems on existence

Numerous definitions and existence theorems of classical, mild and weak solutions to our problem are considered in the literature. These approaches differ with respect to their hypotheses. The following review does not attempt to provide a uniform treatment, but to show connections between different classes of solutions.

3.2.1 From mild to classical solutions

The construction of solutions of the initial-boundary problem begins with the construction of mild solutions and then turns to classical solutions.

Here u is considered as a function of time t with values in a Banach space X.

We define $C([t_1,t_2],X)$ to be the set of continuous functions u defined on $t_1 \leq t \leq t_2$ with values in a Banach space X.

The space X must be chosen such that the domain of the operator A, $\mathcal{D}(A) \subset X$.

Later we consider what is the regularity of the solutions depending on the regularity of the initial conditions. Therefore, we consider different functional spaces, i.e. $X = (L^\infty(\Omega))^r \times (H^2(\Omega))^{m-r}$ (see Section 3.3.2) or X a subspace of bounded continuous $(C(\Omega))^r \times (C^2(\Omega))^{m-r}$ - functions (see Section 3.3).

We consider the problem in the form,

$$\begin{aligned} u_t &= Au + f(u), \\ u(0) &= u_0 \end{aligned} \tag{3.4}$$

In order to rewrite (3.2) as an abstract problem of the form (3.4) we define the operator $A = D\Delta$ with the domain $\mathcal{D}(A) := \{(u^1, u^2) \in (L^\infty(\Omega))^r \times (H^2(\Omega))^{m-r} : \partial_n u^2 = 0 \text{ on } \partial\Omega\}$.

We note that A has the form, $A = A_1 \times A_2$, where $A_1 = 0$, $A_2 = D_+\Delta$ and $(A_1 \times A_2)(u^1, u^2) = (A_1 u^1, A_2 u^2)$ for $u^1(t) \in \mathcal{D}(A_1)$ and $u^2(t) \in \mathcal{D}(A_2)$ for $u^1 = (u_1, ..., u_r)$ and $u^2 = (u_{r+1}, ..., u_m)$.

Remark 3.1. Later we show that A defined above is a sectorial operator. Therefore, A generates a C^0-semigroup (see Theorem 4.6 in [12]).

We use the following notation:

Definition 3.2. Let A be the infinitesimal generator of a C_0 semigroup $P(t)$. Let $u_0 \in X$ and $f \in L^1([0,T], X)$. A function $u \in C([0,T], X)$ satisfying

$$u(.,t) = P(t)u_0 + \int_0^t P(t-s)f(u(.,s))ds \quad for \quad all \quad t \in [0,T]$$

is a mild solution of the initial value problem (3.4) on $[0,T]$.

Definition 3.3. A function $u : [0,T) \to X$ is a classical solution of (3.4) on $[0,T)$ if u is continuous on $[0,T)$, continuously differentiable on $(0,T)$, $u(t) \in \mathcal{D}(A)$ for $0 < t < T$, (3.4) is satisfied on $(0,T)$ and $u(0) = u_0$.

For $f \in L^1([0,T], X)$ the initial value problem (3.4) has a unique mild solution [63]. We are interested in imposing further conditions on f so that for $u_0 \in \mathcal{D}(A)$ the mild solution becomes a classical solution.

Rothe [65] considers systems of the form,

$$u_t = D\Delta u - Du + F(x,t,u), \quad for \quad all \quad x \in \Omega, t > 0, \tag{3.5}$$

where D is a diagonal matrix with diagonal entries $d_i = 0$ for $i = 1, ..., r$ and $d_i > 0$ for $i = r+1, ..., m$, together with the initial condition

$$u(x,0) = u_0(x) \tag{3.6}$$

and boundary conditions

$$u_i(x,.) = 0 \quad for \quad i = r+1, ..., s \tag{3.7}$$

$$and \qquad b_i(x)u_i(x,t) + \partial_n u_i(x,t) = 0 \quad for \quad i = s+1, ..., m \quad on \quad \partial\Omega. \tag{3.8}$$

In other words, components, which do not diffuse, may occur. The boundary conditions considered include the case of zero-flux boundary conditions if $b_i(x) = 0$. Rothe [65] uses the $E_{\infty,0,T}$-mild solution, which is defined in the following way,

Definition 3.4. Let $T \in (0,\infty) \cup \infty$. An $E_{\infty,0,T}$-mild solution of the initial boundary value problem for the initial data $u_0 \in L^\infty(\Omega, \mathbb{R}^m)$ on the time interval $[0,T)$ is a measurable function $u : (x,t) \in \Omega \times (0,T) \to \mathbb{R}^m$ satisfying

$u(.,t) \in L^\infty(\Omega)$ and $sup\{\|u(.,s)\|_\infty | s \in (0,t)\} < \infty$ for all $t \in (0,T)$,

$u(.,t) = P(t)u_0 + \int_0^t P(t-s)F(.,s,u(.,s))ds$ for all $t \in (0,T)$,

where the integral is an absolutely converging Bochner integral in $L^\infty(\Omega)$. P is an operator: $P_i(t) = I$ for $i = 1, ..., r$ and $P_i(t) = S_i(d_i t)$ for $i = r+1, ..., m$, where I denotes the identity operator and $S_i(t)$ denotes the semigroup generated by the operator $-\Delta + 1$ and the boundary conditions (3.7) or (3.8) for $i = r+1, ..., s$ or $i = s+1, ..., m$ respectively.

For $p \in \mathbb{N}$, $\alpha \in (0,1)$ let $C^p(\bar{\Omega})$ and $C^{p+\alpha}(\bar{\Omega})$ be the Banach spaces of continuously p-times differentiable and α-Hölder functions. A function f is Hölder continuous with exponent $\alpha \in (0,1)$ if there is a constant L such that

$$\|f(x) - f(y)\| \leq L|x-y|^\alpha.$$

Rothe [65] formulated a theorem on the existence of mild and classical solutions of the system of reaction-diffusion equations coupled with ordinary differential equations. We may apply it to our models to show the existence of solutions in the spaces of continuously differentiable and α-Hölder functions.

Theorem 3.5.

Assume that:

(i) $u_0 \in L^\infty(\Omega, \mathbb{R}^m)$.

(ii) A function $F(.,.,u) : (x,t) \in \bar{\Omega} \times [0,\infty) \to F(x,t,u) \in \mathbb{R}^m$ *is measurable in* (x,t) *for all* $u \in \mathbb{R}^m$.

(iii) For every bounded set $B \subset \bar{\Omega} \times [0,\infty) \times \mathbb{R}^m$, there exists a constant $L(B)$ such that

$$\begin{aligned} |F(x,t,u)| &\leq L(B) \quad for \quad all \quad (x,t,u) \in B, \\ |F(x,t,u) - F(x,t,v)| &\leq L(B)|u-v| \quad for \quad all \quad (x,t,u),(x,t,v) \in B. \end{aligned}$$

Then the following holds:

(1) For each initial function $u_0 \in L^\infty(\Omega, \mathbb{R}^m)$, there exists $T \in [0,\infty)$ such that the initial-boundary value problem (3.5) has a unique $E_{\infty,0,T}$-mild solution on the interval $[0,T)$.

(2) Consider the existence time T as a functional of the initial data $u_0 \in L^\infty(\Omega, \mathbb{R}^m)$. Then this functional $T = T(u_0)$ satisfies

$$inf\{T(u_0) | u_0 \in L^\infty(\Omega, \mathbb{R}^m), \|u_0\|_\infty \leq \bar{u}_0\} > 0 \quad for \quad all \quad \bar{u}_0 \in [0,\infty).$$

(3) The existence time $T \in (0,\infty) \cup \infty$ can be chosen maximal, i.e. Definition 3.2 does not hold for a larger time. In that case we let $T = T_{max}$ and obtain

$$lim_{t \to T_{max}} \|u(t)\|_\infty = \infty \ \ if \ \ T_{max} < \infty.$$

(4) Assume regular initial data u_0, i.e.

$$\begin{aligned} u_{0i} &\in C^\alpha, \quad \alpha \in (0,1) \quad for \quad i = 1,...,r, \\ u_{0i} &\in C^{2+\alpha} \quad for \quad i = r+1,...,m, \end{aligned}$$

where r is the size of the ODEs subsystem (as defined before: $d_i = 0$ for $i = 1,...,r$ and $d_i > 0$ for $i = r+1,...,m$) and that, for every bounded set $B \in \bar{\Omega} \times [0,\infty) \times \mathbb{R}^m$, there exists a constant $L(B)$ such that

$$|F(x,t,u)| \leq L(B) \quad for \quad all \quad (x,t,u) \in B, \tag{3.9}$$

$$\begin{aligned} |F(x,t,u) - F(y,s,v)| &\leq L(B)(|x-y|^\alpha + |t-s|^{\alpha/2} + |u-v|) \\ &\quad for \quad all \quad (x,t,u),(y,s,v) \in B. \end{aligned} \tag{3.10}$$

Then the mild solution is smooth, in the sense that, with $u(.,0) = u_0$ we have

$$\begin{aligned} u_i &\in C^{\alpha,1+\alpha/2}(\bar{\Omega} \times [0,T]) \quad for \quad i = 1,...,r \quad all \quad T \in (0,T_{max}), \\ u_i &\in C^{2+\alpha,1+\alpha/2}(\bar{\Omega} \times [0,T]) \quad for \quad i = r+1,....m, \quad all \quad T \in (0,T_{max}). \end{aligned}$$

Remark 3.6. In the models considered by us F does not depend explicitly on x or t. Thus the condition (3.10) is equivalent with the assumption (iii).

3.2.2 Weak solutions

Ball [5] defines a weak solution of the equation (3.4) in the following way

Definition 3.7. A function $u \in C([0,T],X)$ is a weak solution of (3.4) on $[0,T]$ if for every $v^* \in \mathcal{D}(A^*)$ the function $\langle u, v^* \rangle$ is absolutely continuous on $[0,T]$ and

$$\frac{d}{dt}\langle u, v^* \rangle = \langle u, A^* v^* \rangle + \langle f(u), v^* \rangle \quad a.e. \ on \ [0,T]. \tag{3.11}$$

A^* is an adjoint operator of A from $\mathcal{D}(A^*) \subset X^*$ into X^*, where X is a dual Banach space to X and $D(A^*)$ is the set of elements $u^* \in X^*$ for which there is a $v^* \in X^*$ such that $\langle u^*, Au \rangle = \langle v^*, u \rangle$ for all $u \in \mathcal{D}(A)$, and if $u^* \in \mathcal{D}(A^*)$ then $v^* = A^* u^*$.

Ball [5] proved that

Theorem 3.8.
There exists for each $x \in X$ a unique weak solution u of (3.4) on $[0,T]$ satisfying $u(0) = u_0$ if and only if A is the infinitesimal generator of a C_0 semigroup $P(t)$ of bounded linear operators on X, and in this case u given by

$$u(.,t) = P(t)u_0 + \int_0^t P(t-s)f(u(.,s))ds \quad for \ \ all \ \ t \in [0,T] \tag{3.12}$$

Remark 3.9. Relationship (3.12) implies that weak solutions are also mild solutions of (3.4).

3.3 Invariant rectangles and stability of solutions

3.3.1 Existence and uniqueness of solutions

To show the global existence and uniqueness of solutions to our receptor-based models, we apply the theory of a priori estimates and bounded invariant rectangles. Using this theory we also show that the solutions of all considered receptor-based models for positive initial conditions stay positive and that in some case they are uniformly bounded (e.g. in the four-equation model considered in Section 4). Bounded invariant rectangles are bounded regions, Σ, in a phase space, with the property that if the initial data lie in Σ, then the solution $u(x,t)$ lies in Σ for all $x \in \Omega$ and all $t > 0$. Thus Σ provides an a priori supremum-norm bound on u. We recall elements of the theory,

which can be applied to our models. The corresponding theorems and proofs can be found e.g. in [72].

We consider the system (3.2) with zero flux boundary conditions in a single space variable, $\bar{\Omega} = [0, 1]$, where $D = diag(d_1, ..., d_m)$ with $d_i \geq 0$ for all i, and f is a smooth mapping from an open set $U \in \mathbb{R}^m$ to $\mathbb{R}^m$. Solutions of (3.2) are continuous functions of time with values in a Banach space, B.

Let us suppose that B is a Banach space of functions on Ω with values in $\mathbb{R}^m$; $\|\cdot\|_B$ denotes the B-norm and $\|\cdot\|_\infty$ the L^∞-norm.

Smoller introduces the following notation of an admissible Banach space

Definition 3.10. B is admissible if the following conditions hold:

(1) B is a subset of the space of bounded continuous functions on $\Omega \subseteqq \mathbb{R}$, and if $w \in B$, $\|w\|_B \geq \|w\|_\infty$.

(2) If $f : \mathbb{R}^m \to \mathbb{R}^m$ is smooth and $f(0) = 0$ then $f(w) \in B$ for every $w \in B$, and for any $M > 0$, there is a constant $k(M)$ such that

$$\|f(w) - f(w')\|_B \leq k(M)\|w - w'\|_B,$$

for all $w,\ w'$ in B with $\|w\|_\infty, \|w'\|_\infty \leq M$.

And, additionally, for unbounded $\Omega = \mathbb{R}$:

(3) B is translation-invariant, i.e. $w \circ \tau \in B$ for every $w \in B$ and every translate $\tau : \mathbb{R} \to \mathbb{R}$. In addition $\|w \circ \tau\|_B \leq \|w\|_B$.

(4) If $\tau_h : \mathbb{R} \to \mathbb{R}$ denotes translation by h (i.e. $\tau_h(x) = x + h$), then for each $w \in B$,

$$\|w \circ \tau_h - w\|_B \to 0 \ \ as \ \ h \to 0.$$

We define $C([0, T], B)$ to be the Banach space of continuous functions on $[0, T]$ with values in the admissible Banach space B, normed by

$$\|w\| = \sup_{0 \leq t \leq T} \|w(t)\|_B.$$

First we recall the concept of an invariant region, which allows to prove global existence theorems. Our formulations are taken from the book of Smoller [72].

Definition 3.11. A closed subset $\Sigma \in \mathbb{R}^m$ is called a (positively) invariant region for the local solution of (3.2), if any solution $u(x, t)$ having all of its boundary and initial values in Σ, satisfies $u(x, t) \in \Sigma$ for all $x \in \Omega$ and for all $t \in [0, \delta)$.

We consider regions Σ of the form

$$\Sigma = \cap_{i=1}^{m}\{u \in U : G_i(u) \leq 0\} \tag{3.13}$$

where, for each i, G_i are smooth real-valued functions defined on open subsets of U, and the gradient dG_i never vanishes.

To show the existence of invariant rectangles for the system (3.2) we can use the following Theorem being a modified version of the Theorem 14.7 in [72].

Theorem 3.12.
Any region of the form $\Sigma = \cap_{i=1}^{m}\{u \in U : G_i(u) \leq 0\}$ is invariant for (3.2) provided that f points strictly into Σ on $\delta\Sigma$, i.e. provided that for every $v_0 \in \delta\Sigma$ (so $G_i(v_0) = 0$ for some i), the following condition holds,

$$dG_i(f) < 0 \quad at \quad v_0, \quad for \quad all \quad t \in \mathbb{R}^+. \tag{3.14}$$

Remark 3.13. Since D in (3.2) is a diagonal matrix with nonnegative coefficients, then any region of the form $\Sigma = \cap_{i=1}^{m}\{u : a_i \leq u \leq b_i\}$ is invariant provided that the condition (3.14) is fulfilled (see Corollary 14.8 in [72]).

Suppose we can prove the existence of such a bounded invariant rectangle for the system (3.2) for a particular choice of the function f. Then, to show the existence of a global solution, we can use the following result in [72].

Corollary 3.14.
Consider the system (3.2) with data $u_0 \in B$. If the system admits a bounded invariant region Σ, and $u_0(x) \in \Sigma$ for all $x \in \mathbb{R}$, then the solution exists for all $t > 0$.

It can happen that the vector field f satisfies the weaker condition: $dG_i(f) \leq 0$ at v_0, i.e. f is tangent to $\delta\Sigma$ at certain places. If the system (3.2) is f-stable, we can replace the condition (3.14) in the Theorem 3.12 by

$$dG_i(f) \leq 0 \quad at \quad v_0, \quad for \quad all \quad t \in \mathbb{R}^+. \tag{3.15}$$

Definition 3.15. The system (3.2) is called f-stable if, whenever f is the limit of functions f_n in the C^1-topology on compacta, for all $t \geq 0$, then any solution of (3.2) is the limit in the compact-open topology of solutions of (3.2) (i.e. u_n converges to u uniformly on compact subsets of $\Omega \times \mathbb{R}$), where f is replaced by f_n.

We can formulate the following:

Theorem 3.16.
Any region of the form $\Sigma = \cap_{i=1}^{m}\{u \in U : G_i(u) \leq 0\}$, *where for each* i, G_i *are smooth real-valued functions defined on open subsets of* U, *and the gradients* dG_i *never vanish, is invariant for the system (3.2), provided that for every* $v_0 \in \partial\Sigma$ *(so* $G_i(v_0) = 0$ *for some* i*) the system is* f*-stable and the following condition holds,*

$$dG_i(f) \leq 0 \quad at \quad v_0, \quad for \quad all \quad t \in \mathbb{R}^+. \tag{3.16}$$

For many choices of the kinetics function f the bounded invariant set does not exist but we can find an a priori bound; namely, there is a constant $c > 0$, depending only on $\|u_0\|_\infty$ such that if u is any solution of (3.2) in $0 \leq t \leq T$, for all time t, $0 \leq t \leq T$, then $\|u(\cdot, t)\|_\infty \leq c$. Then the solution of this problem exists for times $t \in [0, T]$ (see [72], Theorem 14.4).

Theorem 3.17.
Let B *be an admissible Banach space, and let* $u_0 \in B$. *If the solution is a priori bounded in the* L^∞*-norm on* $0 \leq t \leq T < \infty$, *then the solution of (3.2) exists for all* t, $0 \leq t < T$ *and* $u(\cdot, t) \in B$, $0 \leq t \leq T$.

Remark 3.18. In the systems containing ordinary differential equations jumps may occur at $t = \infty$, i.e. one may loose regularity at $t = \infty$ and solutions for continuous initial conditions may become asymptotically discontinuous.

It is of interest to note that invariant sets exist for many systems of reaction-diffusion equations modelling biological phenomena, for example the Fitzhugh-Nagumo system, Hodgkin-Huxley equation, Field-Noyes or Belousov-Zhabotinski model (see [72]).

The uniqueness and the contiuous dependece of the solution on the initial data follows from the following theorem (for the proof see [72])

Theorem 3.19.
Let $u, v \in C([0, T], B)$ *be solutions of (3.2) on* $0 \leq t \leq T$, *where* $\|u\|_\infty$, $\|v\|_\infty \leq M$. *Then there is a constant* $k = k(M)$ *such that*

$$\|u(t) - v(t)\|_B \leq e^{kt}\|u(0) - v(0)\|_B, \quad 0 \leq t \leq T.$$

3.3.2 Stationary solutions and their stability

It is a well-known phenomenon in nonlinear reaction-diffusion system that several static or dynamic patterns may coexist. If we change parameters, the number of patterns may change due to, for example, a bifurcation. For these reasons it is important to investigate the asymptotic behavior of solutions as $t \to +\infty$.

Let $\bar{u}(x)$ be a stationary solution to Eq. (3.2).

We define the stability and asymptotic stability of the stationary solution in the terms of the norm of some Banach space $B(\Omega)$.

Definition 3.20. $\bar{u}(x)$ is a stable solution if, for every $\epsilon > 0$, there exists δ such that for every initial function $u^0(x)$, $\|u^0(\cdot) - \bar{u}^0(\cdot)\|_{B(\Omega)} < \delta$ the solution u for this initial function exists for all $t \geq 0$ and $\|u(\cdot, t) - \bar{u}(\cdot)\|_{B(\Omega)} < \epsilon$ for all $t > 0$.

Definition 3.21. A stationary solution $\bar{u}(x)$ of (3.2) is asymptotically stable if it is stable and there exists a neighbourhood N of $\bar{u}$ such that if u is a solution to Eq. (3.2) with $u(0, \cdot) \in N$ then u exists for all $t \geq 0$ and $\lim_{t\to\infty} \|u(\cdot, t) - \bar{u}(\cdot)\|_{B(\Omega)} = 0$.

The stability of smooth stationary solutions of reaction-diffusion equations may be analysed by considering the eigenvalues of the linearised system (compare [7], [72]). The stability problem of the stationary discontinuous solutions is more subtle. The reason is that the spectral criterion on linearised stability cannot be applied since the system cannot be linearised at a discontinuous solution. As an example, in [21] Heinze and Schweizer consider the system of one reaction-diffusion equation coupled with one ODE describing the dynamics of two competing species. They show the instability of discontinuous solutions for a particular class of small perturbations which cannot be obtained from a linearisation argument.

Let us now consider functions $(u_i(t), u_j(t)) \in L^\infty(\Omega) \times H^2(\Omega)$, where $i = 1, ..., r$, $j = r + 1, ..., m$. It means that first r equations (ODE) hold almost everywhere in Ω while the next $m - r$ equations (reaction-diffusion equations) hold in the usual weak sense.

We consider continuous maps

$$f : (L^\infty(\Omega))^r \times (H^1(\Omega))^{m-r} \to (L^\infty(\Omega))^r \times (L^2(\Omega))^{m-r}. \tag{3.17}$$

Remark 3.22. Since in considered models $\Omega = [0, 1]$ is one-dimensional, from embedding theorems (see e.g. [22]) we obtain that $H^1(\Omega) \hookrightarrow L^\infty(\Omega)$. Therefore (3.17) holds for all the nonlinear functions f considered in receptor-based models.

To study the stability of the smooth stationary solutions we can apply the theorem about stability and instability by the linear approximation, which is a modified version of the theorem of Henry [22] (Theorem 5.1.1). This criterion is formulated for the equations with sectorial operators. It justifies the usage of the linear stability analysis in the next sections.

Definition 3.23. [22] We call a linear operator A in a Banach space X a sectorial operator if it is a closed densely defined operator such that, for some ϕ in $(0, \pi/2)$ and some $M \geq 1$ and real a, the sector

$$S_{a,\phi} = \{\lambda : \phi \leq |arg(\lambda - a)| \leq \pi, \ \ \lambda \neq a\}$$

is in the resolvent set of A and

$$\|(\lambda - A)^{-1}\| \leq \frac{M}{|\lambda - a|} \ \ for \ \ all \ \ \ \lambda \in S_{a,\phi}.$$

Definition 3.24. Suppose A is a sectorial operator and $Re\sigma(A) > 0$; then for any $\alpha > 0$,

$$A^{-\alpha} = \frac{1}{\Gamma(\alpha)} \int_0^\infty t^{-\alpha-1} e^{-At} dt.$$

A^α is the inverse of $A^{-\alpha}$; $A^0 = Id$ on X.

Definition 3.25. If A is a sectorial operator in a Banach space X, define for each $\alpha \geq 0$

$$X^\alpha = \mathcal{D}(A_1^\alpha)$$

with the norm $\|u\|_\alpha = \|A_1^\alpha u\|$, $u \in X^\alpha$

where $A_1 = A + aI$ with a chosen so $Re\ \sigma(A_1) > 0$, where σ is the spectrum of the operator A_1.

Theorem 3.26.

Let -A be a sectorial linear operator in a Banach space X and let $f : U \to X$ where U is a cylindrical neighborhood in X^α (for some $\alpha < 1$) of $(\tau, \infty) \times u_0$ and let u_0 be the equilibrium point of

$$u_t = Au + f(t, u),$$

i.e. $u_0 \in \mathcal{D}(A)$ and $Au_0 + f(t, u_0) = 0$.

Suppose that $f(t, u_0 + z) = f(t, u_0) + Bz + g(t, z)$, where B is a bounded linear map from X^α to X and $\|g(t, z)\| = o(\|z\|_\alpha)$ as $\|z\|_\alpha \to 0$, uniformly in $t > \tau$, and f is locally Holder continuous in t, locally Lipschitzian in u, on U.

(1) If the spectrum $A+B$ lies in $Re\lambda < -\beta$ for some $\beta > 0$, then the original equation has the solution u_0 asymptotically stable in X^α.

(2) If the spectrum $A+B$ intersects $\{Re\lambda > 0\}$, then the equilibrium solution u_0 is unstable.

We may apply the above theorem to the systems of reaction-diffusion equations coupled with ordinary differential equations while studying the stability of a smooth solution.

Let us note that

$$-A = \begin{pmatrix} 0 & 0 \\ 0 & -D_+\Delta \end{pmatrix}. \tag{3.18}$$

is a sectorial operator. To show this we use the statement from [22] saying

Corollary 3.27.
If A_1 is sectorial in X and A_2 is sectorial in Y, then $A_1 \times A_2$ is sectorial in $X \times Y$, where $(A_1 \times A_2)(u^1, u^2) = (A_1u^1, A_2u^2)$ for $u^1(t) \in \mathcal{D}(A_1)$ and $u^2(t) \in \mathcal{D}(A_2)$.

We consider $X = (L^\infty(\Omega))^r$, $Y = (L^2(\Omega))^{m-r}$ and $Y^{\frac{1}{2}} = (H^1(\Omega))^{m-r}$ (for details see [22]).

$A_2 := -\Delta$ is a sectorial operator in Y (see e.g. [22]). $A_1 = 0$ is also a sectorial operator. Hence $-A$ defined by (3.18) is also sectorial. All the kinetics functions f used in receptor-based models considered in this thesis satisfy $f(u) \in (L^\infty(\Omega))^r \times (L^2(\Omega))^{m-r}$ for $u(t) \in (L^\infty(\Omega))^r \times (H^1(\Omega))^{m-r}$ (see Remark 3.22).

Remark 3.28. Another theorem about the linearised stability of the spatially homogeneous solutions of the reaction-diffusion system coupled with ODEs is given in [8]. The authors formulate sufficient conditions for the stability of a constant stationary solution.

In the following sections we apply the linear stability analysis to find the conditions for the destabilisation of the spatially homogeneous steady state (e.g. to find conditions for the diffusion-driven instability).

We are also interested in studying the inhomogeneous stationary solutions. For $m = 1$ it can be shown (compare [60], [72]) that

Theorem 3.29.
There exists no stable spatial pattern (i.e. spatially inhomogeneous solution) for a scalar reaction-diffusion equation in one dimension with Neumann boundary conditions.

Proof : We consider the system (3.2) for $m = 1$ in one-dimensional space, i.e. $\Omega = [0, 1]$ and

$$\begin{aligned} u_t &= u'' + f(u), \\ u'(0) &= u'(1) = 0, \end{aligned} \tag{3.19}$$

where u' denotes the derivative of u in respect to x and u_t derivative in respect to t.

Stationary spatially inhomogeneous solution U satisfies

$$\begin{aligned} U'' + f(U) &= 0, \\ U'(0) &= U'(1) = 0. \end{aligned} \tag{3.20}$$

We will show that if U is a spatially nonuniform solution of (3.20) then U is unstable.

The linearisation of (3.19) is

$$\begin{aligned} \lambda y &= y'' + f'(U(x))y, \\ y'(0) &= y'(1) = 0. \end{aligned} \tag{3.21}$$

We realistically assume that $f'(U)$ is bounded by $K > 0$, which implies that the discrete eigenvalues λ of (3.21) must be bounded above so there must exist the largest eigenvalue, λ_0 (see [72]). We have $\lambda_0 > \lambda_1 \geq \lambda_2 ... \geq \lambda_i \geq ...$

Now consider the eigenvalue problem with fixed boundary values,

$$\begin{aligned} \mu y &= y'' + f'(U(x))y, \\ y(0) &= y(1) = 0. \end{aligned} \tag{3.22}$$

with eigenvalues $\mu_0 > \mu_1 \geq \mu_2 ...$

From (3.20) we obtain

$$\begin{aligned} U''' + f'(U)U' &= 0, \\ U'(0) &= U'(1) = 0, \end{aligned}$$

Now we notice that $z = U'(x)$ is an eigenfunction of (3.22) if $\mu = 0$.

This implies that $\mu = 0$ is an eigenvalue of (3.22). Thus, we obtain that the largest eigenvalue $\mu_0 \geq 0$.

Now, consider the two eigenvalue problems defined by (3.21) and (3.22), that is with zero flux and zero boundary conditions on y. Using the Sturm comparison principle

(see e.g. [31]) we can show that $\lambda_0 > \mu_0$. In fact, if $\lambda_0 \leq \mu_0$, then we would have $f'(U) - \mu \leq f'(U) - \lambda$. So, from the Sturm comparison principle (see e.g. [31]) we obtain that the principal eigenfunction corresponding to λ has a zero in $(0, 1)$. This is impossible since the principal eigenfunction is of one sign (see [72]). Now, since $\mu_0 \geq 0$, we obtain also $\lambda_0 > 0$. It means that the largest eigenvalue of (3.21) is positive and so w grows exponentially with time and hence $U(x)$ is linearly unstable. Thus there are no stable spatially patterned solutions of (3.2) for $m = 1$, and consequently the only stable solutions $u(x, t)$ of (3.20) are homogeneous steady states and satisfy $f(U) = 0$. ■

3.4 Turing-type patterns in reaction-diffusion systems

Diffusion-driven instability (Turing-type instability) arises in a reaction-diffusion system. It occurs when there exists a spatially homogeneous solution, which is asymptotically stable in the sense of linearised stability in the space of constant functions, but it is unstable with respect to spatially inhomogeneous perturbation.

We study the linear instabilities of the homogeneous steady state to classify the patterns, which may grow, in terms of their wavenumber.

We consider a dimensionless reaction-diffusion system with zero-flux boundary conditions of the form (3.2). For such a system, we consider a bifurcation from the homogeneous (spatially uniform) steady state by examining the response of the system to an initially small perturbation $\tilde{u}$ from the steady state $\bar{u}$, $|\tilde{u}_i| \ll 1$.

Setting

$$u = \bar{u} + \tilde{u}, \tag{3.23}$$

we linearise (3.2) in the variable $\tilde{u}$ (substituting (3.23) into (3.2), using a Taylor expansion and ignoring quadratic and higher order terms).

We obtain

$$\frac{\partial \tilde{u}}{\partial t} = D \triangle_x \tilde{u} + B\tilde{u} \tag{3.24}$$

with zero-flux boundary conditions, where B is the Jacobian matrix of the kinetics system f evaluated at the homogeneous state $\bar{u}$.

We seek solutions to the system (3.24) of the the form,

$$\tilde{u} = exp(\lambda t)\Phi(x),$$

where Φ is a vector.

Substituting into equation (3.24) we obtain

$$D\triangle_x\Phi + (B - \lambda I)\Phi = 0. \tag{3.25}$$

Eigenfunctions of the spatial eigenvalue problem (3.25) can be written as $\Phi_m = y_m\phi_m$, where y_m is a constant vector and ϕ_m are eigenfunctions of the Laplacian

$$\begin{aligned} \triangle_x\phi_m &= -{\mu_m}^2\phi_m \quad in \quad \Omega, \\ \partial_n u &= 0 \quad on \quad \partial\Omega \end{aligned}$$

and μ_m is a wavenumber associated with ϕ_m.

For nontrivial solutions of (3.25) we require

$$det(B - {\mu_m}^2 D - \lambda({\mu_m}^2)I) = 0. \tag{3.26}$$

This condition yields the dispersion relation $\lambda = \lambda({\mu_m}^2)$ which is an algebraic equation for the growth rate.

The solution of the linear stability problem is then given by

$$\tilde{u}(x,t) = \Sigma_{m=0}^{\infty} exp(\lambda({\mu_m}^2)t)y_m\phi_m(x) \tag{3.27}$$

with y_m being vectors determined by the initial data. The label m is called the mode number. For certain nonlinearities in the reaction term it can be shown that the amplitudes of growing modes are bounded by a finite value.

The linear stability of the homogeneous steady state to spatially heterogeneous perturbation of mode m is determined by the sign of the real part of $\lambda({\mu_m}^2)$ (see Theorem 3.26 about linearised stability). The steady state is stable (asymptotically) for $Re\lambda({\mu_m}^2) < 0$ for all m and unstable for $Re\lambda({\mu_m}^2) > 0$ for some m. When it is unstable a perturbing mode of appropriate wavenumber may grow. The requirement about the stability of the steady state in the absence of diffusion is equivalent to the nonexistence of growing modes for the wavenumbers with ${\mu_m}^2 = 0$. This provides conditions on the Jacobian matrix B.

There are two kinds of Turing-type patterns (depending on the imaginary part of the eigenvalue with positive real part).

• Stationary patterns, when a single eigenvalue of the Jacobian matrix B becomes positive and the bifurcating solution is a nonconstant steady state. In such case long-time solutions are stationary and spatially heterogeneous structures.

• Wave patterns [40], when 2 complex conjugate eigenvalues of B cross the imaginary axis. It is a supercritical Hopf bifurcation from a homogeneous solution to a stable periodic and nonconstant solution. The result is a pattern which oscillates in time.

The majority of theoretical studies in theory of pattern formation due to the diffusion-driven instability focus on the analysis of the systems of only 2 reaction-diffusion equations. They are activator-inhibitor systems and involve kinetics chosen in the way necessary for a diffusion-driven instability. One variable describes the density of chemical (activator) which activates its own production and the production of the other one (inhibitor) which in turns inhibits the production of activator. In a recent paper [66] the Turing's theory was extended to the systems of n reacting and diffusing chemicals.

The simplest model we consider here consists of three equations but only one with non-zero diffusion. It seems interesting to check whether in such models patterns can arise due to the diffusion-driven instability and how they depend on the initial conditions.

Models (2.1) and (2.2) are not activator-inhibitor models. We analyse the possible diffusion-driven instabilities, which can arise in both models and show the necessary restrictions regarding kinetics.

4

Receptor-based models with diffusion-driven instability for pattern formation in hydra

4.1 Three-variable model

4.1.1 Dimensionless system

First let us consider the model (2.1). We aim to find out whether in this model any patterns can evolve due to a diffusion-driven instability. We convert the model (2.1) into a dimensionless form using the following rescaling $x^* = \frac{x}{L}$, where L is a domain length and $\gamma = \frac{L^2}{d_l}$. Symbol x^* denotes the dimensionless version of x. It will be called x throughout.

We obtain

$$
\begin{aligned}
\frac{\partial}{\partial t} r_f &= -\mu_f(r_f) + p_r(r_f, r_b) - b(r_f, l) + d(r_b), \\
\frac{\partial}{\partial t} r_b &= -\mu_b(r_b) + b(r_f, l) - d(r_b), \\
\frac{\partial}{\partial t} l &= \frac{1}{\gamma}\frac{\partial^2}{\partial x^2} l - \mu_l(l) - b(r_f, l) + p_l(r_f, r_b) + d(r_b), \qquad (4.1) \\
r_f &: [0,1] \times \mathbb{R}^+ \to \mathbb{R}^+, \\
r_b &: [0,1] \times \mathbb{R}^+ \to \mathbb{R}^+, \\
l &: [0,1] \times \mathbb{R}^+ \to \mathbb{R}^+.
\end{aligned}
$$

For ligands we assume zero flux boundary conditions. All the functions used in the reaction terms are nonnegative for nonnegative arguments. The model has biological interpretation for such functions. For simplicity we use a notation

$$
\begin{aligned}
f^1 &= -\mu_f(r_f) + p_r(r_f, r_b) - b(r_f, l) + d(r_b), \\
f^2 &= -\mu_b(r_b) + b(r_f, l) - d(r_b), \\
f^3 &= -\mu_l(l) - b(r_f, l) + p_l(r_f, r_b) + d(r_b).
\end{aligned}
$$

For further analysis we consider the following functions

$$\begin{aligned} \mu_f(r_f) &= \mu_f r_f, \\ b(r_f, l) &= b r_f l, \\ d(r_b) &= d r_b, \\ \mu_b(r_b) &= \mu_b r_b, \\ \mu_l(l) &= \mu_l l. \end{aligned} \tag{4.2}$$

The proposed functions are the simplest functions usually used to describe decay or binding processes (compare models described in [60]), modelled by the law of mass action. As a simplest case scenario they seem biologically reasonable.

4.1.2 Linear stability analysis

For a dimensionless reaction-diffusion system with zero-flux boundary conditions we consider bifurcation from the steady state by examining the response of the system to an initially small perturbation from the steady value $(\bar{r}_f, \bar{r}_b, \bar{l})$. The analytical investigation proceeds by identifying a control parameter in the system (here the scaling parameter γ) which may be varied until the homogeneous steady state loses stability and bifurcates to a particular heterogeneous solution. We consider a nontrivial steady state. The trivial one is always stable and there is no bifurcation possible from the trivial steady state for any positive value of γ. Considering a bifurcation from nontrivial, nonnegative steady state is biologically reasonable. We consider our model in the parameter space, in which there exists such nontrivial steady state.

The formation of a spatial pattern is a nonlinear phenomenon. However, a good indication of the pattern in one dimension can be obtained by a simple linear analysis. We carry out a linear stability analysis to derive the conditions under which instability can arise (for details see i.e [60], [61] [72], [20]). We consider stationary solutions $\bar{r}_f \in L^\infty([0,1])$, $\bar{r}_b \in L^\infty([0,1])$, $\bar{l} \in H^2([0,1])$ of the system (4.1) and apply spectral criterion on linearised stability, i.e. Theorem 3.26 formulated in Section 3.3.2.

4.1.2.1 Notations

A is the Jacobian matrix of kinetics system of (4.1) evaluated at the spatially homogeneous state $(\bar{r}_f, \bar{r}_b, \bar{l})$.

The submatrix of A consisting of the i_1-th and i_2-th column and i_1-th and i_2-th row will be denoted $A_{i_1 i_2}$. We have

$$\begin{aligned} trA_{i_1 i_2} &= a_{i_1 i_1} + a_{i_2 i_2}, \\ |A_{i_1 i_2}| &= a_{i_1 i_1} a_{i_2 i_2} - a_{i_1 i_2} a_{i_2 i_1}, \end{aligned}$$

The tilde " ˜ " always denotes the PDE system. $\tilde{A}$ is then linearisation of the full system (4.1) at a constant solution,

$$\tilde{A}(\mu_m) = A - \frac{1}{\gamma} D {\mu_m}^2, \tag{4.3}$$

where D, the matrix of diffusion coefficients has the form

$$D = \begin{pmatrix} 0 & 0 & 0 \\ 0 & 0 & 0 \\ 0 & 0 & 1 \end{pmatrix}. \tag{4.4}$$

From the linear stability analysis we obtain the dispersion relation $\lambda = \lambda({\mu_m}^2)$ as a solution of the characteristic polynomial,

$$det(\tilde{A} - \lambda I) = 0. \tag{4.5}$$

Note that γ occurs in the system in such way that we may consider $\lambda = \lambda(\frac{{\mu_m}^2}{\gamma})$ with γ appearing nowhere explicitly. The function $\lambda({\mu_m}^2, \gamma)$ as a function of γ for different ${\mu_m}^2$ is simply scaled along the γ axis. We call $\lambda = \lambda(\frac{{\mu_m}^2}{\gamma})$ the dispersion relation throughout.

Jacobian A has the form

$$A = \begin{pmatrix} a_{11} & a_{12} & a_{13} \\ a_{21} & a_{22} & a_{23} \\ a_{31} & a_{32} & a_{33} \end{pmatrix}, \tag{4.6}$$

where

$$\begin{aligned} a_{11} &= \partial_{r_f} f^1 = -\partial_{r_f} \mu_f(\bar{r}_f) + \partial_{r_f} p_r(\bar{r}_f, \bar{r}_b) - \partial_{r_f} b(\bar{r}_f, \bar{l}), \\ a_{12} &= \partial_{r_b} f^1 = \partial_{r_b} p_r(\bar{r}_f, \bar{r}_b) + \partial_{r_b} d(\bar{r}_b), \\ a_{13} &= \partial_l f^1 = -\partial_l b(\bar{r}_f, \bar{l}), \\ a_{21} &= \partial_{r_f} f^2 = \partial_{r_f} b(\bar{r}_f, \bar{l}), \\ a_{22} &= \partial_{r_b} f^2 = -\partial_{r_b} \mu_b(\bar{r}_b) - \partial_{r_b} d(\bar{r}_b), \\ a_{23} &= \partial_l f^2 = \partial_l b(\bar{r}_f, \bar{l}), \\ a_{31} &= \partial_{r_f} f^3 = -\partial_{r_f} b(\bar{r}_f, \bar{l}) + \partial_{r_f} p_l(\bar{r}_f, \bar{r}_b), \\ a_{32} &= \partial_{r_b} f^3 = \partial_{r_b} p_l(\bar{r}_f, \bar{r}_b) + \partial_{r_b} d(\bar{r}_b), \\ a_{33} &= \partial_l f^3 = -\partial_l \mu_l(\bar{l}) - \partial_l b(\bar{r}_f, \bar{l}). \end{aligned}$$

Guided by biological interpretation we assume that all the constants in (4.2) are positive, so for all $\bar{r}_f, \bar{r}_b, \bar{l} \geq 0$ we have the following signs for some of these derivatives

$$\begin{aligned} a_{12} &> 0, \\ a_{21} &> 0, \\ a_{13} &< 0, \\ a_{22} &< 0, \\ a_{23} &> 0, \\ a_{32} &> 0, \\ a_{33} &< 0. \end{aligned} \tag{4.7}$$

Let us note that the sign of a_{11} depends on the form of p_r and the sign of a_{31} on the form of p_l. We will derive formal conditions on functions p_r and p_l that make it possible to destabilise the constant solution. Let us recall now that for the system of three linearised ODEs the characteristic polynomial has the form

$$\chi_A(\lambda) = \lambda^3 - trA\lambda^2 + \sum_{i<j} |A_{ij}|\lambda - detA = 0. \tag{4.8}$$

The Hurwitz matrix is

$$H = \begin{pmatrix} -\sigma_1 & -\sigma_3 & 0 \\ 1 & \sigma_2 & 0 \\ 0 & -\sigma_1 & -\sigma_3 \end{pmatrix} = \begin{pmatrix} -trA & -detA & 0 \\ 1 & \sum_{i<j} |A_{ij}| & 0 \\ 0 & -trA & -detA \end{pmatrix}. \tag{4.9}$$

Let $\triangle_i$ be the successive principal minors of matrix H. We have

$$\begin{aligned} \triangle_1 &= -trA = -\sigma_1, \\ \triangle_2 &= -trA(\sum_{i<j} |A_{ij}|) + detA = -\sigma_1\sigma_2 + \sigma_3, \\ \triangle_3 &= -\triangle_2 detA = -(-\sigma_1\sigma_2 + \sigma_3)\sigma_3. \end{aligned}$$

From the Routh-Hurwitz theorem [17]: The number k of roots of the real polynomial which lie in the right half-plane is given by the formula

$$k = V(1, \triangle_1) + V(\triangle_1, \triangle_3) + V(1, \triangle_2),$$

where V is the number of changes of sign of adjacent numbers in a sequence.

For the ODE system, $k = 0$, the equilibrium is asymptotically stable, if and only if all $\triangle_i > 0$.

For the full reaction-diffusion system we obtain

$$\chi_{\tilde{A}}(\lambda) = \lambda^3 - tr\tilde{A}\lambda^2 + \sum_{i<j} |\tilde{A}_{ij}|\lambda - det\tilde{A} = 0. \tag{4.10}$$

$$\begin{aligned}
\tilde{\triangle}_1 &= -trA + \frac{1}{\gamma}{\mu_m}^2 = \triangle_1 + \frac{1}{\gamma}{\mu_m}^2, \\
\tilde{\triangle}_2 &= (-trA + \frac{1}{\gamma}{\mu_m}^2)(\sum_{i<j} |A_{ij}| - trA_{12}\frac{1}{\gamma}{\mu_m}^2) + (detA - |A_{12}|\frac{1}{\gamma}{\mu_m}^2) = \\
&= -trA_{12}(\frac{1}{\gamma})^2{\mu_m}^4 + (|A_{23}| + |A_{13}| + trA_{12}trA)\frac{1}{\gamma}{\mu_m}^2 + \triangle_2, \\
\tilde{\triangle}_3 &= -\tilde{\triangle}_2 det\tilde{A} = \tilde{\triangle}_2(-detA + |A_{12}|\frac{1}{\gamma}{\mu_m}^2).
\end{aligned}$$

So for a diffusion-driven instability we require firstly that $Re\lambda({\mu_m}^2) < 0$ for ${\mu_m}^2 = 0$, that is, the uniform steady state is stable in the absence of diffusion.

We have

$$Re\lambda(\mu_m^2 = 0) < 0 \quad \equiv \quad -trA > 0, \tag{4.11}$$

$$\wedge - trA(\sum_{i<j} |A_{ij}|) + detA > 0, \tag{4.12}$$

$$\wedge - detA > 0. \tag{4.13}$$

Secondly we require that there exists a positive ${\mu_m}^2$ for which $\lambda({\mu_m}^2)$ has a positive real part. Using the Routh-Hurwitz conditions we obtain,

$$Re\lambda(\mu_m^2) > 0 \quad \equiv \quad \tilde{\triangle}_1 < 0, \tag{4.14}$$

$$\vee \quad \tilde{\triangle}_2 < 0, \tag{4.15}$$

$$\vee \quad \tilde{\triangle}_3 < 0. \tag{4.16}$$

Adding diffusive terms to the trace can only decrease the trace and therefore increase $\tilde{\triangle}_1$. Hence $\tilde{\triangle}_1$ is always positive if $\triangle_1$ is positive. We analyse the above conditions (4.11)-(4.16) and obtain that a steady state which is stable in the absence of diffusion can be destabilised due to the diffusion if and only if $|A_{12}| < 0$.

Theorem 4.1.

For the system (4.1) a steady state which is stable in the absence of diffusion (conditions (4.11)-(4.13) are fulfiled), is destabilised when diffusion is introduced if and only if $|A_{12}| < 0$.

Proof :

(*Sufficiency*)

If $|A_{12}| < 0$ then there exists $\frac{{\mu_m}^2}{\gamma} > 0$ such that

$$-det\tilde{A} = -detA + |A_{12}|\frac{1}{\gamma}{\mu_m}^2 < 0.$$

If $\tilde{\triangle}_2 > 0$ then $\tilde{\triangle}_3 < 0$ and if $\tilde{\triangle}_2 < 0$ then $\tilde{\triangle}_3 > 0$, i.e. in both cases $k = 1$.

(*Necessity*) Assume that $|A_{12}| > 0$. Then $a_{11} < 0$ ($|A_{12}| = a_{11}a_{22} - a_{12}a_{21}$) and also $trA < 0$ and $trA_{12} < 0$.

We can show that $\tilde{\triangle}_2 > 0$.

$$\tilde{\triangle}_2 = -trA_{12}(\frac{1}{\gamma})^2{\mu_m}^4 + (|A_{23}| + |A_{13}| + trA_{12}trA)\frac{1}{\gamma}{\mu_m}^2 + \triangle_2 < 0$$

only if $(|A_{23}| + |A_{13}| + trA_{12}trA) < 0$.

From this condition we obtain

$$a_{23}a_{32} > (a_{11} + a_{22})^2 + 2(a_{11} + a_{22})a_{33} - a_{13}a_{31}.$$

On the other hand if $\triangle_2 > 0$, then $\sum_{i<j} |A_{ij}| > 0$. And we obtain the following condition

$$a_{23}a_{32} < a_{11}a_{22} + a_{11}a_{33} + a_{22}a_{33} - a_{13}a_{31} - a_{12}a_{21}.$$

Combining the two above inequalities we obtain

$$a_{11}^2 + a_{22}^2 + a_{11}a_{22} + a_{11}a_{33} + a_{22}a_{33} < -a_{12}a_{21}$$

which cannot be verified considering inequalities in (4.7) and the fact that $a_{11} < 0$.

If $|A_{12}| > 0$ then also $\tilde{\triangle}_3 > 0$ for every μ_m.

So for $|A_{12}| > 0$, $\tilde{\triangle}_i > 0$, $i = 1, 2, 3$ and the destabilisation of the steady state is impossible. This concludes the proof. ■

Now we can formulate necessary and sufficient conditions for Turing-type patterns in the three-variable model with one diffusion operator in third equation

$$-trA > 0, \tag{4.17}$$

$$-trA(\sum_{i<j} |A_{ij}|) + detA > 0, \tag{4.18}$$

$$-detA > 0, \tag{4.19}$$

$$|A_{12}| < 0. \tag{4.20}$$

Analysing these conditions we can show how they determine production functions.

Theorem 4.2.
There is a diffusion-driven instability for the system (4.1) only if

$$p_r(\bar{r}_f, \bar{r}_b) < \bar{r}_f \frac{\partial}{\partial r_f} p_r(\bar{r}_f, \bar{r}_b).$$

Proof : It follows directly from the calculation of $|A_{12}|$ using (4.2) and steady states equations. We obtain

$$|A_{12}| = (d + \mu_b)(\frac{p_r}{\bar{r}_f} - \frac{\partial}{\partial r_f} p_r).$$

From Theorem 4.1 $|A_{12}| < 0$ is a necessary condition for the diffusion-driven instability for the system (4.1). Hence

$$|A_{12}| = (d + \mu_b)(\frac{p_r}{\bar{r}_f} - \frac{\partial}{\partial r_f} p_r) < 0$$

is a condition for the diffusion-driven instability. ■

Conclusion 4.3. For the Turing-type instability, the function describing *de novo* production of free receptors must depend on the density of free receptors and this dependence must be a power function of the order $\alpha + 1$, where $\alpha > 0$.

Hence Turing-type patterns can occur if

$$p_r(r_f) = m_1 {r_f}^{\alpha+1}, \quad \alpha > 0.$$

This function can depend also on the density of bound receptors, but it is crucial here that it depends on the density of free receptors. For the numerical simulations we use the simplest function fulfiling the above condition, namely $p_r(r_f) = m_1 {r_f}^2$.

To model the production rate of ligands p_l we also take a function of the concentration of free receptors.

In numerical simulations we use a function similar to p_r

$$p_l(r_f) = m_2 {r_f}^2.$$

Remark 4.4. It appears that model (4.1) cannot exhibit a wave bifurcation.

We can show that

Lemma 4.5.
For the wave bifurcation to arise in system (4.1) we need:

$$\sum_{i<j} |A_{ij}| - trA_{12} \frac{detA}{|A_{12}|} < 0 \tag{4.21}$$

Proof : For a wave bifurcation we need that $k = 2$. So, from Routh-Hurwitz theorem we need: $\tilde{\triangle}_1 > 0$, $\tilde{\triangle}_2 < 0$ and $\tilde{\triangle}_3 > 0$, while $\tilde{\triangle}_1,\ \tilde{\triangle}_2,\ \tilde{\triangle}_3 > 0$,

This is equivalent to: $\tilde{\triangle}_2 < 0$ and $-det\tilde{A} > 0$. From Theorem (4.1) we have $|A_{12}| < 0$. If $-trA_{12} > 0$ then $\tilde{\triangle}_2 > 0$ for every $\frac{{\mu_m}^2}{\gamma}$. So for a wave bifurcation we need $-trA_{12} < 0$. Since $\tilde{\triangle}_2 < 0$, we have $\tilde{\triangle}_3 < 0$ if and only if $-det\tilde{A} > 0$, which is possible if and only if $\tilde{\triangle}_2 < 0$ for $\frac{{\mu_m}^2}{\gamma} = \frac{detA}{|A_{12}|}$.

Hence after some algebraic calculations we obtain the condition (4.21). ■

Under condition (4.19), i.e. $-detA > 0$, no parameter values were found for which (4.21) could be satisfied in system (4.1).

4.1.3 Discussion of pattern selection

The mechanism of pattern selection, by which one mode is chosen to grow to heterogeneous steady state from many admissible modes, is an important issue. The dispersion relation, algebraic equation for the growth rate, indicates which modes can grow to determine the final long term pattern. All wavenumbers in the region where $Re\lambda({\mu_m}^2) > 0$ are linearly unstable. The best-known dispersion relation (i.e. known from activator-inhibitor system) determines the bounded range of unstable modes the size of which depends on the bifurcation parameter γ. Then a certain range of γ can be determined for which there exists only one unstable mode. This feature of the Turing-type systems is usually used in the applications [60], [61]. It allows to select (changing the scaling parameter γ) the mode which grows to the long-term heterogeneous pattern. If the range of unstable modes is finite but includes more values then there is a competition between patterning modes. Murray [61] suggests that the mechanism of initiation of pattern formation may determine the mode selected.

Let us have a closer look at the dispersion relation, which we obtain for the model (4.1). From the proof of Theorem 4.1 we observe that the destabilisation of the homogeneous steady state is possible if and only if

$$det\tilde{A} = detA - |A_{12}|\frac{{\mu_m}^2}{\gamma} > 0. \tag{4.22}$$

Fig. 4.1 shows $det\tilde{A}$ as a function of $\frac{{\mu_m}^2}{\gamma}$.

We can see that for every γ there exist infinitely many different integer μ_m for which inequality (4.22) is fulfiled. It means that there is an infinite range of unstable modes.

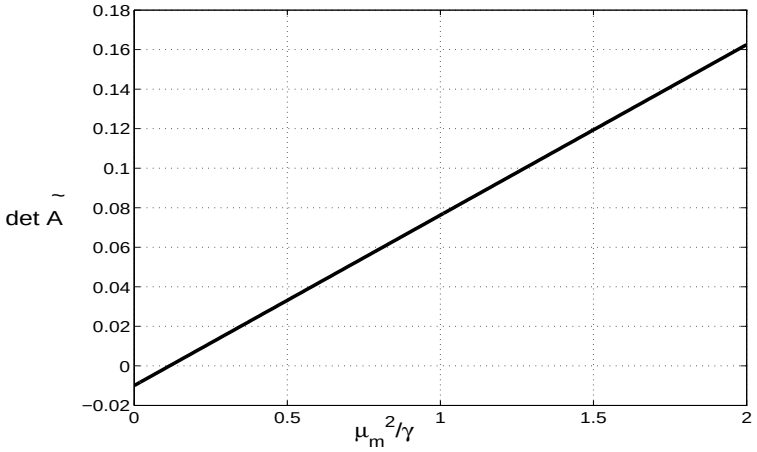

Figure 4.1. $det\tilde{A}$ as a function of $\frac{{\mu_m}^2}{\gamma}$ for three-variable model (4.1). It shows that condition $det\tilde{A} > 0$ (4.22) for the destabilisation of the homogeneous steady state is fulfiled for infinitely many wavenumbers ${\mu_m}^2$. The values of Jacobian matrix A are calculated for the parameters for which the conditions (4.17)-(4.20) are satisfied ($m_1 = 1.466$, $m_2 = 2$, $\mu_f = 0.2$, $\mu_b = 0.02$, $d = 0.02672$, $b = 0.7$, $\mu_l = 0.2$). The value of the smallest integer μ_m for which $det\tilde{A} > 0$ depends on γ.

The dispersion relation $\lambda = \lambda(\frac{{\mu_m}^2}{\gamma})$ is showed in Fig. 4.2. It is fundamentally different than the typical (so called 'vanilla') dispersion relation, obtained among other in activator-inhibitor models (compare [60]).

Asymptotic analysis for the systems with such dispersion relation is still lacking.

In the model with such dispersion relation we cannot select a single unstable mode. There even does not exist a wavenumber with maximal $Re(\lambda)$. $Re(\lambda)$ grows monotonously with $\frac{{\mu_m}^2}{\gamma}$. However, we can show that $Re(\lambda)$ is bounded from above. From the dispersion relation we cannot decide which eigenfunctions, that is, which spatial patterns, are linearly unstable and grow with time. We could conjecture that the number of growing mode depends on initial conditions as it is also suggested by Murray [60] and [61].

However, simulations show that for a given domain size (given scaling parameter γ), the ultimate spatial structure depends on the initial data (initial perturbation) but only with regard to the place of peak formation (see the results of simulations shown in Fig. 4.5). The wavenumber of the growing pattern does not depend on the initial data. It seems that the solution which survives is related to the minimum possible wavenumber admitted by the dispersion relation, i.e., that the wavenumber which determines the final pattern corresponds to the smallest possible $Re(\lambda)$.

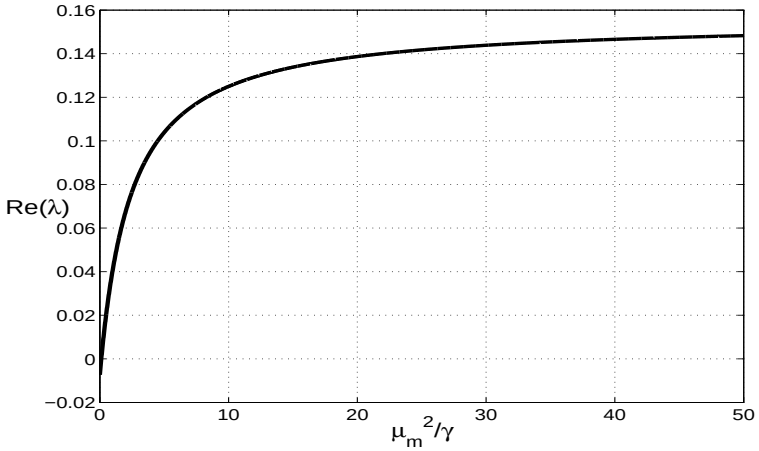

Figure 4.2. Dispersion relation $\lambda = \lambda(\frac{{\mu_m}^2}{\gamma})$ for the model (4.1) with parameters as in Fig. 4. Real part of linear growth rate λ plotted as a function of $\frac{{\mu_m}^2}{\gamma}$. It shows that for a given γ there exists an infinite range of unstable modes, i.e. $Re(\lambda) > 0$ for infinitely many ${\mu_m}^2$. A single unstable mode cannot be selected.

We perform simulations for different initial conditions and they always lead to the same number of peaks which, however, are situated in different positions. By changing γ we can change the position of the peak and for γ big enough also the number of the peaks (Fig. 4.4b). It means that for a problem of a given scale (given the domain size and diffusion coefficient) a specific number of pattern units (peaks) is reliably reproduced.

4.1.4 Numerical investigations

For the model (4.1) we found the stable steady state $\bar{r}_f, \bar{r}_b, \bar{l}$ with the help of the computer algebra program MAPLE. The diagrams (4.3) show the dependence of equilibrium of kinetics system on the production coefficient m_1. For $m_1 < 1.465$ there is only one steady state $(0, 0, 0)$. So our model makes sense only for the $m_1 \geq 1.465$. For such m_1 there are 2 nontrivial steady states: one, which is always unstable and one, which satisfies conditions (4.17)-(4.20). Further numerical values used do not represent a systematic review of the parameter space. This requires a separate exhaustive study. Rather, it is our purpose to establish, numerically, the capabilities of the models to display the desired types of behaviour (see Discussion).

We carry out simulations for the following set of parameters:

$$m_1 = 1.466, \quad m_2 = 2, \quad \mu_f = 0.2, \quad \mu_b = 0.02, \quad d = 0.02672, \quad b = 0.7, \quad \mu_l = 0.2.$$

The equilibrium point ($\bar{r}_f = 1.259,\ \bar{r}_b = 103.642,\ \bar{l} = 5.493$) satisfies conditions (4.17)-(4.20). The discretised system of ODEs is numerically solved using the CVODE package and numerical estimates of the Jacobian matrix. Space discretisation is a gridpoint on a unit interval. Time discretisation is performed implicitly. Homogeneous Neumann boundary conditions (zero flux) are implemented as a reflection at the boundary. Simulations are in agreement with the analysis and show that one-dimensional spatially uniform initial data evolve into a spatially inhomogeneous pattern, which is stationary in time. Simulations are performed for different initial values of the perturbation and different scaling parameter γ. Let us remind that $\gamma = \frac{L^2}{d_l}$ and the model (4.1) is nondimensionalised and defined on the interval $[0, 1]$ with diffusion coefficient $d_l = 1$. It means that an increasing γ corresponds to the increase of a domain size or decrease of diffusion coefficient of the initial problem (2.1).

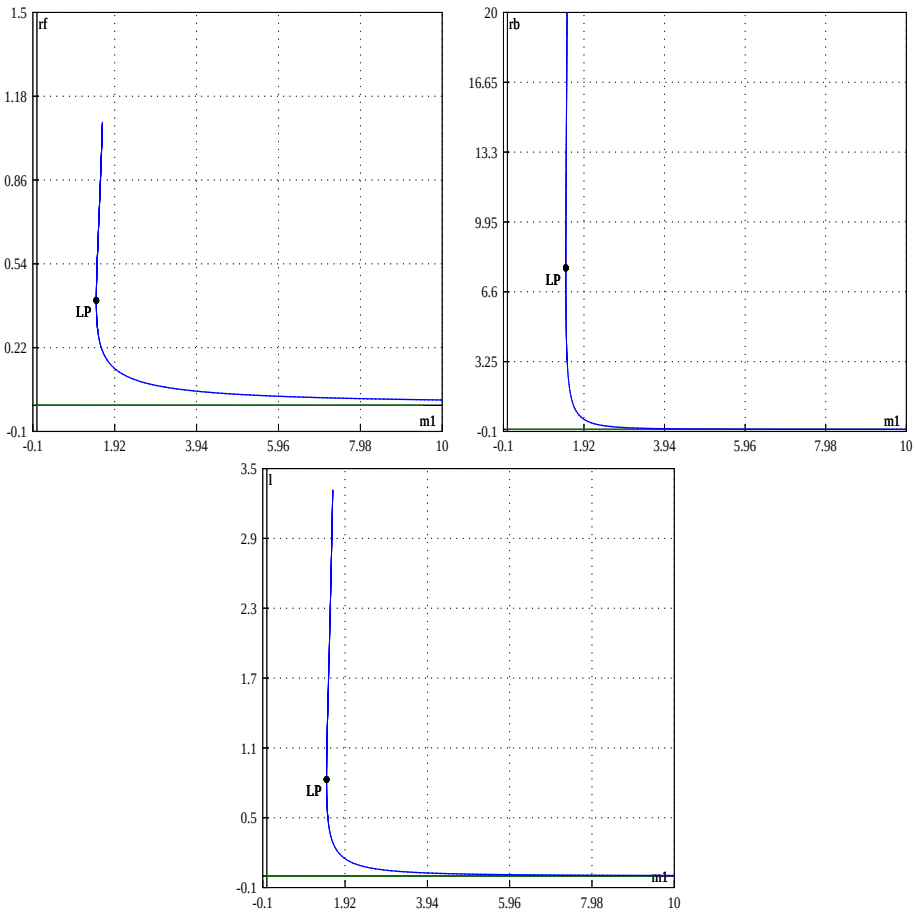

Figure 4.3. Bifurcation diagrams for the steady states of r_f, r_b and l. We plot the steady states of the system (4.1) as functions of the parameter m_1. The other parameters: $m_2 = 2$, $\mu_f = 0.2$, $\mu_b = 0.02$, $d = 0.02672$, $b = 0.7$, $\mu_l = 0.2$.

Simulations show that (compare with the discussion in Section 4.1.3):

• The number of peaks in the final pattern depends on the domain size but not on the initial perturbation. For γ small enough (which can be calculated from the dispersion relation) the final pattern consists of only one "hump" as shown in Figs. 4.4a and 4.5.

Figs. 4.4a and 4.5 depict the space profile of the solution after a long time. The profile is stationary in time. The scaling parameter $\gamma = 1$.

• When γ is growing, new peaks appear (the number of peaks always increases by one). Fig. 4.4b shows the space profile after a long time for the parameter $\gamma = 60$.

• If the parameter γ is small enough, the final solution strongly resembles initial condition. This behaviour is not implied by the dispersion relation.

• Even for a given γ the location of the peak strongly depends on initial condition. It is illustrated by Fig. 4.5. The figures show that the peak is formed at the coordinate of the largest gradient in initial function. For a symmetric initial perturbation at first two peaks are formed but finally only one of them persists.

In summary, we showed that for the simplest receptor-based model consisting of 3 equations, Turing-type patterns can arise only if there is a self-enhancement (autocatalysis) of free receptors. The final pattern strongly depends on the initial perturbation.

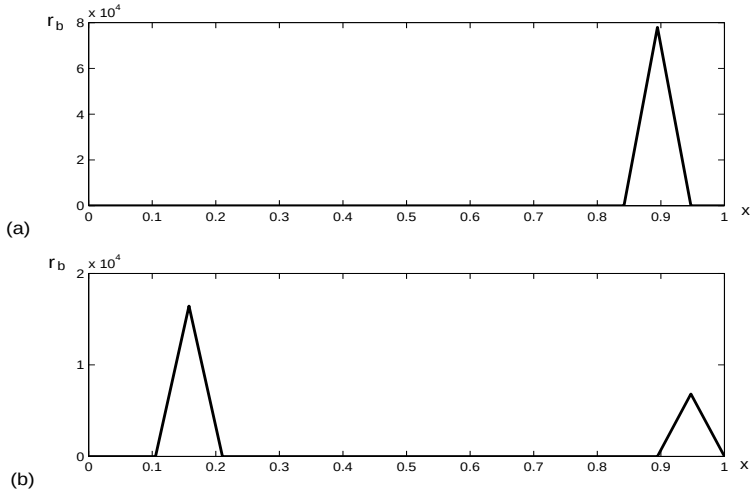

Figure 4.4. (a) Spatial profile of solution r_b of the model (4.1) after a long time. Simulations are performed for parameters: $m_1 = 1.466$, $m_2 = 2$, $\mu_f = 0.2$, $\mu_b = 0.02$, $d = 0.02672$, $b = 0.7$, $\mu_l = 0.2$ and $\gamma = 1$. In the density bound receptors we observe formation of a single peak (spike solution). (b) Spatial profile of r_b for the scaling parameter $\gamma = 60$ and the other parameters as above. We observe formation of two peaks.

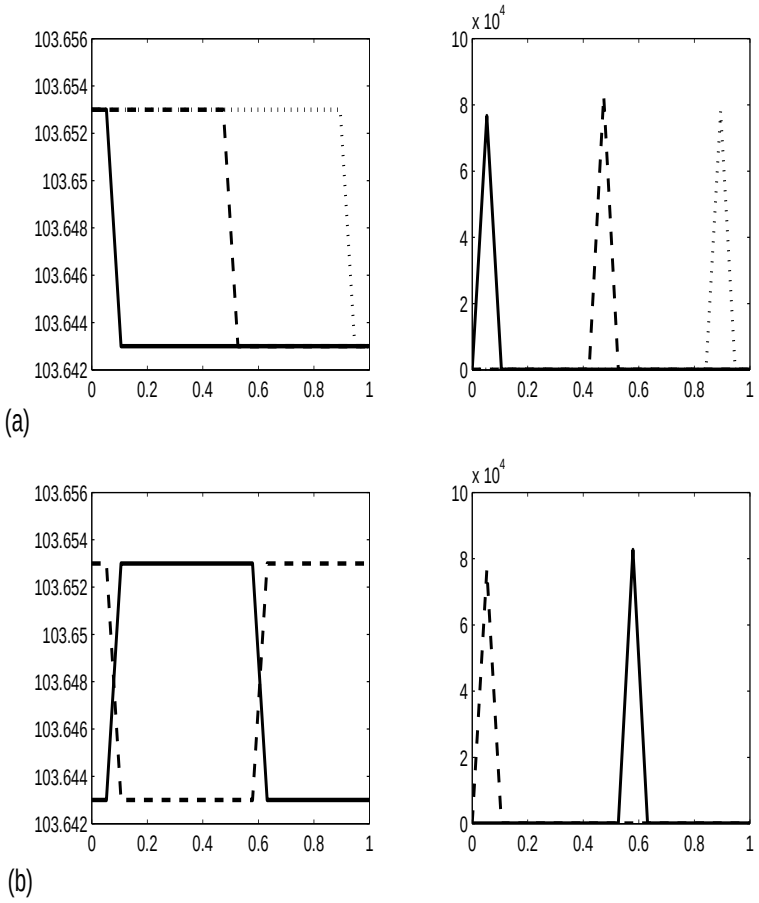

Figure 4.5. Spatial profile of r_b for different initial perturbations and $\gamma = 1$ and the other parameters as in Fig. 6. On the left hand-side we present the initial condition and on the right-hand side the final pattern originating from such initial condition. The perturbation in initial data is of order 10^{-2} (it can be arbitrarily small) while the final peak is of height 8×10^4. We observe that the number of the peaks in the final pattern does not depend on initial perturbation of the homogeneous steady state. (a) Different initial conditions and corresponding solutions depicted using matching line styles. The location of the peak strongly depends on the initial condition. The peak is formed at the coordinate of the largest gradient in the initial function. (b) The results for the initial conditions with two maxima or two minima - the result is always one peak (depicted using matching line styles).

4.2 Four-variable model

4.2.1 Invariant sets and existence of solutions

Now we analyse the model defined by equation system (2.2). We convert the system into a dimensionless form in a manner similar as for the three-variable model. We use rescaling $x^* = \frac{x}{L}$, where L is the domain length, $\gamma = \frac{L^2}{d_l}$ and $d_2 = \frac{d_e}{d_l}$ and obtain the system

$$\begin{aligned}
\frac{\partial}{\partial t} r_f &= -\mu_f(r_f) + p_r(r_f, r_b) - b(r_f, l) + d(r_b), \\
\frac{\partial}{\partial t} r_b &= -\mu_b(r_b) + b(r_f, l) - d(r_b), \\
\frac{\partial}{\partial t} l &= \frac{1}{\gamma}\frac{\partial^2}{\partial x^2} l - \mu_l(l) - b(r_f, l) + p_l(r_f, r_b) + d(r_b) - b_e(l, e), \\
\frac{\partial}{\partial t} e &= \frac{d_2}{\gamma}\frac{\partial^2}{\partial x^2} e - \mu_e(e) + p_e(r_b, l).
\end{aligned} \tag{4.23}$$

We show the global existence and uniqueness of solutions to the four-variable model of hydra (4.23) with initial conditions,

$$\begin{aligned}
r_f(0, x) &= r_{f0}(x), \\
r_b(0, x) &= r_{b0}(x), \\
l(0, x) &= l_0(x), \\
e(0, x) &= e_0(x)
\end{aligned} \tag{4.24}$$

and boundary conditions,

$$\begin{aligned}
\frac{\partial l}{\partial x}|_{x=0,1} &= 0, \\
\frac{\partial e}{\partial x}|_{x=0,1} &= 0.
\end{aligned} \tag{4.25}$$

First we consider production functions defined in (4.44), i.e.

$$\begin{aligned}
p_r &= m_1 \frac{r_b}{1 + r_b}, \\
p_l &= m_2 \frac{r_b}{1 + r_b}, \\
p_e &= m_3 \frac{r_b}{1 + r_b}.
\end{aligned}$$

Now $u = [r_f, r_b, l, e]^T$ and $f(u) = [-\mu_f r_f + p_r(r_b) - br_f l + dr_b, -\mu_b r_b + br_f l - dr_b, -\mu_l l + p_l(r_b) - br_f l + dr_b - b_e el, -\mu_e e + p_e(r_b)]^T$.

Note that $f : R^4 \to R^4$ is Lipschitz continuous on R^4. Solution on $\bar{\Omega}_T = [0,1] \times [0,T]$ for any $T > 0$ is a function $u : \Omega_T \to R^4$ which is continuous in $\bar{\Omega}_T$ and suitably differentiable in $\Omega_T = [0,1] \times (0,T]$. In addition $u = [r_f, r_b, l, e]^T$ must satisfy conditions (4.24) and (4.25)

We introduce the set

$$\Sigma = \{(r_f, r_b, l, e) : 0 \le r_f \le a_f, 0 \le r_b \le a_b, 0 \le l \le a_l, 0 \le e \le a_e\}. \tag{4.26}$$

Then we show that the vector field generated by $f(u)$ ($V = [-\mu_f r_f + p_r(r_b) - br_f l + dr_b, -\mu_b r_b + br_f l - dr_b, -\mu_l l + p_l(r_b) - br_f l + dr_b - b_e el, -\mu_e e + p_e(r_b)]$) does not point out of Σ (Σ is invariant for the four-variable system).

Theorem 4.6.
Let $(r_f(x,t), r_b(x,t), l(x,t), e(x,t))$ be a solution to (4.23) on Ω_T (for any $T \ge 0$. Then there exist a bounded invariant rectangle $\Sigma = \{(r_f, r_b, l, e) : 0 \le r_f \le a_f, 0 \le r_b \le a_b, 0 \le l \le a_l, 0 \le e \le a_e\}$ on Ω_T.

Proof: First we show that all the solutions are nonnegative for the nonnegative initial conditions. Then we show that the solutions for $r_f + r_b$ and $r_b + l$ and e are bounded from above. Hence we can conclude that the solutions for r_f, r_b and l are also bounded and there exist the invariant bounded rectangle for the model (4.23).

The first claim is that $\Sigma_0 = \{(r_f, r_b, l, e) : r_f, r_b, l, e \ge 0\}$ is an invariant set. To see it we apply Theorem (3.16).

We set $G = -r_f$ (note that $(-1, 0, 0, 0)$ is a left eigenvector of D).

$\nabla G(V)|_{r_f=0} = -(p_r + dr_b) \le 0$ in Σ, so $r_f \ge 0$.

If $G = -r_b$ then $\nabla G(V)|_{r_b=0} = -br_f l < 0$ in Σ. Hence $r_b \ge 0$.

If $G = -l$ then $\nabla G(V)|_{l=0} = -dr_b - p_l < 0$ in Σ. Hence $l \ge 0$.

If $G = -e$ then $\nabla G(V)|_{e=0} = -p_e < 0$ in Σ. Hence $e \ge 0$.

Thus, we obtain that all the solutions of model (4.23) are nonnegative for nonnegative initial conditions.

To show that the solutions are bounded from above we add two first equations and obtain,

$$\frac{\partial(r_f + r_b)}{\partial t} = p_r(r_b) - \mu_f r_f - \mu_b r_b. \tag{4.27}$$

Let us calculate it in $r_f + r_b = a_1$. Since $p_r = \frac{m1 r_b}{1+r_b} < m_1$ for every r_b, we obtain $p_r(r_b) - \mu_f r_f - \mu_b r_b < m_1 - min(\mu_f, \mu_b)a_1 \leq 0$ for every $r_f, r_b, l, e \in \Sigma$ if $a_1 > m_1/min(\mu_f, \mu_b)$.

Thus, we obtain that $r_f + r_b \leq a_1$. Since $r_f \geq 0$ and $r_b \geq 0$, we can conclude that both r_f and r_b are bounded from above, $r_f \leq a_f$ and $r_b \leq a_b$.

If $G(r_f, r_b, l, e) = e - a_e$ then $\nabla G(V)|_{e=a_e} = p_e - \mu_e a_e < m_3 - \mu_e a_e \leq 0$ for $a_e \geq \frac{m_3}{\mu_e}$ (since $p_e = \frac{m_3 r_b}{1+r_b}$) Hence $e \leq a_e$.

If $G(r_f, r_b, l, e) = l - a_l$ then $\nabla G(V)|_{l=a_l} = p_l - br_f l - \mu_l l - b_e le + dr_b \leq m_2 + dr_b - \mu_l a_l$ for every $r_f, r_b, l, e \in \Sigma$, because $p_l = \frac{m2 r_b}{1+r_b}$ and e and r_f are nonnegative. Now since r_b is bounded from above by a_b, we can choose $a_l \geq \frac{m_2 + da_b}{\mu_l}$.

Then $\nabla G(V)|_{l=a_l} \leq 0$ and hence $l \leq a_l$. ■

The existence of solutions for all $t > 0$ comes from the Theorem 3.12 and the Corollary 3.14. Uniqueness then follows from Theorem 3.19.

To show the existence of solutions of model (4.23) with the production functions (4.45),

$$\begin{aligned} p_r &= m_1 \frac{r_b}{1 + r_b}, \\ p_l &= m_2 {r_b}^2, \\ p_e &= m_3 \frac{l}{1 + l}. \end{aligned}$$

we use the same methods and notice that, if r_b is bounded from above by a_b, then $p_l = m_2 {r_b}^2$ is also bounded from above and we can choose a_l such that $p_l - br_f l - \mu_l l - b_e le + dr_b \leq 0$ in Σ.

We obtained the nonnegativity of solutions which is important for biological applications of the model.

Conclusion 4.7. For the nonnegative initial data the solutions of the system (4.23) stay nonnegative.

4.2.2 Conditions for diffusion-driven instability

For the system (4.23) we also perform linear stability analysis and consider the characteristic polynomial

$$\chi_A(\lambda) = \lambda^4 - trA\lambda^3 + \sum_{i<j} |A_{ij}|\lambda^2 - \sum_{i<j<k} |A_{ijk}|\lambda + detA,$$

where $|A_{ijk}|$ is a determinant of submatrix A_{ijk}. A_{ijk} is a submatrix of A consisting of the i-th, j-th and k-th column and i-th, j-th and k-th row.

The Hurwitz matrix has the form

$$H = \begin{pmatrix} -\sigma_1 & -\sigma_3 & 0 & 0 \\ 1 & \sigma_2 & \sigma_4 & 0 \\ 0 & -\sigma_1 & -\sigma_3 & 0 \\ 0 & 1 & \sigma_2 & \sigma_4 \end{pmatrix},$$

where

$$\begin{aligned} -\sigma_1 &= -trA, \\ \sigma_2 &= \sum_{i<j} |A_{ij}|, \\ -\sigma_3 &= -\sum_{i<j<k} |A_{ijk}|, \\ \sigma_4 &= detA. \end{aligned}$$

We have

$$\begin{aligned} \triangle_1 &= -\sigma_1 = -trA, \\ \triangle_2 &= -\sigma_1\sigma_2 + \sigma_3, \\ \triangle_3 &= \triangle_2(-\sigma_3) - \sigma_4{\sigma_1}^2 = \\ &= \sigma_1(\sigma_2\sigma_3 - \sigma_1\sigma_4) - {\sigma_3}^2, \\ \triangle_4 &= \triangle_3\sigma_4. \end{aligned}$$

From the Routh-Hurwitz theorem [17] we obtain that

$$k = V(1, \triangle_1) + V(\triangle_1, \triangle_3) + V(1, \triangle_2) + V(\triangle_2, \triangle_4).$$

For the full reaction-diffusion system we have

$$(4.28)\text{–}\tilde{\sigma_1} = -tr\tilde{A} = -trA + \frac{{\mu_m}^2}{\gamma}(1 + d_2),$$

$$(4.29)\ \tilde{\sigma}_2 = \sum_{i<j} |\tilde{A}_{ij}| = \sum_{i<j} |A_{ij}| - \frac{{\mu_m}^2}{\gamma}[trA_{12}(1 + d_2) + a_{33}d_2 + a_{44}] + \frac{{\mu_m}^4}{\gamma^2}d_2,$$

$$(4.30)\text{–}\tilde{\sigma}_3 = -\sum_{i<j<k} |\tilde{A}_{ijk}| = -\sum_{i<j<k} |A_{ijk}| + \frac{{\mu_m}^2}{\gamma}[(|A_{12}| + |A_{13}| + |A_{23}|)d_2$$

$$(4.31)\qquad +|A_{12}| + a_{44}trA_{12}] - \frac{{\mu_m}^4}{\gamma^2}trA_{12}d_2,$$

$$(4.32)\ \tilde{\sigma_4} = det\tilde{A} = detA + \frac{{\mu_m}^2}{\gamma}(-|A_{12}|a_{44} - d_2|A_{123}|)$$

$$(4.33)\qquad +\frac{{\mu_m}^4}{\gamma^2}d_2|A_{12}|.$$

From the Routh-Hurwitz theorem we obtain necessary and sufficient conditions for a diffusion-driven instability of the system (4.23),

$$(4.34)\qquad \triangle_1 > 0,$$

$$(4.35)\qquad \triangle_2 > 0,$$

$$(4.36)\qquad \triangle_3 > 0,$$

$$(4.37)\qquad \triangle_4 > 0.$$

$$(4.38)\qquad \textit{There exist integers } \mu_m \textit{ and } i \textit{ such that } \tilde{\triangle}_i < 0.$$

Conditions (4.34)-(4.37) guarantee a stable constant equilibrium of the kinetic system, while condition (4.38) is necessary for the spatial pattern to grow.

Now we assume that the production of free receptors depends only on the density of bound receptors so that $a_{11} < 0$ (now $a_{ii} < 0$ for every i.) It follows from the requirement of no self-enhancement of free receptors.

Remark 4.8. In the model with self-enhancement of free receptors we obtain patterns similar to those in the three-variable model previously considered (see discussion in Section 4.2.4).

Now we can formulate the conditions for pattern formation in model (4.23).

Theorem 4.9.

Necessary and sufficient conditions for diffusion-driven pattern formation in model (4.23) are

$$-trA > 0, \tag{4.39}$$

$$\sum_{i<j} |A_{ij}| > 0, \tag{4.40}$$

$$-\sum_{i<j<k} |A_{ijk}| > 0, \tag{4.41}$$

$$detA > 0. \tag{4.42}$$

$$\text{There exists } \frac{{\mu_m}^2}{\gamma} \text{ such that } det\tilde{A} < 0. \tag{4.43}$$

Proof : Conditions (4.39)-(4.42) guarantee that the steady state $(\bar{r}_f, \bar{r}_b, \bar{l}, \bar{e})$ is stable in the absence of diffusion (i.e. for the spatially homogeneous perturbation).

We show that the above conditions are equivalent to conditions (4.34)-(4.38).

(4.39) follows directly from (4.34). (4.42) follows from (4.36) and (4.37), which is satisfied if and only if $detA > 0$.

$\triangle_4 > 0$ and $\triangle_3 > 0$ if and only if $-\sigma_3 > 0$ and we obtain the condition (4.41). Since $-\sigma_3 > 0$ then $\triangle_2 > 0$ if and only if $\sigma_2 > 0$ what is equivalent to the condition (4.40).

Now we analyse the condition (4.38). We can show that it is fulfiled if and only if $det\tilde{A} < 0$. Analogically as in the three-variable model, $\tilde{\triangle}_1 > 0$ if $\triangle_1 > 0$. It is easy to check that if $\sigma_2 > 0$ then also $\tilde{\sigma}_2 > \sigma_2 > 0$. And analysing the formula for $\tilde{\triangle}_2$ we can show that in every point $\frac{{\mu_m}^2}{\gamma}$ $\tilde{\triangle}_2 > \triangle_2$. Then $\tilde{\triangle}_2$ stays positive. So only $\tilde{\triangle}_3$ or $\tilde{\triangle}_4$ can change the sign.

$\tilde{\sigma}_4 < 0$ guarantees that $\tilde{\triangle}_4 < 0$ or $\tilde{\triangle}_3 < 0$. It means that $k = 1$ and we have a stationary pattern. $\tilde{\sigma}_4 < 0$ is equivalent to $det\tilde{A} < 0$ and we obtain condition (4.43). Analysing the formula (4.31) and (4.33) we notice that $\tilde{\sigma}_3$ cannot change sign unless $\tilde{\sigma}_4$ does not. $-\tilde{\sigma}_3 < 0$ only if $|A_{23}| < 0$ what is possible only for the special choice of function p_l and then also $\tilde{\sigma}_4 < 0$. It means that condition (4.43) is also necessary for diffusion-driven instability in model (4.23). ■

The last condition guarantees that a spatially homogeneous steady state is unstable for a spatially heterogeneous perturbation if γ is such that $det\tilde{A} < 0$ for some integer μ_m. Analysing the formula (4.33) we see that $det\tilde{A} < 0$ is possible only if $|A_{123}| > 0$ or

$|A_{12}| < 0$. The last condition is fulfiled if and only if $p_r(\bar{r}_b) < \bar{r}_b \frac{\partial}{\partial r_b} p_r(, \bar{r}_b)$. In numerical simulations we consider kinetics for which this condition is not fulfiled (see (4.44) and (4.45)). Then the necessary condition is $|A_{123}| > 0$.

The dependence of $\tilde{\sigma_4} = det\tilde{A}$ on $\frac{{\mu_m}^2}{\gamma}$ is shown in Fig. 4.6.

We can see that $det\tilde{A}$ changes sign in some interval of $\frac{{\mu_m}^2}{\gamma}$ and for every γ we have a finite range of unstable modes which can grow. We can isolate a specific mode to be excited by choosing γ (for details see [40]). For hydra modelling we select ${\mu_m}^2 = 1$ to be driven unstable. In this way we obtain a gradient-like solution.

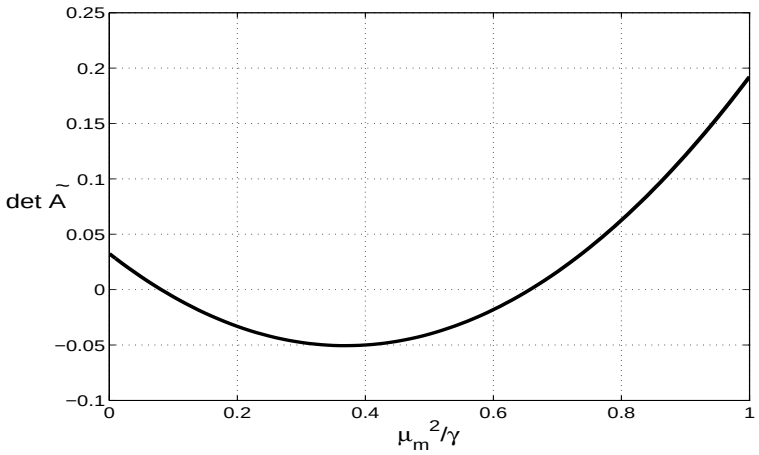

Figure 4.6. $det\tilde{A}$ as a function of $\frac{{\mu_m}^2}{\gamma}$ calculated for the four-variable model (4.23). The figure illustrates that for a certain range of γ the single mode (equal 1) can be selected that becomes unstable.

4.2.3 Numerical results

4.2.3.1 Pattern formation from a randomly perturbed homogeneous steady state

We assumed that functions describing production of free receptors and production of ligands depend on the density of bound receptors. It means that there is no self-enhancement of free receptors. In fact the model cannot be simplified to one with autocatalysis of free receptors without assuming that the changes in the density of bound receptors are much faster than the other processes what would be highly unrealistic. We consider two different cases of model (4.23).

(1) We assume, in addition, that the function describing the production of enzyme (p_e) depends on the density of bound receptors. It seems to be biologically reasonable that all the *de novo* productions are regulated by bound receptors which give the signal to the cells. Consequently we assume that the production functions have the following form

$$\begin{aligned} p_r &= m_1 \frac{r_b}{1+r_b}, \\ p_l &= m_2 \frac{r_b}{1+r_b}, \\ p_e &= m_3 \frac{r_b}{1+r_b}. \end{aligned} \tag{4.44}$$

(2) It is also possible that the production of enzyme depends on the density of ligands. It could be regulated via some other receptors not considered in our model. Thus we assume that the production of enzyme depends on the density of ligands and is a Michaelis-Menten function. We can consider the following production functions

$$\begin{aligned} p_r &= m_1 \frac{r_b}{1+r_b}, \\ p_l &= m_2 {r_b}^2, \\ p_e &= m_3 \frac{l}{1+l}. \end{aligned} \tag{4.45}$$

In both cases functions describing decay, binding and dissociation have the form as in the three-variable model (see (4.2)), also $\mu_e(e) = \mu_e e$, $b_e(l,e) = b_e l e$.

In fact, the particular form of p_e (whether it is a function of r_b or l) has no influence on our previous analysis. In both cases we find the parameter space and nontrivial homogeneous steady state for which the conditions (4.39)-(4.43) are fulfiled (see bifurcation diagrams in Fig. 4.7).

Similarly as previously, further particular numerical values are chosen to establish, numerically, the capabilities of the model to display the desired types of behaviour.

In case (1) we perform simulations for the following parameters:

$$\begin{gathered} m_1 = 0.93, \quad m_2 = 3, \quad m_3 = 1.2, \\ \mu_f = 0.2, \quad \mu_b = 0.3, \quad \mu_l = 0.1, \quad \mu_e = 0.1, \\ d = 0.9, \quad b = 2.0, \quad b_e = 0.7. \end{gathered}$$

and homogeneous steady state: $\bar{r}_f = 0.787$, $\bar{r}_b = 1.095$, $\bar{l} = 0.834$, $\bar{e} = 5.458$.

In case (2) we perform simulations for the same parameters as before, only m_1 is changed and equal 1.0. Homogeneous steady state: $\bar{r}_f = 0.842$, $\bar{r}_b = 0.413$, $\bar{l} = 0.294$, $\bar{e} = 3.513$.

The diagrams (4.7) show the dependence of the equilibrium of kinetics system on the production coefficient m_1. Similarly as in the three-variable model there exists such value $m_1{}^*$ that for $m_1 < m_1{}^*$ there is only one steady state (0,0,0,0), while for $m_1 > m_1{}^*$ there are two additional steady states: one, which is always unstable and one, which satisfies conditions for diffusion-driven instability (4.39)-(4.43).

Simulations show that in both cases one-dimensional spatially uniform initial data evolves into a gradient pattern (we do not distinguish between the two polarities). The model turns out to be robust against changes in the initial conditions. It means that the final pattern does no depend on the way we perturbed initially the homogeneous steady state. Different spatially nonuniform perturbations lead to the same final pattern. We perform simulations for the random initial perturbation, i.e. the initial value in every discretisation point is the value of the spatially uniform steady state perturbed by a small value which is randomly generated.

The results for both cases are shown in parallel in the Fig. 4.8. On the left-hand side - the plots for the case (1), on the right-hand side for the case (2).

The formation of the gradient pattern depends only on the scaling parameter γ which means on the domain size and diffusion coefficient of the original problem. It is the intrinsic property of Turing-type mechanism that the complexity of pattern depends on the scaling parameters. The question is only how large is the space of parameter γ such that a gradient like solution can be obtained. In our model, γ can be changed even 2 orders of magnitude without changing the complexity of the pattern. It seems to be reasonable for hydra. It was shown in experiments that the minimum tissue size for reorganisation of the whole organism is 0.2 mm only, while the grown up hydra is 5 mm long.

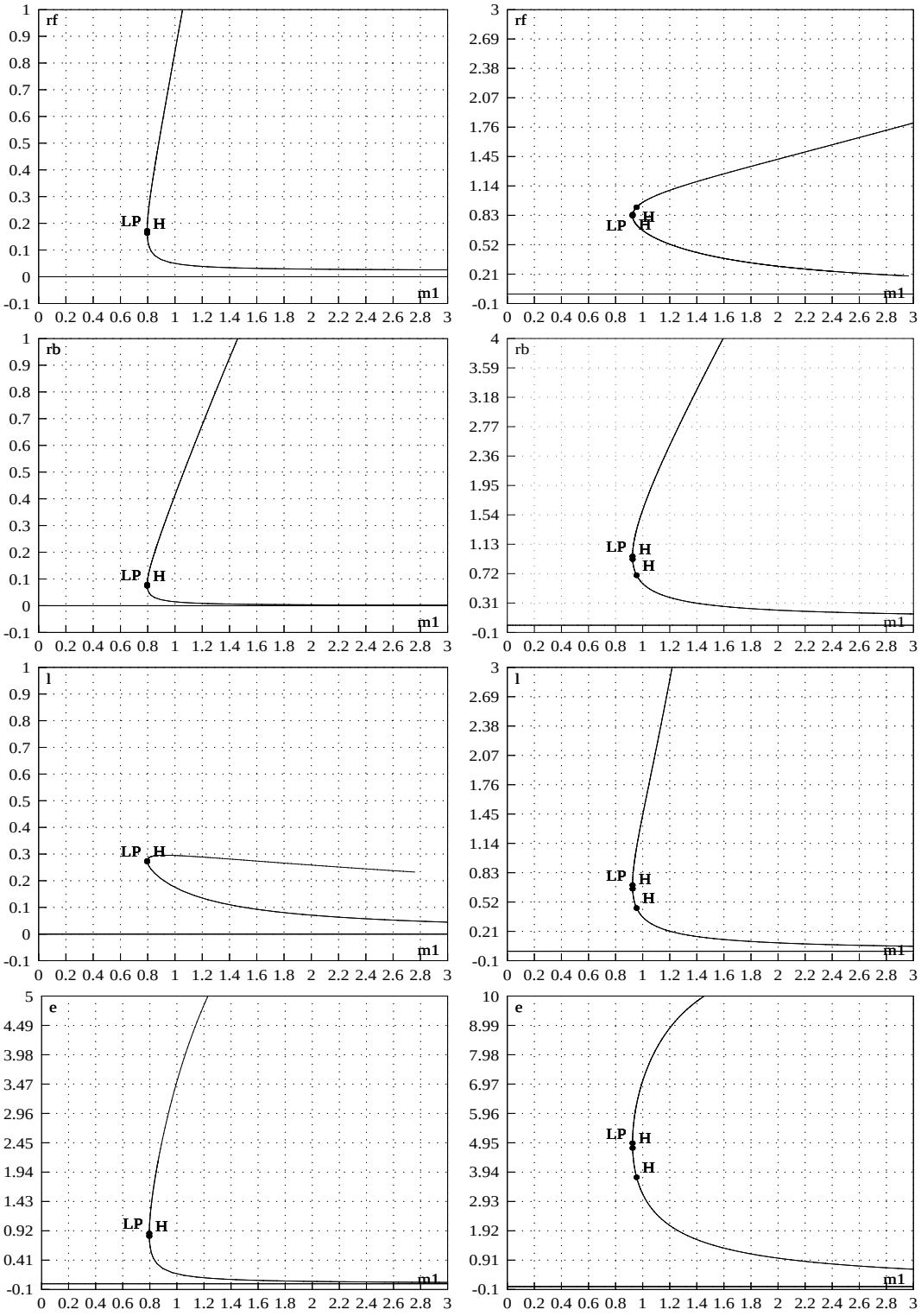

Figure 4.7. Bifurcation diagrams for the steady states of r_f, r_b, l and e. We plot the steady states of the system (4.23) as functions of the parameter m_1. On the left-hand side we present the plots for the case (1), with the kinetics (4.44), on the right-hand side for the case (2), with the kinetics (4.45) with parameters: $m_2 = 3$, $m_3 = 1.2$, $\mu_f = 0.2$, $\mu_b = 0.3$, $\mu_l = 0.1$, $\mu_e = 0.1$, $d = 0.9$, $b = 2.0$, $b_e = 0.7$.

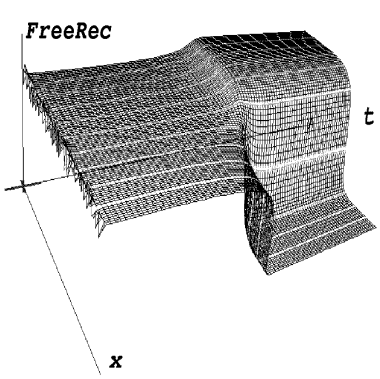
FreeRec
t
x

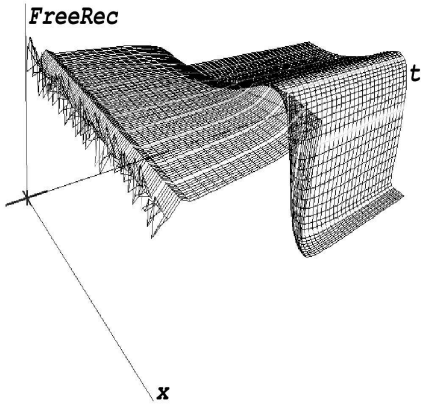
FreeRec
t
x

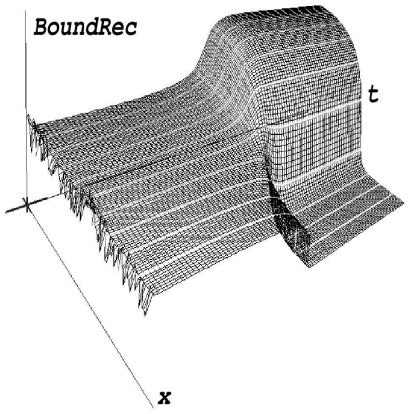
BoundRec
t
x

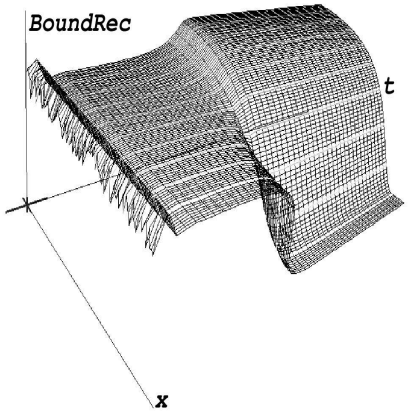
BoundRec
t
x

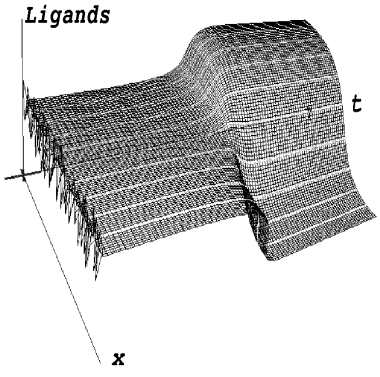
Ligands
t
x

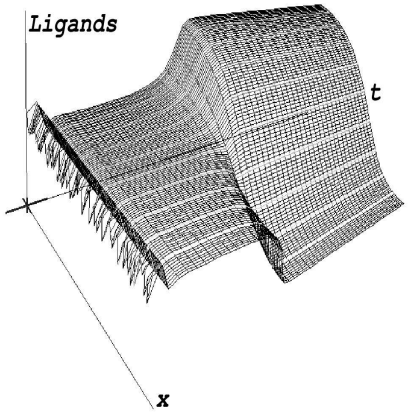
Ligands
t
x

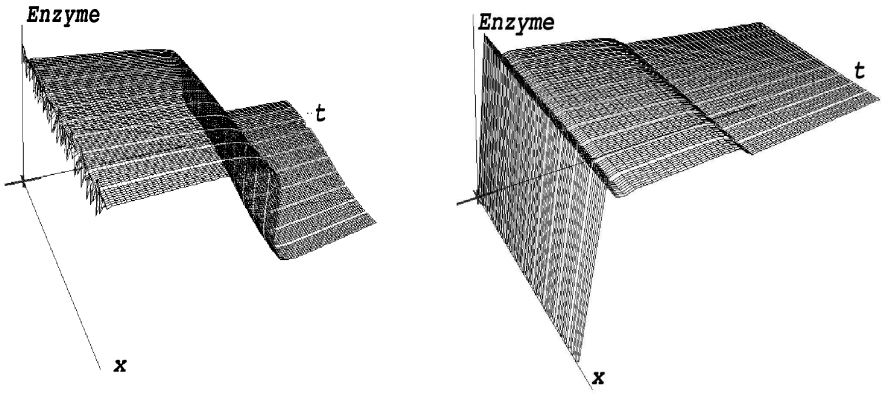

Figure 4.8. Solutions of the four-variable model (4.23). Time evolution of r_b. On the left-hand side we present the plots for the case (1), with the kinetics (4.44), on the right-hand side for the case (2), with the kinetics (4.45). In both cases we observe the formation of a gradient-like structure in the density of bound receptors. Simulations are performed for a random perturbation of the homogeneous steady state $\bar{r}_f = 0.787$, $\bar{r}_b = 1.095$, $\bar{l} = 0.834$, $\bar{e} = 5.458$ in case (1) and $\bar{r}_f = 0.842$, $\bar{r}_b = 0.413$, $\bar{l} = 0.294$, $\bar{e} = 3.513$ in case (2) and γ equal to 1 with parameters: $m_2 = 3$, $m_3 = 1.2$, $\mu_f = 0.2$, $\mu_b = 0.3$, $\mu_l = 0.1$, $\mu_e = 0.1$, $d = 0.9$, $b = 2.0$, $b_e = 0.7$ and $m_1 = 0.93$ for the kinetics (4.44) and $m_1 = 1$ for the kinetics (4.45).

4.2.3.2 Simulation of cutting and grafting experiments

We have solved numerically the model equations for initial conditions corresponding to the cutting and grafting experiments. The mathematical formulation of considered models of cutting and grafting experiments is presented in Appendix B.

Simulations of this model predict outcome of some cutting experiments, what is shown in Figs. 4.9 and 4.10. In the experiments a head and a foot regenerate when they are cut off, even after cutting the half of the animal as it is shown in the Fig. 2.2. This is reflected by our model. To simulate cutting experiments we take as an initial conditions the data corresponding to the normal development (which we obtained as a solution of the model for the perturbed homogeneous steady state) and consider only these which correspond to the part of the body column. We perform simulations with the parameter γ corresponding to the new size of the domain. Regeneration of the initial structure is observed.

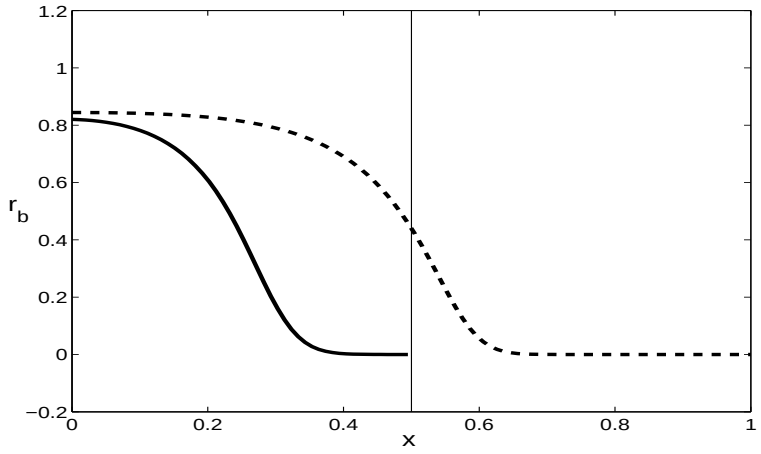

Figure 4.9. The solution of the model (4.23) with the kinetics (4.44) and initial data corresponding to a surgical removal of the lower part (half) of the body column. We perform simulations for the initial data obtained from the data corresponding to the normal development and cutted to the upper part (half) of the domain. With a dashed line we plot initial conditions corresponding to the normal development on the whole domain and with a solid line the result of simulations performed for initial conditions limited to a half of domain. Vertical line shows the place of cutting. We observe reorganisation of the "gradient" on a smaller domain. It corresponds to the formation of a new "foot".

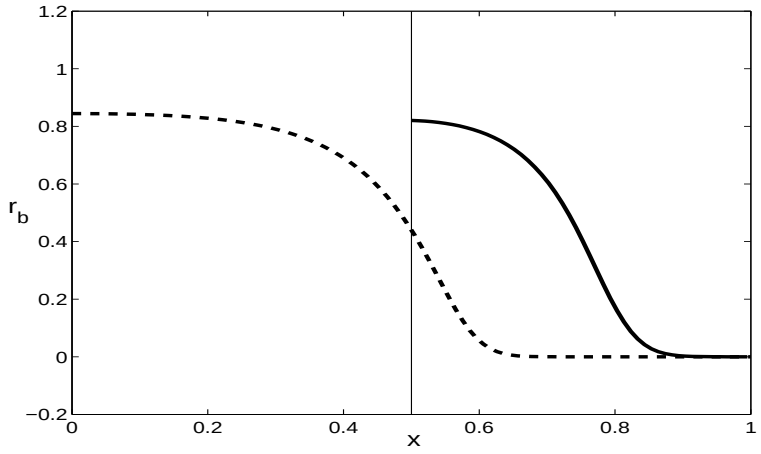

Figure 4.10. The solution of the model (4.23) corresponding to a surgical removal of the upper part (half) of the body column. We perform simulations for the initial data obtained from the data corresponding to the normal development and cutted to the lower part (half) of the domain and observe reorganisation of the "gradient" on a smaller domain. It corresponds to the formation of a new "head".

New "foot" is formed even if the initial data are close to those describing the head in both models. However new "head" cannot be formed if we take as initial data values too close to zero. Fig. 4.10 shows that for the model with kinetics (4.44) after removal of the upper half of body column the regeneration of the pattern is observed. In the model with kinetics (4.45) the removed part of domain must be smaller than a half (or the remained fragment should not include the "foot" end of domain).

Results of the grafting experiments cannot be simulated using the model as it is shown in the fig.(4.12) and (4.11).

The mathematical formulation of the model of grafting experiments is given in the Appendix B. Numerical simulations suggest that the final pattern is stable for spatial perturbation. We can see that a transplantation is nothing but such perturbation. Simulations show that e.g. if in initial conditions we have two peaks (like grafting new head to the lower part of body column), second peak will disappear in short time and we get the gradient pattern.

See Discussion for further comments.

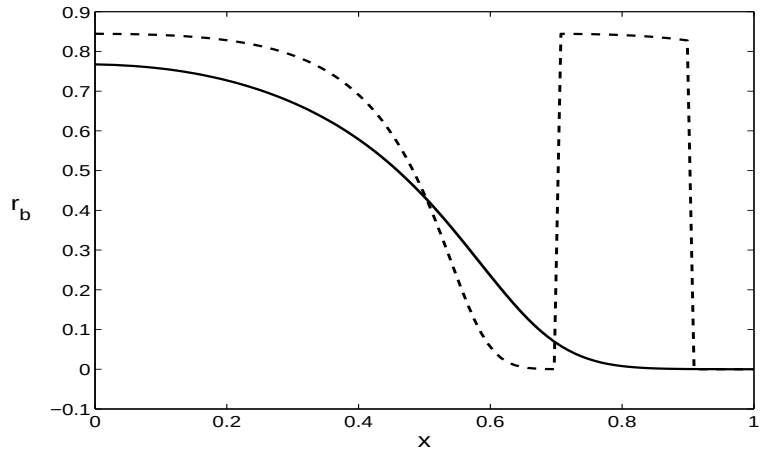

Figure 4.11. The solution of the model corresponding to the transplantation of the tissue from the upper to the lower position along body column. We observe decay in the density of bound receptors in the transplant - there is no formation of a new structure. With a dashed line we plot initial conditions corresponding to the grafting experiment and with a solid line - the density of r_b after some time.

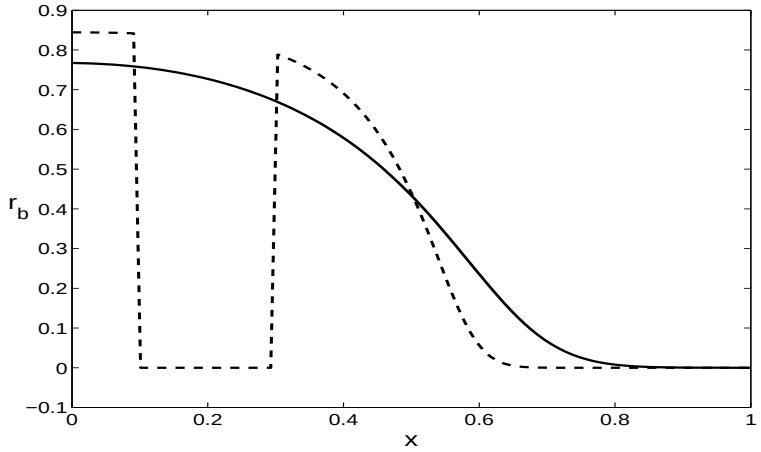

Figure 4.12. The solution of the model corresponding to the transplantation of the tissue from the lower to the upper position along the body column. We observe increase in the density of bound receptors in the transplant - there is no formation of a new structure. With a dashed line we plot initial conditions corresponding to the grafting experiment and with a solid line - the density of r_b after some time.

4.2.4 Four-variable model with autocatalysis of free receptors

Analysing the condition (4.38) and the form of $\tilde{\sigma}_4$ we notice that if $|A_{12}| < 0$ then there exists $\frac{{\mu_m}^2}{\gamma}$ such that $\sigma_4 < 0$ and still $\tilde{\Delta}_3 > 0$. Therefore, if $|A_{12}| < 0$, then (4.38) is fulfiled. As in the three-variable model $|A_{12}| < 0$ only if the function describing *de novo* production of free receptors depends on the density of free receptors (is a power function of the order $1 + \alpha$, $\alpha > 0$).

It means that in the four-variable model (4.23) with self-enhancement of free receptors there is a destabilisation of the homogeneous steady state. It occurs if and only if $\sigma_4 < 0$. The dependence of σ_4 on $\frac{{\mu_m}^2}{\gamma}$ is shown in the Fig. 4.13. From this we see that for every γ there is an infinite range of unstable modes. Fig. 4.13 is plotted for $\gamma = 1$. However we can always choose the γ for which σ_4 is negative already for $\mu_m = 1$.

Simulations show that the model usually behaves similarly to the three-variable model. The final pattern strongly depends on the initial condition and is a spike solution. The number of peaks depends on the domain size. However, for certain domain size it does not depend on the initial function.

The model (4.23) without autocatalysis of free receptors is more robust than the one with autocatalysis in the sense that, for a given scaling parameter γ, the long-time pattern does not depend on the initial perturbation of the homogeneous steady state and the wavelength of the final pattern can be reliably predicted.

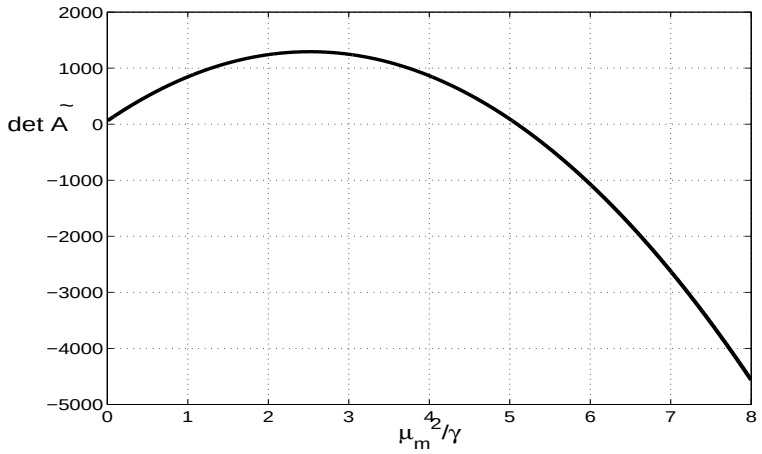

Figure 4.13. σ_4 as a function of $\frac{{\mu_m}^2}{\gamma}$ for four-variable model with autocatalysis of free receptors. It shows that condition for the destabilisation of the homogeneous steady state is fulfiled for infinitely many wavenumbers ${\mu_m}^2$ as it is in three-variable model.

4.3 Discussion

We showed that Turing-type patterns can be obtained in a receptor-based model for hydra. Because of the same mechanism (diffusion-driven instability), a receptor-based model can have properties of solutions similar to an activator-inhibitor model.

The three-variable model requires autocatalysis of free receptors, for the Turing-type patterns to arise. However, in the four-variable model, such patterns arise without autocatalysis. Both *de novo* productions of free receptors and ligands depend only on the density of bound receptors.

In the model based on four equations, the shape of the final pattern does not depend on the initial conditions, i.e. on the way we perturb initially the spatially homogeneous steady state. The values in each point of the domain can be randomly distributed. The range of such values should be between the minimum and the maximum value of the final pattern. It means that simulations of the model resemble *de novo* pattern formation from dissociated cells.

The Turing-type mechanism is one of the simplest theories for the biological pattern formation. In models with such mechanism patterns can arise spontaneously. However, there are several general properties of Turing-type systems that limit their applicability. The parameters must be tightly controlled to obtain the instability at the desired point in parameter space. In particular, the scaling parameter (corresponding to the domain size and diffusion coefficient) and in the model with two diffusion equations also the diffusion coefficients must have the proper relative magnitudes. It is difficult to

obtain a scale-invariance of the degree which is observed in biological systems. Another important problem is that of pattern selection. It arises in the models with multiple stable solutions. Tight control of the initial conditions is needed to select the desired pattern.

The receptor-based models with a Turing-type mechanism can predict the outcome of some cutting experiments but to explain the grafting experiments it is necessary to seek a new mechanism. The reason for this is that the final pattern is stable for spatial perturbation and transplantation is nothing but such perturbation. Simulations show that e.g. if in the initial conditions two peaks are present (corresponding to grafting a new head to the lower part of body column), the second peak will disappear in a short time and we obtain the gradient pattern. The result is valid for three- and four-variable models with both considered kinetics (4.44) and (4.45).

Stable solutions with 2 peaks can be achieved only by an increase, at the same time, of the size of domain. This is precisely how such solutions were obtained in the model of Meinhardt. It is a very important feature of models with the Turing-type mechanism of pattern formation. It encourages us to look for another mechanism, which could explain the results of grafting experiments.

5

Receptor-based model with hysteresis for pattern formation in hydra

5.1 Additional equations modelling the production terms

Let us recall the four-variable model for pattern formation in hydra,

$$\frac{\partial}{\partial t} r_f = -\mu_f(r_f, r_b) + p_r(r_b) - b(r_f, l) + d(r_b), \tag{5.1}$$

$$\frac{\partial}{\partial t} r_b = -\mu_b(r_f, r_b) + b(r_f, l) - d(r_b), \tag{5.2}$$

$$\frac{\partial}{\partial t} l = \frac{1}{\gamma}\frac{\partial^2}{\partial x^2} l - \mu_l(l) - b(r_f, l) + p_l + d(r_b) - b_e(l, e), \tag{5.3}$$

$$\frac{\partial}{\partial t} e = \frac{d_2}{\gamma}\frac{\partial^2}{\partial x^2} e - \mu_e(e) + p_e. \tag{5.4}$$

As stated above (Section 4.3) the results of grafting experiments suggest that the model should involve a memory-based relation.

So far we modelled the p_l and p_e with nonlinear functions depending on r_b and l in case of p_e showing for which nonlinearities system allows Turing type pattern formation. It seems appropriate to consider p_l and p_e as a function determined by the system of ordinary differential equations (modelling the metabolic processes of the cells).

One option would be to consider differential equations for p_l and p_e of the following type,

$$\epsilon \frac{\partial}{\partial t} p_i = g_i(r_f, r_b, l, p_i). \tag{5.5}$$

"Small" number ϵ means that the process of *de novo* production of ligands, receptors or enzyme is much faster than the other processes (binding, dissociation, decay).

For ordinary differential equations the singular perturbation limit $\epsilon \to 0$ is analytically well studied. There is not much known in case of reaction-diffusion systems controlled by the solution to an equation of type (5.5). A van der Pol oscillator with diffusion shows difficulties arising in such a system for small ϵ (see e.g. [60]).

As in many other cases the complexity of the biological process makes it difficult to give a rigorous derivation of these equations. We can only use heuristic reaction terms to depict and investigate the patterning process.

It is very often for the system functioning far from the equilibrium that the uniqueness of the fix point is not guaranteed. It can also happen that the only equilibrium is trivial but the system shows pattern formation (as it is in the model for bacteria growth in [25] and [26]). Here, we consider the mechanism of pattern formation which results from existence of multiple steady states.

5.2 Modelling hysteresis

Hysteresis enters the problem due to the fact that the production of a new biochemical may depend on the history. Hysteresis seems to be important in modelling biological development since according to the observation, inductive signals are present only in the certain time interval of the development. It triggers the changes in the cell's nucleus and evokes differentiation, which does not revert when signal is stopped. The developmental process is irreversible.

Hysteresis results from multiple steady states (see Fig. 5.1). Suppose we have three steady states: the two outer states stable and the inner state unstable. The system may jump from the first stable state to the second when parameters are changed. If parameters are changed back the system remains in the second state till parameters reach another critical value.

Some theories and related bibliography on hysteresis are given in the survey by Macki et al. [42]. It is known that hysteretic kinetics can lead to spatial patterns in chemical systems, such as the Liesegang rings formed by precipitating colloids [53].

A reaction-diffusion model involving a hysteretic functional was proposed by Hoppensteadt and Jäger [25] and Hoppensteadt, Jäger and Pöppe [26] for bacterial growth patterns. They assumed that the cell's growth had a hysteretic dependence on the amount of nutrients and acid present. Pattern formation in this model is caused by the initial instability of the ordinary differential equations. However, as the solution

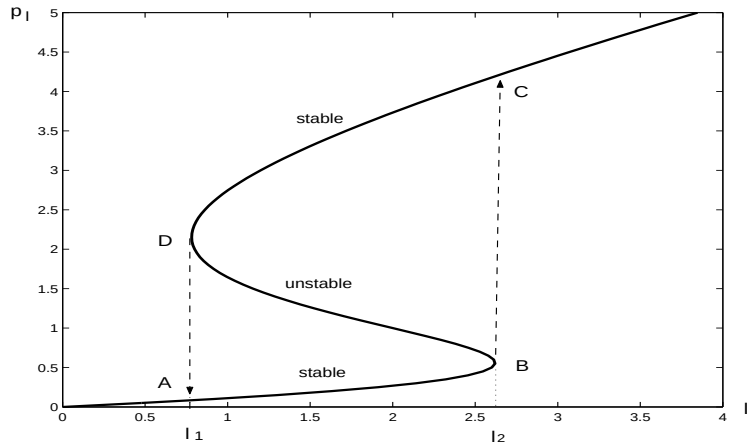

Figure 5.1. Nullclines of g_l - hysteretic dependence of p_l on l. The two outer branches are stable, the inner branch is unstable. If the system evolves on the stable branch AB, the density of ligands l increases and it reaches the value l_2, the system becomes unstable and it jumps to the other stable branch CD. Decreasing the value of l below l_2 does not cause any change, the system remains on the upper stable branch till the value of l approaches l_1 from above. The l value needs to drop below l_1 to shift the system back to the lower stable branch AB.

evolves, nonlinear effects modify the coefficients of these equations so that they become stable [10].

Models based on hysteresis-type bistability were also used in chemistry to describe enzymatic reactions. Seeling and Denzel [69] have deduced a differential equation based on monosubstrate kinetics with substrate inhibition.

Babloyantz and Sanglier [4] developed a model for the regulation of the *lac operon*.

Klein [39] proposed a model for bisubstrate enzymatic reactions when embedded in a metabolic network. He showed how the description of five enzymatic reactions, under the assumption of a partial steady state for the fast variables, can lead to the model of 2 equations with hysteretic nonlinearities. This shows that models with very complicated nonlinear kinetics can be macroscopic descriptions for much larger dynamical networks.

Much of the complexity of such networks usually can be reduced by time-separation arguments, i.e. by reducing the equations for fast variables to algebraic constraints and incorporating slow variables as in the derivation of Michaelis-Menten kinetics, see e.g. [60]. Much work in this respect has been done for chemical reactions but the kinetics for biological interactions are still highly heuristic. There is not enough information about exact rules satisfied by biomolecular processes.

We propose to model the production of ligands and of an enzyme using additional ODEs with hysteresis. We consider

$$g_l = -\delta_l \frac{p_l}{1+p_l^2} + \frac{m_2 l r_b}{(1+\sigma_l p_l^2 - \beta_l p_l)(1+\alpha_l r_b)}, \tag{5.6}$$

$$g_e = -\delta_e \frac{p_e}{1+p_e^2} + \frac{m_3 l e}{(1+\sigma_e p_e^2 - \beta_e p_e)(1+\alpha_e r_b)}. \tag{5.7}$$

Since real biological signal transduction mechanisms are complicated cascades of different enzyme reactions, which are not known so far, we can only consider some particular reaction kinetics which allow to test the possibilities and restrictions of such model. Such functions should be biologically realistic and fulfil some basic assumptions.

We assume that the production of ligands (and enzyme) in a steady state has a hysteretic dependence on the amount of ligands (enzyme) present. It depends also on the density of bound receptors. We assume that the bound receptors trigger the production of ligands and the enzyme. To model the hysteretic dependence of p_l on l we assume that in a steady state the density of ligands l is a third order polynomial of production p_l divided by a second order polynomial. Fig. 5.2 shows nullclines of g_l, (5.6) crossing nullclines of the kinetic system of equation (5.3). We show it in the coordinate system l, p_l. The plot is drawn for $r_b = 1$ but it remains qualitatively the same for all r_b. We choose the parameters to obtain three solutions of the subsystem ($\frac{\partial}{\partial t} p_l = 0$, $\frac{\partial}{\partial t} l = 0$). The third order dependence of l and p_l is involved in the kinetics function. This function also depends on the density of bound receptors since it seems that bound receptors give to cells the signal to produce new molecules (W. Müller, *personal communication*). The production is controlled by its own size, which is reflected by the form of g_l function. To model the production of enzyme we use a similar function. It exhibits a hysteretic dependence between the density of enzyme e and the production of enzyme p_e. We assume that the production of enzyme also depends on the density of ligands. The more ligands there are in the system the more enzyme is produced. Numerical simulations show that the dependence on l is necessary for pattern formation in this model. We also assume a dependence on r_b, but based on the simulations we conclude that it is not as crucial.

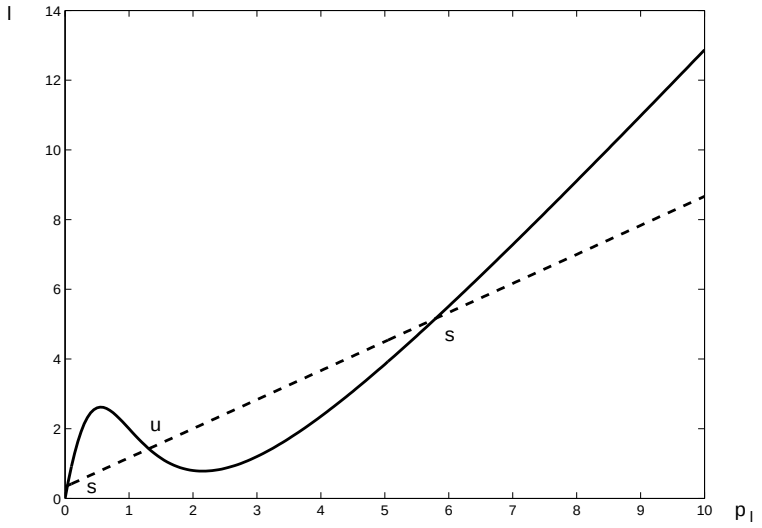

Figure 5.2. Nullclines $\frac{\partial}{\partial t}p_l = 0$ and $\frac{\partial}{\partial t}l = 0$ in the absence of diffusion. The curves cross in three points. This corresponds to the existence of three steady states of the system, two stable and one unstable.

The complete model has the form:

$$
\begin{aligned}
\frac{\partial}{\partial t}r_f &= -\mu_f r_f - b r_f l + d r_b + p_r(r_b), \\
\frac{\partial}{\partial t}r_b &= -\mu_b r_b + b r_f l - d r_b, \\
\frac{\partial}{\partial t}l &= \frac{1}{\gamma}\frac{\partial^2}{\partial x^2}l - \mu_l l - b r_f l + d r_b + p_l - b_e l e, \\
\frac{\partial}{\partial t}e &= \frac{d_2}{\gamma}\frac{\partial^2}{\partial x^2}e - \mu_e e + p_e, \\
\frac{\partial}{\partial t}p_l &= -\delta_l \frac{p_l}{1+p_l^2} + \frac{m_2 l r_b}{(1+\sigma_l p_l^2 - \beta_l p_l)(1+\alpha_l r_b)}, \\
\frac{\partial}{\partial t}p_e &= -\delta_e \frac{p_e}{1+p_e^2} + \frac{m_3 l e}{(1+\sigma_e p_e^2 - \beta_e p_e)(1+\alpha_e r_b)}.
\end{aligned}
\tag{5.8}
$$

where $p_r(r_b) = m_1$ or $p_r(r_b) = m_1 \frac{r_b}{1+r_b}$. The form of p_r is chosen for simplicity.

We also tried to model p_r in a similar way as p_l and p_e but it only makes model more complicated and does not give any qualitatively new results.

5.3 Properties of the system

Similarly as for the four-variable model in Section 4.2.1 using the framework of invariant rectangles and the Theorem 3.12 in Section 3.3, we can show that the solutions of system (5.8) remain positive for positive initial conditions.

The time-behaviour of the solutions depends on parameters. First of all we assume that all the parameters are positive.

To guarantee global existence of the solutions we must assume that σ_l, β_l, σ_l and β_e are chosen in such way that polynomials $1 + \sigma_e p_e^2 - \beta_e p_e$ and $1 + \sigma_l p_l^2 - \beta_l p_l$ have no roots. Otherwise, the solutions might blow up.

Thus we can formulate the following restriction on parameters,

$$\begin{aligned} {\beta_l}^2 - 4\sigma_l < 0, \\ {\beta_e}^2 - 4\sigma_e < 0. \end{aligned} \tag{5.9}$$

These conditions are automatically satisfied for our system since we investigate only parameters which allow the hysteretic relation in equations (5.6) - (5.7) and for such parameters conditions (5.9) are fulfilled.

The existence of global solutions for parameters satisfying (5.9) results from of the theory of bounded invariant rectangles and a priori estimates (Theorem 3.17).

Since the model has a very complicated structure, we investigate the behaviour of solutions numerically. However, in a slightly simplified case, a little more can be accomplished.

5.4 Spatially inhomogeneous stationary solutions in a simplified case

The system of similar type but consisting of one reaction-diffusion equation and one ordinary differential equation, i.e.

$$\begin{aligned} u_t &= \Delta u + f(u, v), \\ v_t &= g(u, v), \end{aligned} \tag{5.10}$$

such that $\partial_v f(u, v) \leq 0$ and $\partial_u g(u, v) \leq 0$ hold, is currently considered by Heinze and Schweizer [21]. They show the existence of stationary and travelling fronts and investigate the stability of these solutions.

Model (5.8) has the form (5.10) for u being a vector of dimension 2 and v a vector of dimension 4. However, in our case, the kinetics system does not define a monotone dynamical system.

Numerical solutions of the model (5.8) with zero flux boundary conditions show similar behaviour. They have the form of stationary or moving fronts depending on the parameters. However, for the model (5.8), analytical results would be difficult to obtain.

We perform analysis proposed in [21] for the system with only one reaction-diffusion equation. We consider $u : \mathbb{R} \times [0, \infty) \to \mathbb{R}$ and $v : \mathbb{R} \times [0, \infty) \to \mathbb{R}^r$. If the equation $g(u, v) = 0$ has multiple solutions, then we may find many stationary solutions of the system (5.10). Now we assume that there exist two solutions, $h_0(u)$ and $h_1(u)$ and that there exist stationary solutions, (u_0, v_0) and (u_1, v_1), of the kinetics system, i.e. $(f, g)(u, v) = 0$, which are stable.

Stationary solutions of of the system (5.10) satisfy,

$$\begin{aligned} 0 &= \Delta u + f(u, v), \\ v(x) &= h_{\phi(x)}(u(x)) \end{aligned} \tag{5.11}$$

for $\phi : \mathbb{R} \to \{0, 1\}$.

We are looking for the solutions of the system satisfying,

$$\begin{aligned} v &= h_0(u), \quad x \leq \bar{x}, \\ v &= h_1(u), \quad x \geq \bar{x}. \end{aligned}$$

Therefore the u must satisfy the following ,

$$\begin{aligned} \frac{u_x^2}{2} + \int_0^u f(s, h_0(s))ds = const = \int_0^{u(-L)} f(s, h_0(s))ds, \quad x < \bar{x}, \\ \frac{u_x^2}{2} + \int_0^u f(s, h_1(s))ds = const = \int_0^{u(+L)} f(s, h_1(s))ds, \quad x > \bar{x}, \end{aligned}$$

where $-L$ and $+L$ are the ends of the domain.

In $u^* = u(\bar{x})$ we obtain,

$$\int_{u^*}^{u(-L)} f(s, h_0(s))ds = \int_{u^*}^{u(+L)} f(s, h_1(s))ds$$

Since we are looking for the solutions connecting u_0 and u_1 we may take $u(-L) = u_0$ and $u(+L) = u_1$.

Therefore, there exists a stationary spatially inhomogeneous solution if and only if there exists u^*, such that the equation,

$$A(u) := \int_{u^*}^{u_0} f(s, h_0(s))ds - \int_{u^*}^{u_1} f(s, h_1(s))ds = 0 \tag{5.12}$$

is satisfied [21].

We consider a model with hysteresis but without an enzyme, i.e.

$$\begin{aligned}
\frac{\partial}{\partial t} r_f &= -\mu_f r_f - b r_f l + d r_b + p_r(r_b), \\
\frac{\partial}{\partial t} r_b &= -\mu_b r_b + b r_f l - d r_b, \\
\frac{\partial}{\partial t} l &= \frac{1}{\gamma}\frac{\partial^2}{\partial x^2} l - \mu_l l - b r_f l + d r_b + p_l, \\
\frac{\partial}{\partial t} p_l &= -\delta_l \frac{p_l}{1+p_l^2} + \frac{m_2 l r_b}{(1+\sigma_l p_l^2 - \beta_l p_l)(1+\alpha_l r_b)}
\end{aligned} \tag{5.13}$$

with $p_r(r_b) = m_1$ or $p_r(r_b) = m_1 \frac{r_b}{1+r_b}$.

Stationary solutions of the system (5.13) satisfy

$$\begin{aligned}
0 &= -\mu_f r_f - b r_f l + d r_b + p_r(r_b), \\
0 &= -\mu_b r_b + b r_f l - d r_b, \\
0 &= \frac{1}{\gamma}\frac{\partial^2}{\partial x^2} l - \mu_l l - b r_f l + d r_b + p_l, \\
0 &= -\delta_l \frac{p_l}{1+p_l^2} + \frac{m_2 l r_b}{(1+\sigma_l p_l^2 - \beta_l p_l)(1+\alpha_l r_b)}.
\end{aligned} \tag{5.14}$$

Solving the first two equations we reduce the system (5.14) to the system of one reaction-diffusion equation coupled with one ordinary differential equation, i.e. of the form (5.10) with $u := l$ and $v := p_l$.

We obtain

$$\begin{aligned}
f(u,v) &= v - \frac{b(\mu_b + d) m_1 u}{b\mu_b u + \mu_f \mu_b \mu_f d} - \mu_l u + \frac{b d m_1 u}{b\mu_b u + \mu_f \mu_b + \mu_f d}, \\
g(u,v) &= -\delta_l \frac{v}{1+v^2} + \frac{m_2 m_1 b u^2}{(b\mu_b u + \mu_f \mu_b \mu_f d)(1+\sigma_l v^2 - \beta_l v)(1 + \frac{\alpha_l b m_1 u}{b\mu_b u + \mu_f \mu_b \mu_f d})}.
\end{aligned} \tag{5.15}$$

The solutions of the algebraic equations $g(u,v)=0$ and $f(u,v)=0$ for the parameter set $b=1.0$, $d=0.9$, $\mu_l=1.2$, $\mu_f=0.1$, $\mu_b=0.01$, $m_1=2$, $m_2=1$, $\alpha_l=9$, $\beta_l=0.8$, $\sigma_l=0.2$ and $\delta_l=1$ are presented in Fig. 5.3.

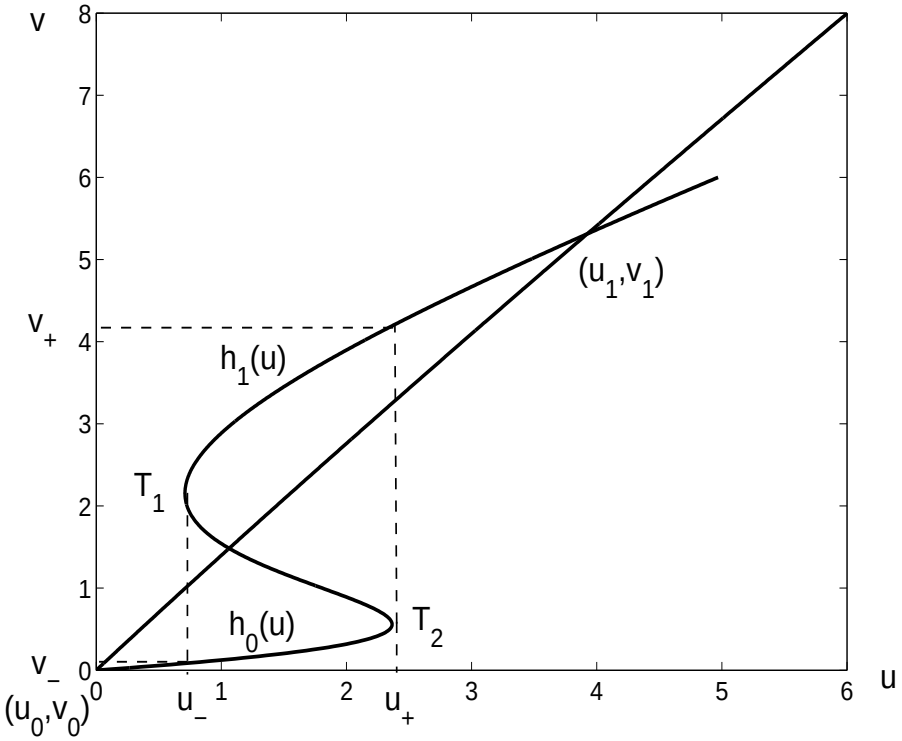

Figure 5.3. Solutions of the algebraic equations $g(u,v)=0$ and $f(u,v)=0$ ($u:=l$, $v:=p_l$) for the parameter set: $b=1.0$, $d=0.9$, $\mu_l=1.2$, $\mu_f=0.1$, $\mu_b=0.01$, $m_1=2$, $m_2=1$, $\alpha_l=9$, $\beta_l=0.8$, $\sigma_l=0.2$ and $\delta_l=1$. (u_0,v_0) and (u_1,v_1) are stable steady states of the kinetics system, u_- is u-coordinate of the lower turning point (T_1), u_+ is u-coordinate of the upper turning point (T_2), v_- is v-coordinate of the point of the curve $g(u_-,v)=0$ laying on the lower branch ($h_0(u)$), v_+ is v-coordinate of the point of the curve $g(u_+,v)=0$ laying on the upper branch ($h_1(u)$).

We find that there are two positive, stable stationary solutions of the kinetic system and that there are two stable branches, $h_0(u)$ and $h_1(u)$ of solutions of the equation $g(u,v)=0$. We look for the value of u^* such (5.12) can be satisfied. Since we cannot explicitly obtain the functions h_i we change the variables in the integrals in (5.12) and consider the equation,

$$A(u) := \int_{h_0(u)}^{v_0} f(H_0(t),t)H_0'(t)dt - \int_{h_1(u)}^{v_1} f(H_1(t),t)H_1'(t)dt, \tag{5.16}$$

where $H_i \circ h_i = Id$, $i=0,1$.

We can explicitly find H and calculate A for a given u. u^* is from the interval $[u_-, u_+]$ such that for $u \in [u_-, u_+]$ there exist both $h_0(u)$ and $h_1(u)$. Thus we can calculate $A(u_-)$ and $A(u_+)$ and if they are of different signs, then there exists u^* such that $A(u^*) = 0$. Numerical calculations show that $A(u) = 0$ exactly in the point u_-.

Numerical simulations performed for the system (5.13) with parameters used above ($b = 1.0$, $d = 0.9$, $\mu_l = 1.2$, $\mu_f = 0.1$, $\mu_b = 0.01$, $m_1 = 2$, $m_2 = 1$, $\alpha_l = 9$, $\beta_l = 0.8$, $\sigma_l = 0.2$ and $\delta_l = 1$) are in agreement with the analysis.

For small enough diffusion coefficients (what is equivalent to the large enough domain size) we observe formation of spatially inhomogeneous solutions (fronts) which are stationary in time (see Fig. 5.4).

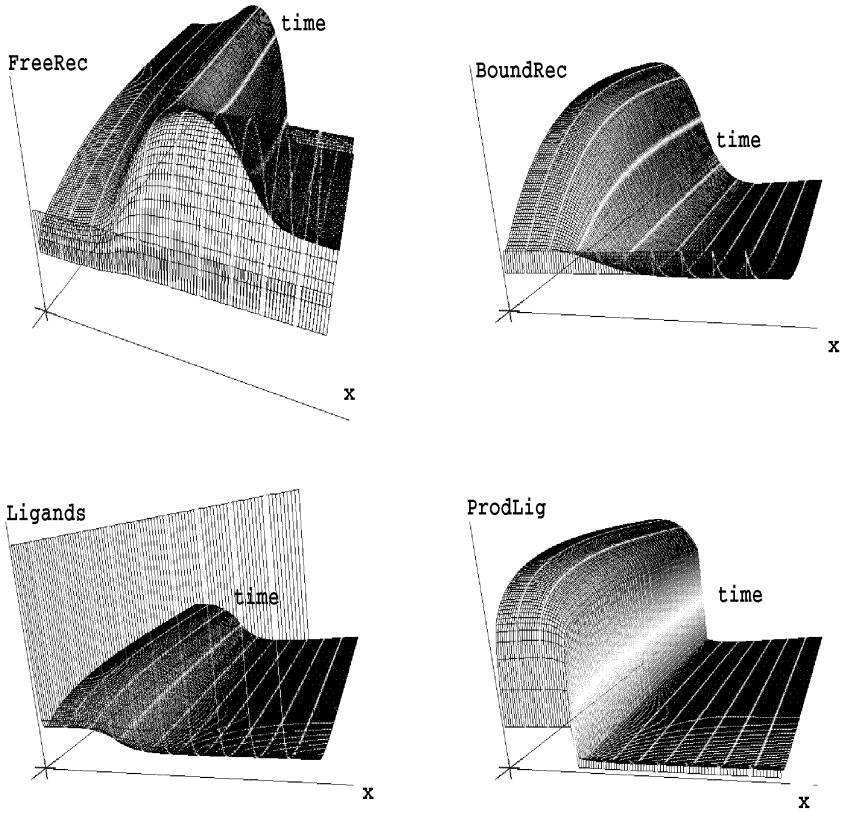

Figure 5.4. The solution of the system (5.13) for parameters $b = 1.0$, $d = 0.9$, $\mu_l = 1.2$, $\mu_f = 0.1$, $\mu_b = 0.01$, $m_1 = 2$, $m_2 = 1$, $\alpha_l = 9$, $\beta_l = 0.8$, $\sigma_l = 0.2$ and diffusion coefficient $d = 0.01$. Simulations are performed for the initial conditions: $r_f(x) = 10$ for $x \in [0, 1]$, $r_b(x) = 10$ for $x \in [0, 1]$, $l(x) = 10$ for $x \in [0, 1]$ and $p_l(x) = 1$ for $x \in [0, 0.3]$, $p_l(x) = 0.1$ for $x \in (0.3, 1]$.

The spatial profile of the solution depends on the diffusion coefficient and it is smoother when the diffusion coefficient is larger (compare Figs. 5.5).

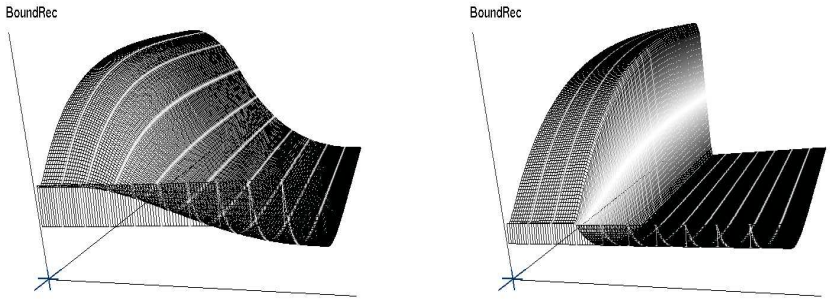

Figure 5.5. The solution of the system (5.13) for different diffusion coefficients. On the left hand-side $d = 0.1$ on the right hand-side $d = 0.0001$. We observe that the profile for the bigger diffusion coefficient is smoother.

Remark 5.1. Considering $p_r = \frac{m_1 r_b}{1+r_b}$ leads qualitatively the same results.

For the complete system we cannot perform similar analysis. Even assuming that one of the diffusion coefficients is equal to zero, we obtain the subsystem of ordinary differential equations which is difficult to reduce to one equation.

5.5 Results of simulations for the complete model with hysteresis

5.5.1 Basic settings

We performed simulations for the model (5.8) with zero flux boundary conditions for l and e.

As initial conditions we chose the homogeneous state, $r_f = 1,\ r_b = 1,\ l = 1,\ e = 1,\ p_l = 1$ and $p_e = 1$ and then perturbed the density of ligands at one end of the domain setting $l = 10$. We set $l = 10$ on the interval of the length 1/10th or 2/10th of the domain.

Simulations show that for the model (5.8) we can have a gradient-like solution for the density of bound receptors (standing wave), which is stationary in time (see Fig. 5.8 or Fig. 5.6) or a spatio-temporal solution oscillating in time (see Fig. 5.7).

Parameters involved in the equations describing production dynamic are chosen in the way allowing the hysteretic dependence of p_l on l. Of course, it is only one particular choice.

Further numerical values used do not represent a systematic review of the parameter space. Rather, it is our purpose to establish, numerically, the capabilities of the models to display the desired types of behaviour.

The diffusion coefficient for the ligands should be smaller than for the enzyme.

For the parameters $b = 2.0$, $d = 0.5$, $\mu_l = 0.1$, $\mu_f = 0.1$, $\mu_b = 0.1$, $\mu_e = 0.3$ $b_e = 0.1$, $m_1 = m_2 = m_3 = 1$, $\alpha_l = \alpha_e = 9$, $\beta_l = \beta_e = 0.8$, $\sigma_l = \sigma_e = 0.2$ and $\delta_l = \delta_e = 1$ we observe the formation of the stationary pattern (standing wave) (see Fig. 5.6). We performed further simulations for different parameters sets, usually changing the d, b and b_e coefficients.

For the parameters $b = 1.0$, $d = 0.9$, $\mu_l = 0.01$, $\mu_f = 0.1$, $\mu_b = 0.1$, $\mu_e = 0.3$ $b_e = 0.8$, $m_1 = m_2 = m_3 = 1$, $\alpha_l = \alpha_e = 9$, $\beta_l = \beta_e = 0.8$, $\sigma_l = \sigma_e = 0.2$ and $\delta_l = \delta_e = 1$, we observe two different behaviours depending on the form of the p_r function. Constant p_r results in a spatio-temporal pattern (see Fig. 5.7), while the Michaelis-Menten function for p_r results in a stationary pattern (see Fig. 5.8).

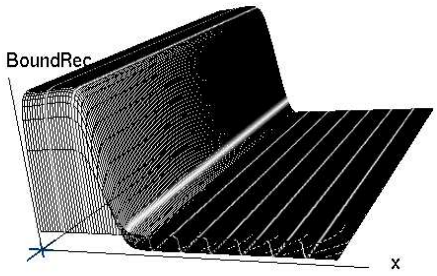

Figure 5.6. Time evolution of r_b for the parameters: $b = 2.0$, $d = 0.5$, $\mu_l = 0.1$, $\mu_f = 0.1$, $\mu_b = 0.1$, $\mu_e = 0.3$ $b_e = 0.1$, $m_1 = m_2 = m_3 = 1$, $\alpha_l = \alpha_e = 9$, $\beta_l = \beta_e = 0.8$, $\sigma_l = \sigma_e = 0.2$ and $\delta_l = \delta_e = 1$ and $p_r = m_1 \frac{r_b}{1+r_b}$

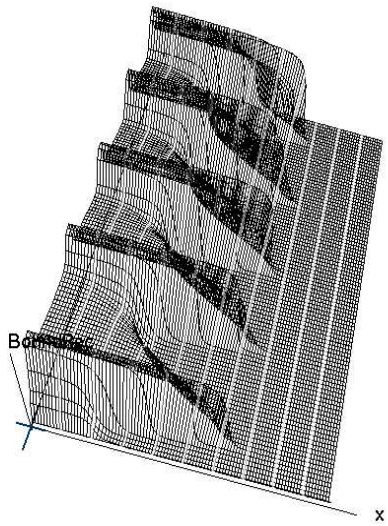

Figure 5.7. Time evolution of r_b for the parameters: $b = 1.0$, $d = 0.9$, $\mu_l = 0.01$, $\mu_f = 0.1$, $\mu_b = 0.1$, $\mu_e = 0.3$ $b_e = 0.8$, $m_1 = m_2 = m_3 = 1$, $\alpha_l = \alpha_e = 9$, $\beta_l = \beta_e = 0.8$, $\sigma_l = \sigma_e = 0.2$ and $\delta_l = \delta_e = 1$ and constant $p_r = m_1$.

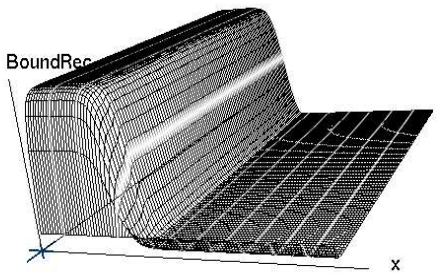

Figure 5.8. Time evolution of r_b for the parameters: $b = 1.0$, $d = 0.9$, $\mu_l = 0.01$, $\mu_f = 0.1$, $\mu_b = 0.1$, $\mu_e = 0.3$ $b_e = 0.8$, $m_1 = m_2 = m_3 = 1$, $\alpha_l = \alpha_e = 9$, $\beta_l = \beta_e = 0.8$, $\sigma_l = \sigma_e = 0.2$, $\delta_l = \delta_e = 1$ and $p_r = m_1 \frac{r_b}{1+r_b}$.

5.5.2 Simulations of cutting and grafting experiments

Simulations can be interpreted as predicting the outcome of grafting experiments. Fig. 5.9 shows the spatio-temporal evolution of the density of bound receptors for initial conditions corresponding to the transplantation of the tissue from the upper part of the body column to the lower one. Mathematical description of the simulated experiments is given in the Appendix B.

We observe the formation of a second peak corresponding to a second head. The formation and persistence of the second maximum is the result of bistability of the reaction terms. For such model we can have various stable solutions, which are transitions between such two stable steady states.

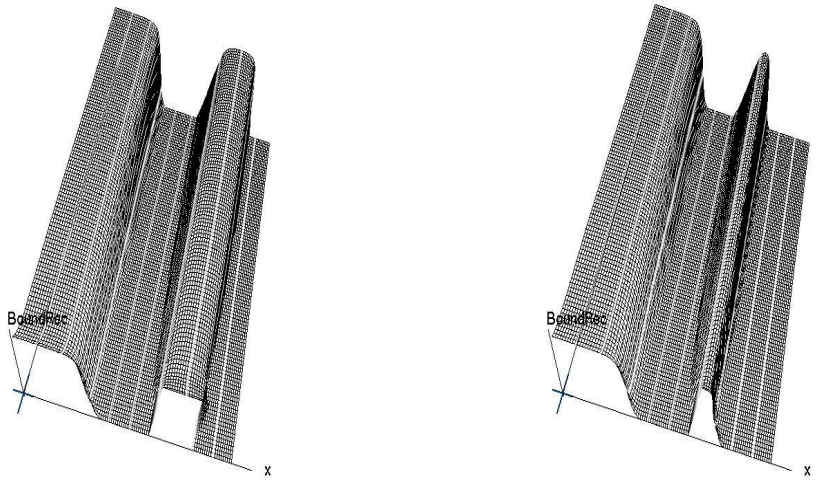

Figure 5.9. The solutions of the model for initial condition corresponding to different transplantations of a head.

We have numerically solved the model equations for initial conditions corresponding to various cutting experiments. If we simulate the cutting of the head end then we can observe the reorganisation. But it happens only in the case when the density of ligands is high enough for the size of production (p_l) to stay in the basin of attraction of the higher steady state. Similarly if we simulate cutting of the foot, we observe formation of the gradient-like solution if the lower end values of the initial state are close enough to the lower steady state. Results of simulations showed that the cutting experiment, in which the body column is cut in half cannot be modelled using such approach. In experiments, cutting in half gives rise to formation of two complete organisms.

The model with hysteresis cannot be used to explain all cutting experiments. Similar observation holds for the SMJM model [70]. The results of the simulations described

by these authors only concern cutting and regeneration of the head or foot. Simulations of the cutting experiments described in [70] concern the cutting of the upper or lower 1/4 of the body column. It means that new simulations are performed for the initial conditions corresponding to the 3/4 of the gradient-like solution. For such initial conditions model (5.8) also reproduces results of experiments.

However, it seems to be meaningful that there is experimental evidence that after cutting hydra in a half, both parts simultaneously regenerate. It means that to model this experiment we should obtain gradient-like pattern formation for the initial conditions corresponding to both parts of the initial domain (as it is for the models with diffusion-driven instability described in Section 4.2.3.2). It is an open problem whether such behaviour can be obtained in model of the form (5.8) for any set of parameters and production kinetics.

5.6 Stationary homogeneous steady states

One of the questions arising is whether it is also possible to obtain, in the model (5.8) diffusion-driven instabilities, and how the corresponding parameter values are related to the parameter space for which we obtained the wave solutions.

Stationary homogeneous steady states satisfy the system,

$$
\begin{aligned}
0 &= -\mu_f r_f - b r_f l + d r_b + m_1 \frac{r_b}{1+r_b}, \\
0 &= -\mu_b r_b + b r_f l - d r_b, \\
0 &= \frac{1}{\gamma}\frac{\partial^2}{\partial x^2} l - \mu_l l - b r_f l + d r_b + p_l - b_e l e, \\
0 &= \frac{d_2}{\gamma}\frac{\partial^2}{\partial x^2} e - \mu_e e + p_e, \\
0 &= -\delta_l \frac{p_l}{1+p_l^2} + \frac{m_2 l r_b}{(1+\sigma_l p_l^2 - \beta_l p_l)(1+\alpha_l r_b)}, \\
0 &= -\delta_e \frac{p_e}{1+p_e^2} + \frac{m_3 l e}{(1+\sigma_e p_e^2 - \beta_e p_e)(1+\alpha_e r_b)}.
\end{aligned}
\tag{5.17}
$$

We solve the 1st, 2nd and 4th equation with respect to r_f, l and e. Assuming that $r_b \neq 0$ we obtain,

$$e = \frac{p_e}{\mu_e}, \tag{5.18}$$

$$r_f = \frac{-r_b(\mu_b + \mu_b r_b - m_1)}{\mu_f(1+r_b)}, \tag{5.19}$$

$$l = -\frac{(\mu_b + d)\mu_f(1+r_b)}{b(\mu_b + \mu_b r_b - m_1)}. \tag{5.20}$$

For $r_b = 0$ we can calculate that the steady states are $(0,0,0,0,0,0)$ and

$(0, 0, \frac{\mu_e \delta_e (b_e^2 + \sigma_e \mu_e^2 \mu_l^2 - \beta_e \mu_e \mu_l b_e)}{m3(b_e^2 + \mu_e^2 \mu_l^2}, -\frac{\mu_l}{b_e}, 0, -\frac{\mu_e \mu_l}{b_e})$, the second of which is nonpositive.

Substituting (5.18)-(5.20) in (5.17) we reduce system (5.17) to the following system of three equations,

$$\begin{aligned}
0 &= p_l - r_b(\mu_b + d) + \frac{\mu_l(\mu_b + d)\mu_f(1+r_b)}{b(\mu_b + \mu_b r_b - m_1)} + dr_b + \frac{b_e(\mu_b + d)\mu_f(1+r_b)p_e}{b(\mu_b + \mu_b r_b - m_1)\mu_e}, \\
0 &= -\frac{\delta_l p_l}{(1+p_l^2)} - \frac{m_2 r_b(\mu_b + d)\mu_f(1+r_b)}{b(\mu_b + \mu_b r_b - m_1)(1+\alpha_l r_b)(1+\sigma_l p_l^2 - \beta_l p_l)}, \\
0 &= -\frac{\delta_e p_e}{(1+p_e^2)} - \frac{m_3(\mu_b + d)\mu_f(1+r_b)}{b(\mu_b + \mu_b r_b - m_1)p_e\mu_e(1+\alpha_e r_b)(1+\sigma_e p_e^2 - \beta_e p_e)}.
\end{aligned} \tag{5.21}$$

We solve the first of the above equations with respect to p_l and obtain,

$$\begin{aligned}
p_l = \quad & (-b_e\mu_f p_e \mu_b - b_e \mu_f p_e d - b_e \mu_f p_e \mu_b r_b - b_e \mu_f p_e d r_b \\
& + r_b b \mu_e \mu_b^2 + r_b^2 b \mu_e \mu_b^2 - r_b b \mu_e \mu_b m_1 - \mu_l \mu_f \mu_e \mu_b \\
& - \mu_l \mu_f \mu_e d - \mu_l \mu_f \mu_e \mu_b r_b - \mu_l \mu_f \mu_e d r_b)/b(\mu_b + \mu_b r_b - m_1)\mu_e.
\end{aligned} \tag{5.22}$$

Finally we obtain two equations,

$$
\begin{aligned}
(5.23)\qquad 0 = {} & -\delta_l(-b_e\mu_f p_e\mu_b - be\mu_f p_e d - b_e\mu_f p_e\mu_b r_b - be\mu_f p_e d r_b + r_b b\mu_e\mu_b^2 \\
& + r_b^2 b\mu_e\mu_b^2 - r_b b\mu_e\mu_b m_1 - \mu_l\mu_f\mu_e\mu_b - \mu_l\mu_f\mu_e d \\
& - \mu_l\mu_f\mu_e\mu_b r_b - \mu_l\mu_f\mu_e d r_b)/b/(\mu_b + \mu_b r_b - m_1)/\mu_e/(1 + (-b_e\mu_f p_e\mu_b \\
& - be\mu_f p_e d - be\mu_f p_e\mu_b r_b - be\mu_f p_e d r_b + r_b b\mu_e\mu_b^2 + r_b^2 b\mu_e\mu_b^2 - r_b b\mu_e\mu_b m_1 \\
& - \mu_l\mu_f\mu_e\mu_b - \mu_l\mu_f\mu_e d - \mu_l\mu_f\mu_e\mu_b r_b - \mu_l\mu_f\mu_e d r_b)^2/b^2 \\
& /(\mu_b + \mu_b r_b - m_1)^2/\mu_e^2) - m_2 r_b(\mu_b + d)\mu_f(1 + r_b)/b/(\mu_b + \mu_b r_b - m_1) \\
& /(1 + \alpha_l r_b)/(1 + \sigma_l(-b_e\mu_f p_e\mu_b - b_e\mu_f p_e d - b_e\mu_f p_e\mu_b r_b - b_e\mu_f p_e d r_b \\
& + r_b b\mu_e\mu_b^2 + r_b^2 b\mu_e\mu_b^2 - r_b b\mu_e\mu_b m_1 \\
& - \mu_l\mu_f\mu_e\mu_b - \mu_l\mu_f\mu_e d - \mu_l\mu_f\mu_e\mu_b r_b \\
& - \mu_l\mu_f\mu_e d r_b)^2/b^2/(\mu_b + \mu_b r_b - m_1)^2/\mu_e^2 - \beta_l(-be\mu_f p_e\mu_b \\
& - b_e\mu_f p_e d - b_e\mu_f p_e\mu_b r_b - b_e\mu_f p_e d r_b + r_b b\mu_e\mu_b^2 + r_b^2 b\mu_e\mu_b^2 \\
& - r_b b\mu_e\mu_b m_1 - \mu_l\mu_f\mu_e\mu_b - \mu_l\mu_f\mu_e d - \mu_l\mu_f\mu_e\mu_b r_b - \mu_l\mu_f\mu_e d r_b) \\
& /b/(\mu_b + \mu_b r_b - m_1)/\mu_e),
\end{aligned}
$$

$$
(5.24)\qquad 0 = -\frac{\delta_e p_e}{(1 + p_e^2)} + \frac{m_3(\mu_b + d)\mu_f(1 + r_b)p_e}{b(-\mu_b - \mu_b r_b + m_1)\mu_e(1 + \alpha_e r_b)(1 + \sigma_e p_e^2 - \beta_e p_e)}.
$$

Second equation is satisfied for $p_e = 0$. Subsequently, r_b is calculated from (5.23).

It is interesting to find the steady states for the values of the parameters used in simulations for which we obtained spatial patterns, i.e. we consider the parameter set $b = 1.0$, $d = 0.9$, $\mu_l = 0.01$, $\mu_f = 0.1$, $\mu_b = 0.1$, $\mu_e = 0.3$ $b_e = 0.8$, $m_1 = m_2 = m_3 = 1$, $\alpha_l = \alpha_e = 9$, $\beta_l = \beta_e = 0.8$, $\sigma_l = \sigma_e = 0.2$, $\delta_l = \delta_e = 1$. In case $p_e = 0$ only one real positive r_b satisfies Eq. (5.23).

Now we assume that $p_e \neq 0$. We solve (5.23) and (5.24) for the parameter set $b = 1.0$, $d = 0.9$, $\mu_l = 0.01$, $\mu_f = 0.1$, $\mu_b = 0.1$, $\mu_e = 0.3$ $b_e = 0.8$, $m_1 = m_2 = m_3 = 1$, $\alpha_l = \alpha_e = 9$, $\beta_l = \beta_e = 0.8$, $\sigma_l = \sigma_e = 0.2$, $\delta_l = \delta_e = 1$.

Equation (5.23) has two solutions, $r_b = 9$, and second solution which is illustrated in Fig. 5.10. Solution of equation (5.24) is shown in Fig. 5.11.

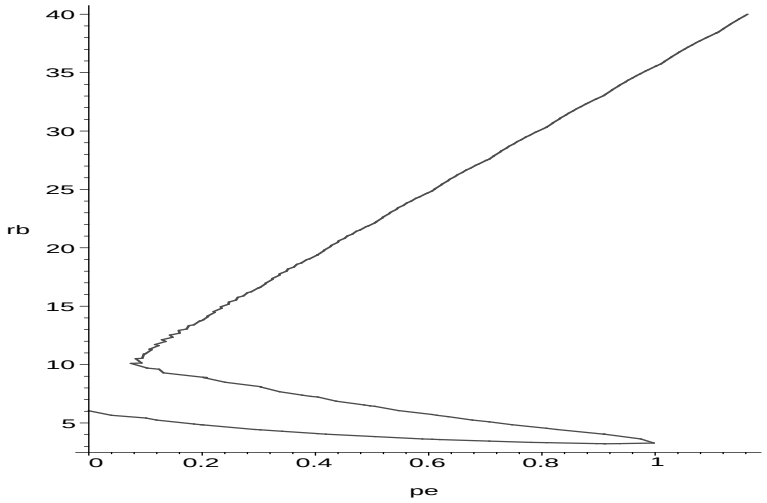

Figure 5.10. Nonconstant solution of (5.23) for the parameters $b = 1.0$, $d = 0.9$, $\mu_l = 0.01$, $\mu_f = 0.1$, $\mu_b = 0.1$, $\mu_e = 0.3$ $b_e = 0.8$, $m_1 = m_2 = m_3 = 1$, $\alpha_l = \alpha_e = 9$, $\beta_l = \beta_e = 0.8$, $\sigma_l = \sigma_e = 0.2$, $\delta_l = \delta_e = 1$.

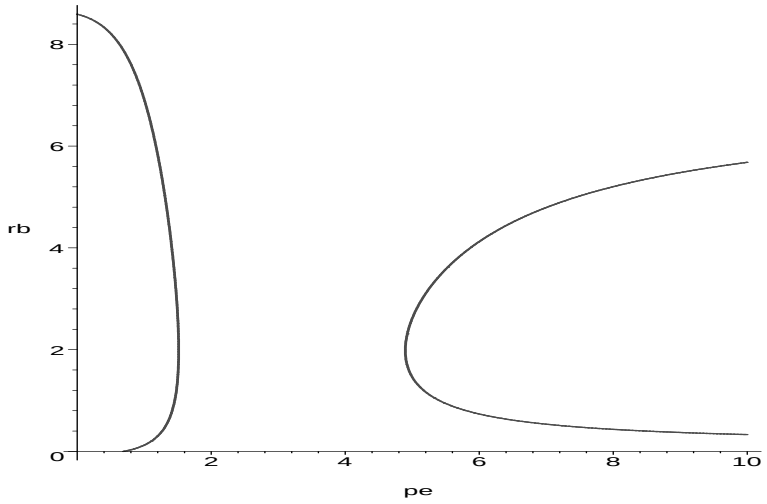

Figure 5.11. Solution of (5.24) for the parameters $b = 1.0$, $d = 0.9$, $\mu_l = 0.01$, $\mu_f = 0.1$, $\mu_b = 0.1$, $\mu_e = 0.3$ $b_e = 0.8$, $m_1 = m_2 = m_3 = 1$, $\alpha_l = \alpha_e = 9$, $\beta_l = \beta_e = 0.8$, $\sigma_l = \sigma_e = 0.2$, $\delta_l = \delta_e = 1$.

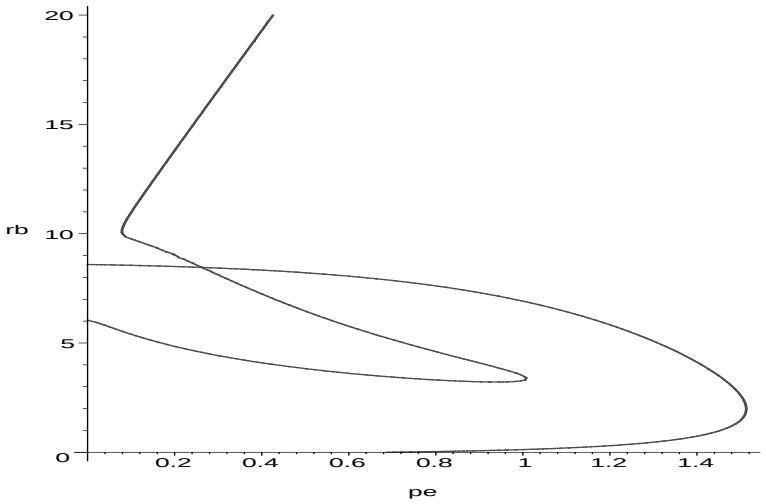

Figure 5.12. Solutions of (5.24) crossing the nonconstant solution of (5.23) for the parameters $b = 1.0$, $d = 0.9$, $\mu_l = 0.01$, $\mu_f = 0.1$, $\mu_b = 0.1$, $\mu_e = 0.3$ $b_e = 0.8$, $m_1 = m_2 = m_3 = 1$, $\alpha_l = \alpha_e = 9$, $\beta_l = \beta_e = 0.8$, $\sigma_l = \sigma_e = 0.2$, $\delta_l = \delta_e = 1$. We can see that there is only one common point.

In summary, we can say that for this set of parameters there is only one positive real solution $\bar{u}_1 = (0.486, 8.456, 17.383, 0.876, 13.208, 0.262)$. There is also one real solution with $p_e = 0$ ($\bar{u}_2 = (2.538, 6.041, 2.379, 0, 0.627, 0)$). For the complete system we have also the trivial solution ($\bar{u}_3 = (0, 0, 0, 0, 0, 0)$)

We perform linear stability analysis of the system (5.17) and obtain that the trivial solution, $\bar{u}_3$, is stable, and the solution $\bar{u}_1$ is also stable. Solution $\bar{u}_2$ is unstable. We investigate whether $\bar{u}_1$ steady state can be destabilised by diffusion. Thus, we study the eigenvalues of the matrix $A - D\frac{\mu_m^2}{\gamma}$, where A is a linearisation of the kinetics system at the state $\bar{u}_1$ (compare Section 3.4), and obtain that there exist diffusion coefficients and γ for which we can select an unstable mode μ_m.

The simulations performed for such values show that the steady state is destabilised. However the solution tends to the trivial equilibrium and no spatially inhomogeneous spatial pattern is obtained. We stress here that for the values of diffusion coefficients (and γ) for which we obtained spatially inhomogeneous pattern (used in previous simulations) the steady state $\bar{u}_1$ is always stable.

For the parameters set $b = 2.0$, $d = 0.5$, $\mu_l = 0.1$, $\mu_f = 0.1$, $\mu_b = 0.1$, $\mu_e = 0.3$ $b_e = 0.1$, $m_1 = m_2 = m_3 = 1$, $\alpha_l = \alpha_e = 9$, $\beta_l = \beta_e = 0.8$, $\sigma_l = \sigma_e = 0.2$ and $\delta_l = \delta_e = 1$ used in simulations presented in Fig. 5.6 we observe qualitatively the same situation (see Fig. 5.14). We did not find numerically any parameters set, for which the number of positive solutions of the system (5.23)-(5.24) would be greater than one.

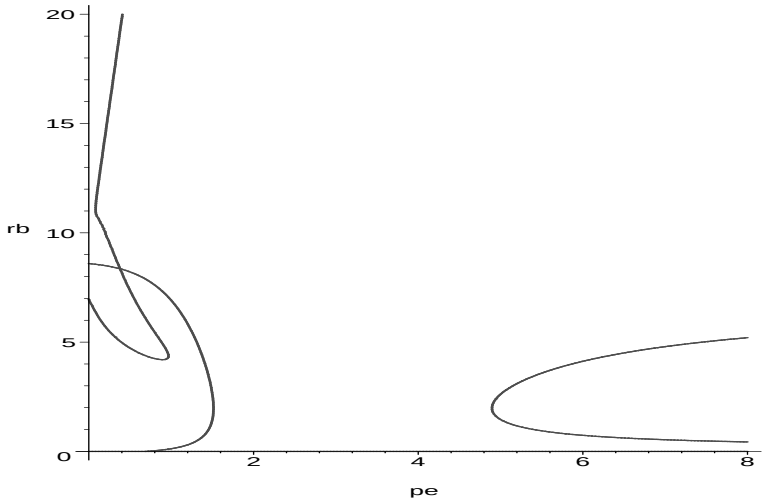

Figure 5.13. Solutions of (5.24) crossing the nonconstant solution of (5.23) for the parameters $b = 1.0$, $d = 0.9$, $\mu_l = 0.01$, $\mu_f = 0.1$, $\mu_b = 0.1$, $\mu_e = 0.3$ $b_e = 0.8$, $m_1 = m_2 = m_3 = 1$, $\alpha_l = \alpha_e = 9$, $\beta_l = \beta_e = 0.8$, $\sigma_l = \sigma_e = 0.2$, $\delta_l = \delta_e = 1$ and constant production of free receptors $p_r = m_1$. We can see that there is only one common point.

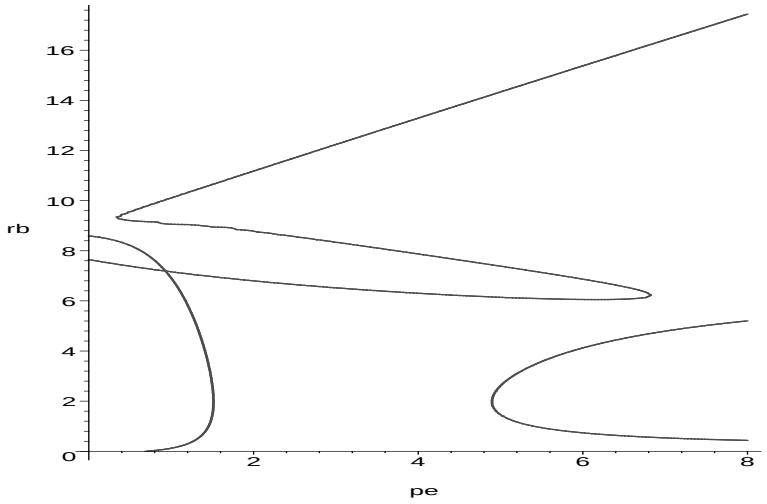

Figure 5.14. Solutions of (5.24) crossing the nonconstant solution of (5.23) for the parameters $b = 2.0$, $d = 0.5$, $\mu_l = 0.1$, $\mu_f = 0.1$, $\mu_b = 0.1$, $\mu_e = 0.3$ $b_e = 0.1$, $m_1 = m_2 = m_3 = 1$, $\alpha_l = \alpha_e = 9$, $\beta_l = \beta_e = 0.8$, $\sigma_l = \sigma_e = 0.2$ and $\delta_l = \delta_e = 1$.

5.7 Another look at the "positional value"

Observing spatio-temporal patterns growing in model (5.8) we arrive at the question of whether such dynamics is possible for the mechanism of pattern formation in hydra. Is it possible that there is no stationary pattern and the density of bound receptors (positional value) oscillates in time? How, then, can cells read such signal and differentiate accordingly?

The idea is that the positional value is not determined by the density of bound receptors at a certain time but by the amount of these receptors over some time period. It can happen that after a ligand binds a receptor, a signal cascade is triggered only if the signal is strong enough and lasts for time long enough (certain number of genes must be activated). Following this idea the positional value might be described by the integral,

$$Pv(t) := \int_0^t r_b(s)ds \tag{5.25}$$

or maybe even more appropriately by

$$Pv(t) := \int_{t-T}^t r_b(s)ds \tag{5.26}$$

or

$$Pv(t) := \int_0^t r_b(s)f(t-s)ds, \quad where \quad f(u) = e^{-\alpha u}. \tag{5.27}$$

Then, regardless of whether the solution for the bound receptors is a stationary wave or it oscillates in time, the solution for so defined positional value Pv is gradient-like (see Fig. 5.15).

Positional value defined by (5.25) could also retain and transmit information about position along the body axes even if the bound receptors dissappear after some time. In simulations of cutting experiments we observe reorganisation of the pattern for Pv, even if there is no pattern formation for r_b, provided we use the definition of Pv such that it "remembers" initial conditions (defined by (5.25)).

Simulating cutting experiments we start from initial conditions, which correspond to the solution, after a long time, of the original problem, truncated to the part of the domain. It means that these are always monotone increasing functions in the coordinate

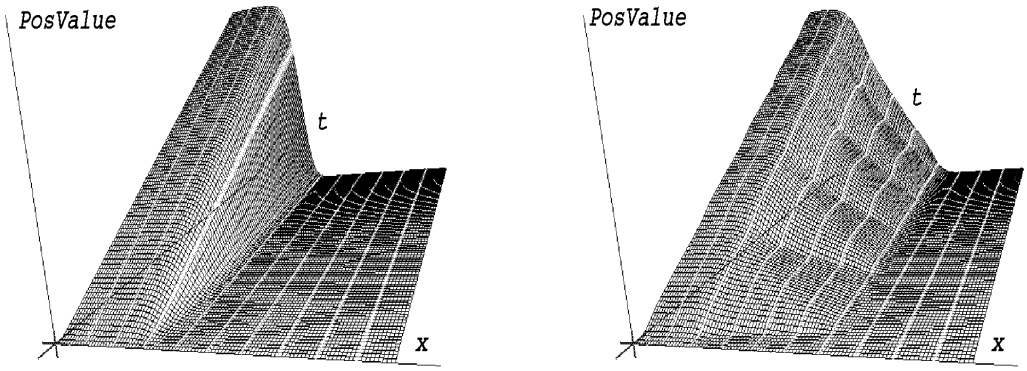

Figure 5.15. Time evolution of Pv corresponding to Fig. 5.8 and 5.7. We can see that even if the solution for r_b is oscillating we get gradient solution for Pv.

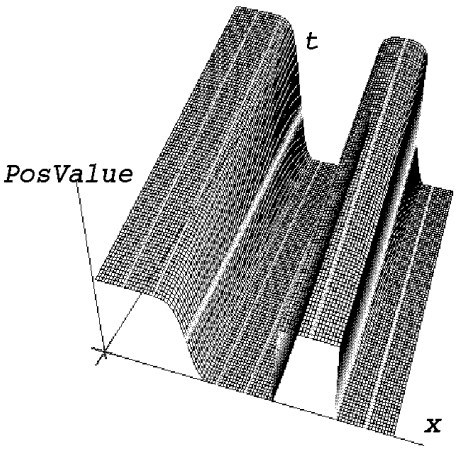

Figure 5.16. Time evolution of Pv for initial conditions corresponding to the grafting experiment

x. Solution for such initial conditions either decays to zero, or it converges to a positive stable homogenous state or it evolves into a gradient-like solution, depending on the initial values. If we look at the integral of the form (5.25), it will stay inhomogeneous but the diversity in the values at both ends of the domain does not increase, it just retains in the form of the initial conditions. This is not satisfactory as an explanation of the regeneration following the cutting experiments.

5.8 Discussion - Turing type model vs model with hysteresis

There are essentially two ways in which a system of identical cells can start to differentiate:

- There is a critical number of cells (size of domain), above which the spatially homogeneous attractor loses stability, which leads to "spontaneous" spatial patterning. It is the case for the models with a Turing-type instability. Such models can explain the *de novo* pattern formation since for some set of parameters and the domain size value, the final pattern is the same and does not depend on the initial perturbation.

- There is an external inducing signal which drives the system into a new, spatially inhomogeneous state. Such signal originates from another group of already differentiated cells. In such case the signal must be strong enough to trigger differentiation. It corresponds to a sufficiently strong initial perturbation of the homogeneous steady state. This type of the initialisation of the pattern-forming mechanism is involved in the model with hysteresis.

The experiments showing *de novo* formation of hydra from the dissociated cells could suggest a Turing-type mechanism. However, usually, in such experiments a few new organisms are formed and then they split and live separately [56]. This means that we do not have to expect the formation of the pattern with a maximum at one end and a minimum at the other end if we start from really random initial distribution. It is rather that initial disturbances lead to the formation of a spatially inhomogeneous solution. Thus, it seems that these kinds of experiments do not exclude models with multiple steady states.

The work shows that the model with multiple steady states can explain the results of grafting experiments, because in such a model many spatially inhomogeneous solutions can coexist. The solution depends on the initial condition similarly as the hydra

resulting from the grafting experiment depends on the graft position and not on the size of the animal.

We showed that stationary fronts can arise already in the simplified model, not including the equations describing the dynamics of an enzyme and its production. For the complete model, we found numerically similar stationary fronts. However, the dynamics of the complete system is more complicated and we observe also spatio-temporal patterns (oscillating in time).

Numerical simulations show that the model cannot fully reproduce the results of cutting experiments. We can simulate only this kind of experiments which shows just the regeneration of head or foot (as in [70]). However, such experiments are modelled by the receptor-based system showing Turing-type instability.

The question is whether these two kinds of experiments can be explained using the same mechanism and whether it could be the combination of the already considered mechanisms. We checked that in the model (5.8) diffusion-driven instabilities does not lead to the formation of the gradient-like pattern. However, the behaviour of the system for different parameter sets and different kinetics describing the production of ligands and enzyme is still an open problem.

6

Models of morphogenesis applied to understand invasion of cancer

6.1 Tumour invasion along a linear or tubular structure

In previous chapters we applied systems of reaction-diffusion equations coupled with ordinary differential equations for studying morphogenesis of hydra. For studying this phenomenon we applied systems with linear structure. It is important to stress that reaction-diffusion models could be applied to model other receptor-ligand systems or the interactions between cells and biochemical molecules.

Growth and morphogenesis in nodular tumours was already studied using the formalism of reaction-diffusion systems. Notably, Chaplain et al. [9] examined spatio-temporal pattern formation in reaction-diffusion systems on the surface of the unit sphere in 3D.

Some human tumours involve tubular or linear structures. For example, some cases of Ductal Carcinoma In Situ (DCIS) show tumour cells spreading amongst normal epithelial cells in the breast ducts away from the primary lesion [11]. The growth pattern is not always contiguous. This histological entity is known as pagetoid spread. A cell automata model of DCIS was developed to study pagetoid spread and to predict its effect on recurrence of DCIS following surgery [11]. In the lung, early lesions, the so-called Ground Glass Opacities, frequently have the form of intertwined linear shadows visible on Computed Tomography (CT) scans [23]. It seems that this type of growth may be present in the vascular and pre-vascular stage of lung cancer development. Since this type of growth does not produce nodular structures in Xray or CT images, its interpretation is ambiguous. It is an interesting question how such structures arise and what are their further invasion paths.

A related mathematical problem has been considered by Gandolfi, Fasano and Bertuzzi [16],[13] who considered the growth of the tumour cord, a cylindrical structure representing a pre-vascular stage of tumour growth.

Motivated by these observations we consider two simple models of the spatial growth of proliferating cells sensitive to a hormonal regulator (called further on "the growth factor"): In the first model, we assume a tubular sheet geometry of the cell population. In the second model, cells are distributed along a straight-line interval. In both models, in the absence of diffusion, the growth factor maintains a stable equilibrium of the number of cells. If the growth factor is allowed to diffuse, the equilibrium, as we will demonstrate, may become unstable to perturbations. Simulations show that the instabilities result in increased growth rates of cells at certain spots of the sheet. Moreover some of the simulations indicate the possibility of chaotic behaviour of the solutions of the model.

Our model attempts to describe a population of cancer cells along linear and tubular structures such as blood vessels, ducts in the breast, or small bronchi in the lungs. Destabilisation of the steady state is interpreted as leading to further growth and invasion of the tumour beyond its original location.

A simplified version of the model was considered by us in [47].

6.2 Model assumptions

6.2.1 Tubular geometry

The first model is defined on a thin sheet of cells, occupying the unit square $(x, y) \in [0,1] \times [0,1]$, rolled to form a cylindrical tube such that the intervals $[x, 0]$ and $[x, 1]$, $x \in [0, 1]$, coincide. There are two substances distributed over the cylinder's surface, cells and growth factor molecules, with surface densities $c(x, y, t)$ and $g(x, y, t)$, respectively. The kinetics equations have the form,

$$\begin{aligned} \dot{c} &= f(c, g), \\ \dot{g} &= h(c, g). \end{aligned} \tag{6.1}$$

Existing cells produce new cells, so $\partial f/\partial c > 0$. Similarly, the more of growth factor is present, the more vigorous is cell proliferation, i.e., $\partial f/\partial g > 0$. On the other hand, the concentration of the growth factor is inhibited both by an increase in cell count and by an increase in growth factor levels, i.e., $\partial h/\partial c < 0$ and $\partial h/\partial g < 0$.

In addition, the growth factor diffuses over the surface of the cylinder, so that the complete set of equations has the form,

$$\begin{aligned} \dot{c} &= f(c,g), \\ \dot{g} &= \frac{1}{\gamma}\Delta_{(x,y)}g + h(c,g). \end{aligned} \tag{6.2}$$

where $\Delta_{(x,y)} = \partial^2_{xx} + \partial^2_{yy}$, with homogeneous Neumann (zero flux) boundary conditions in x,

$$\partial_x g(0,y,t) = \partial_x g(1,y,t) = 0; \;\; y \in [0,1], \tag{6.3}$$

and periodic conditions in y,

$$g(x,0,t) = g(x,1,t); \;\; x \in [0,1], \;\; t \geq 0. \tag{6.4}$$

Coefficient $1/\gamma$ is a composite parameter including the diffusion constant and scaling parameters. We are interested in the conditions for diffusion-driven instability for this problem (compare Section 3.4). Conditions for the linearised stability of the kinetics system of two equations around the spatially homogeneous steady state,

$$\begin{aligned} trA = a_{11} + a_{22} &< 0, \\ \det(A) &> 0, \end{aligned} \tag{6.5}$$

where $A[a_{ij}]$, $a_{11} = \partial f/\partial c$, $a_{12} = \partial f/\partial g$, $a_{21} = \partial h/\partial c$, $a_{22} = \partial h/\partial g$ (derivatives computed at the steady state), can be satisfied under the sign conditions for the partial derivatives of f and h. For the diffusion-driven instability, it is sufficient that

$$\begin{aligned} tr(\tilde{A}) &< 0, \\ \det(\tilde{A}) &< 0, \end{aligned} \tag{6.6}$$

where

$$\tilde{A} = A - \delta D,$$

$D = \begin{pmatrix} 0 & 0 \\ 0 & 1 \end{pmatrix}$ is the diffusion matrix, and $\delta = \mu^2_{n,k}/\gamma$. The wavenumbers $\mu^2_{n,k}$ are obtained from the eigenproblem for the Laplacian on the cylinder's surface

$$\Delta_{(x,y)}\phi_{n,k}(x,y) + \mu^2_{n,k}\phi_{n,k}(x,y) = 0,$$

$$\begin{aligned} \partial_x \phi_{n,k}(0,y) &= \partial_x \phi_{n,k}(1,y) = 0; \;\; y \in [0,1], \\ \phi_{n,k}(x,0) &= \phi_{n,k}(x,1); \;\; x \in [0,1]. \end{aligned} \tag{6.7}$$

We obtain,

$$\left.\begin{array}{l}\phi_{n,k}(x,y)=\cos(n\pi x)\cos(2k\pi y),\\ \mu^2_{n,k}=(n^2+4k^2)\pi^2,\end{array}\right\}\quad n,k\geq 0,\ (n,k)\neq(0,0).$$

Now, the conditions (6.6) can be written as

$$\begin{aligned} a_{11}+a_{22}-\delta &< 0,\\ \det(A)-\delta a_{11} &< 0,\end{aligned}$$

which, considering that $a_{11}>0$, are verified if δ is large enough.

The condition (6.8) is fulfilled for infinitely many δ, i.e. there is an infinite range of unstable modes. As we already mentioned in Section 4.1.3 a complete asymptotic analysis for such systems is still lacking.

6.2.2 Linear geometry

We will also consider a one-dimensional model, in which the tube is replaced by the unit interval, i.e., $x\in[0,1]$. In such model, cells and growth factor molecules have linear densities $c(x,t)$ and $g(x,t)$, respectively. The kinetics equations have the same form as in Eq. (6.1).

The growth factor now diffuses over the unit interval, so that the complete set of equations has the form,

$$\begin{aligned}\dot{c} &= f(c,g),\\ \dot{g} &= \frac{1}{\gamma}\Delta_x g+h(c,g),\end{aligned}\tag{6.8}$$

where $\Delta_x=\partial^2_{xx}$, with homogeneous Neumann (zero flux) boundary conditions

$$\partial_x g(0,t)=\partial_x g(1,t)=0;\ \ t\geq 0.\tag{6.9}$$

The conditions for diffusion-driven (Turing-type) instability for this problem are formally the same as in the two dimensional problem, and given by expressions (6.5) and (6.6). The only difference is that the wavenumbers $\mu^2_{n,k}$ are now obtained from the eigenproblem for the Laplacian on the unit interval

$$\Delta_x\phi_n(x)+\mu_n^2\phi_n(x)=0,\tag{6.10}$$

$$\partial_x\phi_n(0)=\partial_x\phi_n(1)=0.$$

We obtain,

$$\left.\begin{aligned}\phi_n(x) &= \cos(n\pi x),\\ \mu_n^2 &= n^2\pi^2,\end{aligned}\right\}, \quad n > 0.$$

This linear geometry model has been introduced since it is easier to simulate and interpret.

6.2.3 Kinetics of cell proliferation and growth factor production

The philosophy of building a model of the cell cycle is explained in Fig. 6.1.

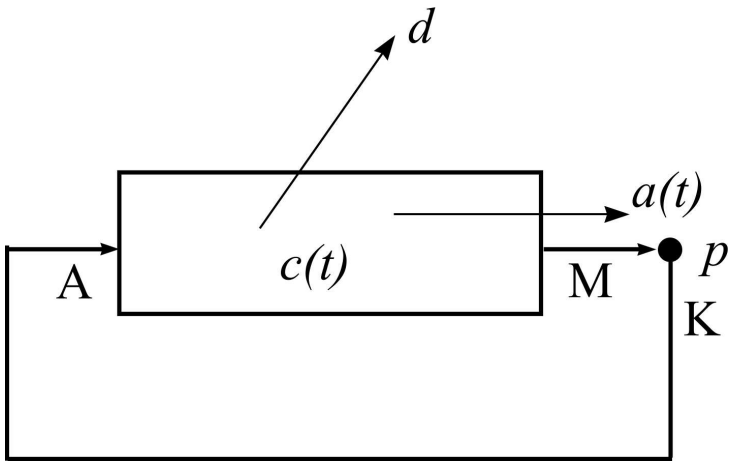

Figure 6.1. Model of the cell cycle of proliferating cells. A newborn cell enters the cell cycle at point A. Cell cycle is treated as a well-mixed tank, from which cells may either enter division at rate $a(t)$, or death at rate d considered constant in time. As a result, if the number of cells present in the cycle at time t is equal to $c(t)$, the flux to mitosis (M) is equal to $a(t)c(t)$, while the flux to death is equal to $dc(t)$. Cells divide with efficiency $p \in [0,1]$ constant in time. Therefore, the flux of just divided cells from mitosis (point K) is equal to $2pa(t)c(t)$. These cells constitute the influx at point A of one of progeny cells. In summary, the rate of change of $c(t)$ is equal to $dc/dt = 2pa(t)c(t) - a(t)c(t) - dc(t)$.

Let us denote by $c(t)$ the number of cells and by $g(t)$ the level of growth factor bound to an average cell, at time t. Equation of cell cycle kinetics has the form

$$\frac{dc}{dt} = [(2p-1)a(t) - d]c(t), \tag{6.11}$$

where function $a(t)$ is the rate of cells flux towards division. We consider it a function of the total amount of bound growth factor present, $c(t)g(t)$,

$$a = \frac{a_0 k(cg)^b}{1 + k(cg)^b}. \tag{6.12}$$

This function is increasing in cg and then saturating at the level a_0, the pattern of increase adjusted by constants k and b ($k, b > 0$). As a consequence,

$$f(c,g) = [(2p-1)\frac{a_0 k(cg)^b}{1+k(cg)^b} - d]c. \tag{6.13}$$

6.2.4 Derivation of models of growth factor kinetics

In this Section, we derive a model of growth factor kinetics. The form of the equation for growth factor kinetics is implied by the following considerations: The growth factor is supplied by a hormonal mechanism extraneous with respect to the sheet of tumour cells. Its supply remains constant. However, its availability to the tumour cells is inversely related with the number of cells. One possible mechanism leading to the inverse relation is that the molecules of the growth factor are bound to receptors on the cell's membrane and therefore are not available to other cells.

We use the formalism of time-continuous Markov chains [2].

We assume that cells are embedded in a "field" of growth factor particles and consider probabilities,

$$P_{ij}(t) = Pr[F(t) = i, B(t) = j], \tag{6.14}$$

where $F(t)$ is a number of free growth factor particles and $B(t)$ is a number of bound growth factor particles. Pair (i,j) is the state of the process.

We assume that in a short time interval $(t, t+\Delta t)$ a transition from state (i,j) to state (k,l) occurs with probability $q_{(i,j)\to(k,l)}\Delta t + o(\Delta t)$. For our model, we specify the following non-zero transition intensities:

$q_{(i,j)\to(i-1,j+1)} = \alpha C i$ - binding of free growth factor particles,

$q_{(i,j)\to(i+1,j)} = \beta$ - constant influx of free growth factor particles,

$q_{(i,j)\to(i-1,j)} = \delta i$ - loss of free growth factor particles,

$q_{(i,j)\to(i,j-1)} = uj$ - loss of bound growth factor particles.

Factor $C = C(c)$ depends on cell density.

The loss and binding intensities are proportional to the number of existing particles of the free or bound growth factor and we assume that they are linear functions. The influx of the free growth particles is constant. A model specified in this way is a time-continuous Markov chain.

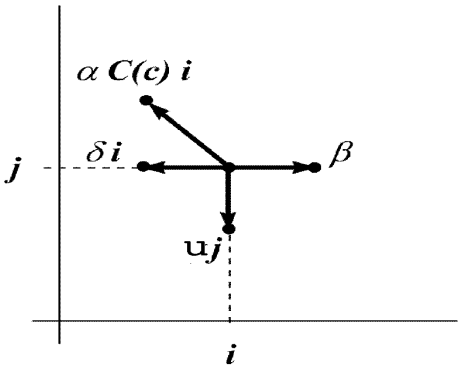

Figure 6.2. Transition intensities, for the numbers of growth factor particles, free (i) and bound (j) in the growth factor state space.

The chain dynamics are described by the following infinite system of Chapmann-Kolmogorov ordinary differential equations for probabilities P_{ij}:

$$\begin{aligned} \dot{P}_{i,j} = \quad & \beta\{i \geq 1\}P_{i-1,j} + u(j+1)P_{i,j+1} \\ & +\delta(i+1)P_{i+1,j} + \alpha C(i+1)\{j \geq 1\}P_{i+1,j-1} \\ & -(\beta + u(j) + \delta(i) + \alpha C(i))P_{ij}, \end{aligned} \tag{6.15}$$

where $\{s\} = 0$ or 1 is the logical value of a statement.

6.2.5 *Expected-value kinetics*

Let us define expected counts of free and bound receptor particles as,

$$E[F(t)] = \Sigma_{i,j\geq 0} i P_{ij}(t), \tag{6.16}$$

$$E[B(t)] = \Sigma_{i,j\geq 0} j P_{ij}(t)). \tag{6.17}$$

Combining equations in (6.15), we obtain

$$\dot{F}(t) = \beta - \delta F - \alpha CF, \tag{6.18}$$

$$\dot{B}(t) = \alpha CF - uB, \tag{6.19}$$

where, by an abuse of notations, $F(t)$ and $B(t)$ denote expectations $E[F(t)]$ and $E[B(t)]$, respectively.

We assume that the total number of growth factor particles is constant and so we obtain,

$$\dot{F}(t) + \dot{B}(t) = \beta - \delta F - uB = 0.$$

Hence,

$$F = \frac{\beta}{\delta} - \frac{u}{\delta}B.$$

and

$$\dot{B}(t) = \alpha C(\frac{\beta}{\delta} - \frac{u}{\delta}B) - uB = \alpha C\frac{\beta}{\delta} - Bu(\frac{\alpha}{\delta}C + 1). \tag{6.20}$$

Since we are interested in the number of particles of bound growth factor per cell, we define $g(t) = \frac{B(t,x)}{c(t,x)}$ and from (6.20) we obtain,

$$\dot{g}(t) = \frac{\alpha\beta}{\delta}\frac{C(c)}{c} - g(t)[u + \frac{\alpha u}{\delta}C(c) + \frac{\dot{c}}{c}]. \tag{6.21}$$

We assume also that $C(c)$ initially grows but then is affected by a crowding effect, i.e.,

$$C(c) = \frac{c^e}{1 + rc^s}, \quad s \geq e > 0.$$

Using (6.11) and (6.12) we can rewrite (6.21) and obtain the kinetics model for the growth factor.

$$\dot{g}(t) = \frac{\alpha\beta}{\delta}\frac{c^{e-1}}{1 + rc^s} - g(t)[u + \frac{\alpha u}{\delta}\frac{c^e}{1 + rc^s} + \frac{(2p-1)a_0k(cg)^b}{1 + k(cg)^b} - d]. \tag{6.22}$$

6.2.6 Model analysis

To reduce the number of parameters we perform the following rescaling,

$$\begin{aligned} a_1 &= (2p-1)a_0, \\ c^* &= ck^{1/b}, \\ r_1 &= rk^{-s/b}, \\ h_0 &= \frac{\alpha}{\delta}k^{-e/b}, \\ \beta_1 &= \beta k^{1/b} \end{aligned}$$

and dropping the superscript "*", for clarity, we obtain the following equations,

$$
\begin{aligned}
\frac{\partial c}{\partial t} &= (\frac{a_1(cg)^b}{1+(cg)^b} - d)c, \\
\frac{\partial g}{\partial t} &= \frac{1}{\gamma}\Delta_x g + h_0\beta_1\frac{c^{e-1}}{1+r_1c^s} - g(t)[u + h_0u\frac{c^e}{1+r_1c^s} + \frac{a_1(cg)^b}{1+(cg)^b} - d].
\end{aligned} \tag{6.23}
$$

We assume that in the absence of cells the density of growth factor cannot increase, hence $u > d$. For the solution of the system (6.23) we can prove the following:

Proposition 6.1.
For nonnegative initial conditions, the solutions of the system (6.23) stay nonnegative and g stays bounded.

Proof : Let $\Sigma = (c,g) : c(t,x) \geq 0$ *and* $g_1 \geq g(t,x) \geq 0$. Then we show that the vector field $V = [(\frac{a_1(cg)^b}{1+(cg)^b} - d)c, h_0\beta_1\frac{c^{e-1}}{1+r_1c^s} - g(t)[u + h_0u\frac{c^e}{1+r_1c^s} + \frac{a_1(cg)^b}{1+(cg)^b} - d]]$ does not point outwards of Σ (so that Σ is invariant for the system (6.23)).

Our results follow from Corollary 3.16 in Section 3.3.

We set $G(c,g) = -c$. $\nabla G(V)|_{c=0} = 0$ in Σ. Hence $c \geq 0$.

If $G(c,g) = -g$ then $\nabla G(V)|_{g=0} = -h_0\beta_1\frac{c^{e-1}}{1+r_1c^s} < 0$ in Σ. Hence $g \geq 0$.

Also if we set $G(c,g) = g - g_1$ then $\nabla G(V)|_{g=g_1} = h_0\beta - g_1[u-d]] < 0$ for $g_1 > \frac{h_0\beta}{u-d}$ since $u > d$. Hence $g \leq g_1$. ■

Thus, we obtain a bounded invariant set for g and nonnegativity of c. For the solution c the bounded invariant set does not exist but we can find an a priori bound. Since $\frac{\partial c}{\partial t} \leq (a_1 - d)c$ we have an a priori bound for solution c, $c \leq c(0)e^{(a_1-d)t}$.

As a consequence, the solution of the whole problem exists for all times $t \geq 0$ (Corollary 3.17).

We calculate that the homogeneous positive steady state (c_i, g_i) must fulfil the following implicit relationship,

$$
h_0(\beta - uX)c_i^e = uX + uXrc_i^s, \;\; c_ig_i = X, \tag{6.24}
$$

where

$$
X = \left\{\frac{d}{a_1 - d}\right\}^{1/b}. \tag{6.25}
$$

Conclusion 6.2. The model has positive steady states only if $a_1 > d$ and $\beta > u(\frac{d}{a_1-d})^{1/b}$

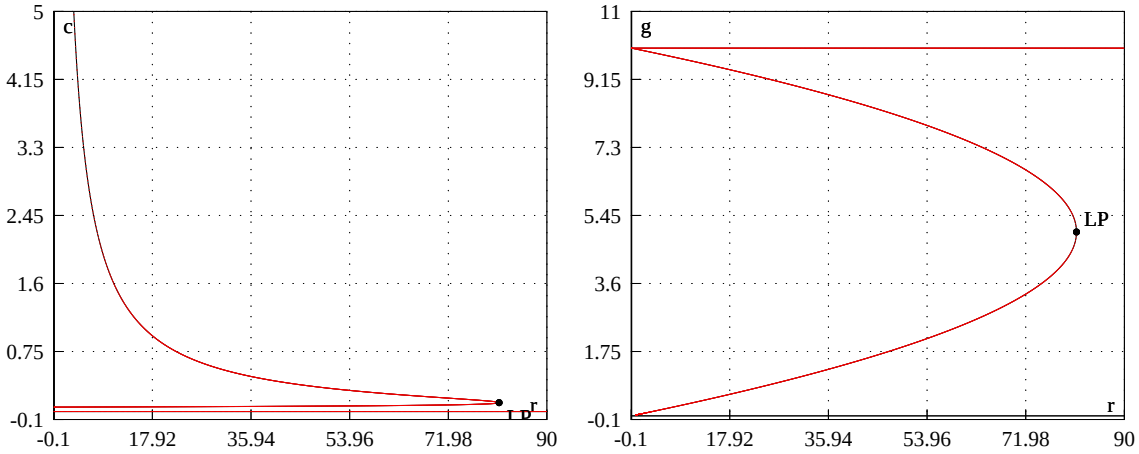

Figure 6.3. Bifurcation diagrams for the steady states of c and g in case $s = 2$ and $e = 1$.

The kinetics system can have 1, 2 or 3 positive steady states (Fig. 6.3). First of all, $(c_0, g_0) = (0, h_0\beta/(u-d))$ for $e = 1$ and $(0, 0)$ for $e > 1$ is a steady state. This steady state is always stable. Further steady states (c_i, g_i) satisfy the relationship (6.24).

The number of (c_i, g_i) fulfilling the condition (6.24) is equal to the number of roots of the function,

$$f(c) = c^s - \frac{h_0(\beta - uX)}{uXr}c^e + \frac{1}{r}, \quad s \geq e > 0$$

If $s = e$ then f has one positive root for $uXr < h_0(\beta - uX)$. Otherwise it has no real positive roots. Now assume that $s > e$. Studying the first and second order derivative of f we find out that f can have zero, one or at most two roots.

Now we consider the special case when $e = 1$. It can be demonstrated that Eq. (6.24) has a pair of solutions, a single solution, or no solution at all, if $r < r_0$, $r = r_0$ and $r > r_0$, respectively, where

$$r_0 = \frac{h_0(\beta - uX)}{suX}\left(\frac{uXs}{h_0(\beta - uX)(s-1)}\right)^{1-s}.$$

6.3 Numerical results

6.3.1 Data

6.3.1.1 Cell kinetics

For preliminary computations, we assume that the expected interdivision time of cells is equal to $1/a_0 = 12$ hours similar to the estimates in [37]. Further, we assume a

perfect efficiency of divisions, $p = 1$, and a low death rate $d = 0.04$. Other coefficients are set arbitrarily at $b = 2$ and $k = 1$.

6.3.1.2 Growth factor kinetics

We use the expected turnover time equal to $1/u = 10$ hours. Also, we use arbitrary values of $h_0 = 1$ and $s = 2$ and $e = 1$. The coefficient r is adjusted to ensure existence of three steady states.

6.3.2 Simulations for the one-dimensional model

The discretised system of ODEs is numerically solved using the CVODE package and numerical estimates of the Jacobian matrix. Space discretisation is a grid on the unit interval. Time discretisation is performed implicitly. Homogeneous Neumann (zero flux) boundary conditions are implemented as a reflection at the boundary.

The spatially homogeneous steady state was perturbed with a small cosinusoidal additive term with different frequencies (for parameter values and further details, cf. the legend to the figures). As evident from Figs. 6.4 and 6.5 cell density $c(x,t)$ remains close to $c(x,0)$ until a threshold time at which it starts exponentially increasing at some x-coordinates and exponentially decreasing at other. The rate of the exponential growth read from the graph is consistent with the saturation rate $(2p-1)a_0 - d$ of Eq. (6.11) when the flux $a(t)$ reaches its maximum value a_0. At the same time, $g(x,t)$ gradually reaches a constant value.

Further figures depict $c(x,t_i)$ as a function of $x \in [0,1]$ (i.e., at discrete points $i\Delta x$, $i = 0, 1, ...100$, $\Delta x = 0.01$), for several times t_i. Series of simulations, depicted in Figs. 6.6 - 6.9 and 6.11 - 6.14 - illustrates the dependence of solutions on parameter γ, the inverse of the diffusion coefficient. As γ increases, i.e., as the diffusion coefficient decreases, the solution profile loses similarity to the initial condition and displays an increasing number of local maxima. For γ large enough, after some time, $c(x,t)$ loses resemblance to $c(x,0)$, which first manifests itself in phase inversion and then appearance of a chaotic-like profile. The transition occurs precisely at the same time when the saturation-rate exponential growth at some x-coordinates commences.

In Figs. 6.15 - 6.18 we present spatial profiles of the numerical simulations for a different parameter set.

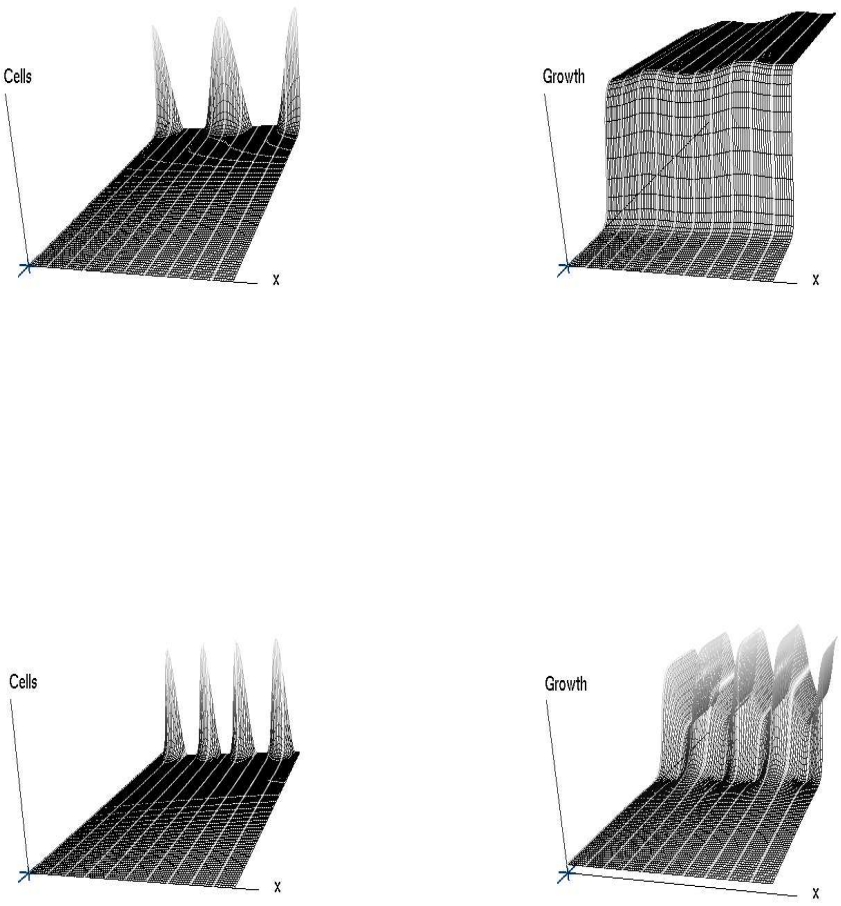

Figure 6.4. Time evolution of the solutions with parameters, $a_1 = 1/12$, $h_0 = 1$, $r = 10$, $s = 2$, $b = 2$, $e = 1$, $d = 0.04$, $u = 0.1$, $\beta_1 = 1$ for $\gamma = 1$ (top row)and $\gamma = 1000$ (bottom row). On the left-hand side we present solution c and on the right-hand side g. Initial perturbation of the steady state value is cosine function with frequency 4 and amplitude 10^{-4}.

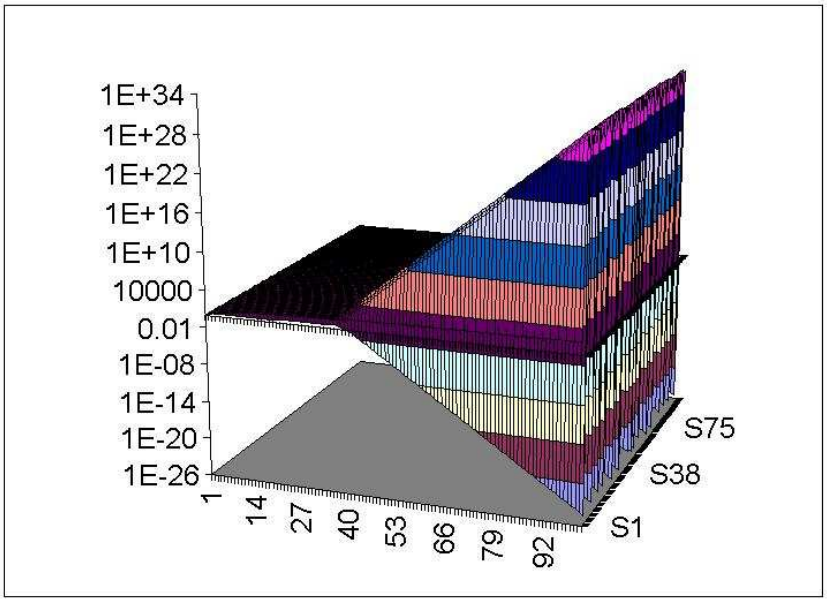

Figure 6.5. Simulated solutions of the one-dimensional model. Parameters, $a_1 = 1/12$, $h_0 = 1$, $r = 10$, $s = 2$, $b = 2$, $d = 0.04$, $e = 1$, $\gamma = 10^4$, $u = 0.1$, $\beta_1 = 1$. Discrete step in x equal to 0.01, time sampled each 10 units - graph of $c(x,t)$ in the semi-logarithmic scale.

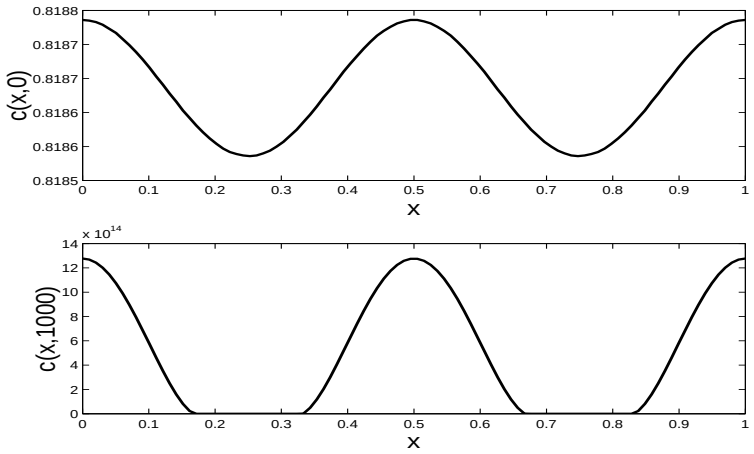

Figure 6.6. Spatial profile of the solution c with parameters, $a_1 = 1/12$, $h_0 = 1$, $r = 10$, $s = 2$, $b = 2$, $e = 1$, $d = 0.04$, $u = 0.1$, $\beta_1 = 1$ $\gamma = 1$. Initial perturbation with cosine function with frequency 4 and amplitude 10^{-4}.

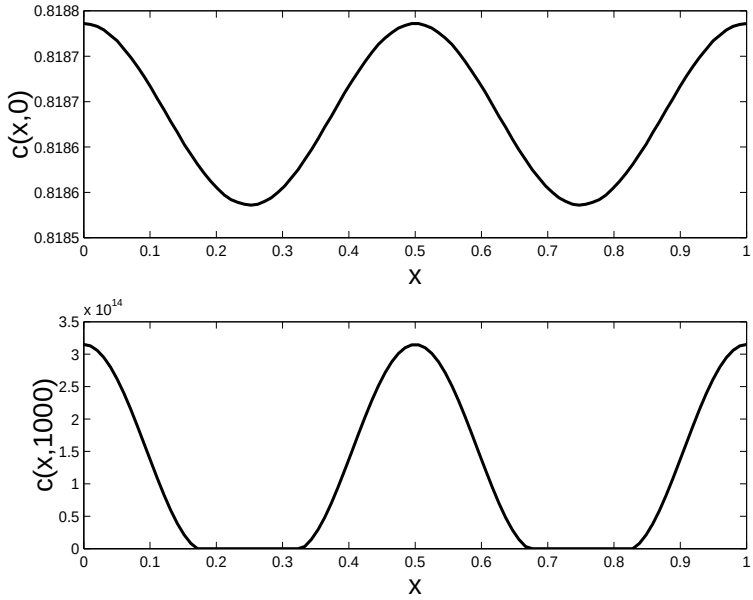

Figure 6.7. Spatial profile of the solution c with parameters and initial condition as in Fig. 6.6 and $\gamma = 10^2$.

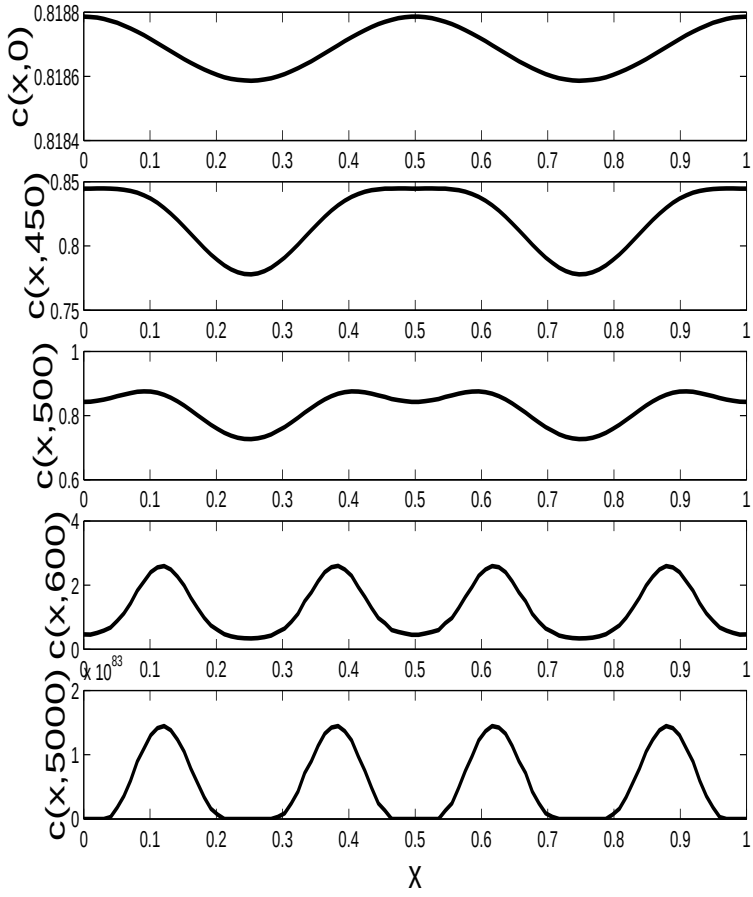

Figure 6.8. Spatial profile of the solution c with parameters and initial condition as in Fig. 6.6 and $\gamma = 10^3$.

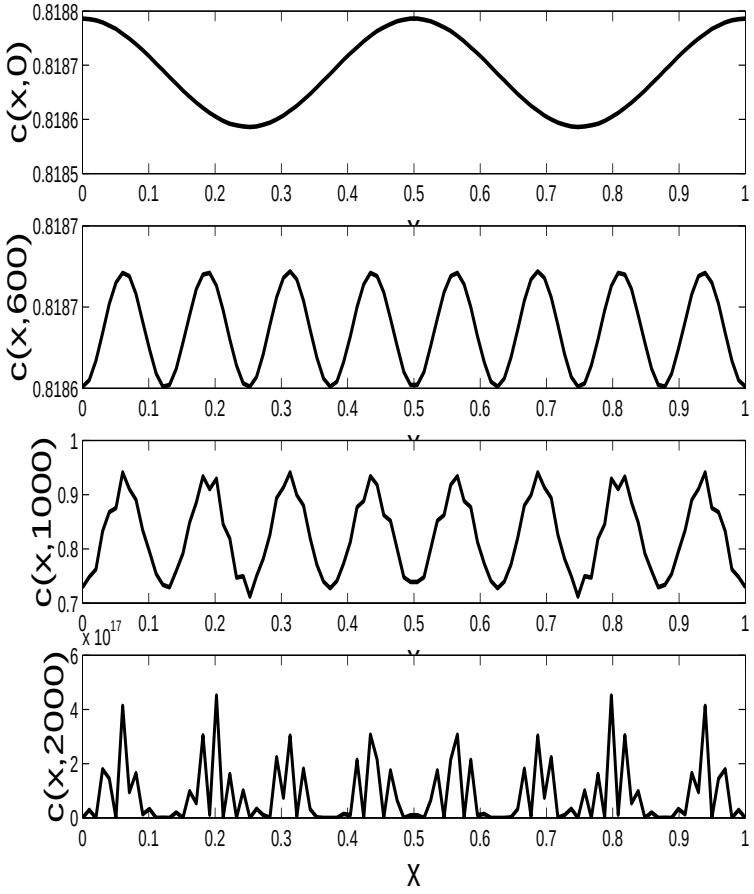

Figure 6.9. Spatial profile of the solution c with parameters and initial condition as in Fig. 6.6 and $\gamma = 10^4$.

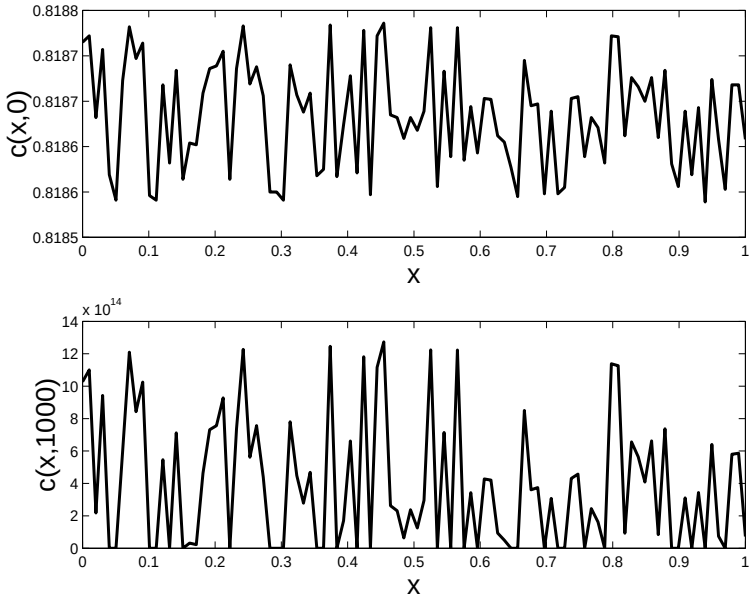

Figure 6.10. Spatial profile of the solution c with parameters and initial condition as in Fig. 6.6 and $\gamma = 1$. Random initial perturbation with amplitude 0.0001.

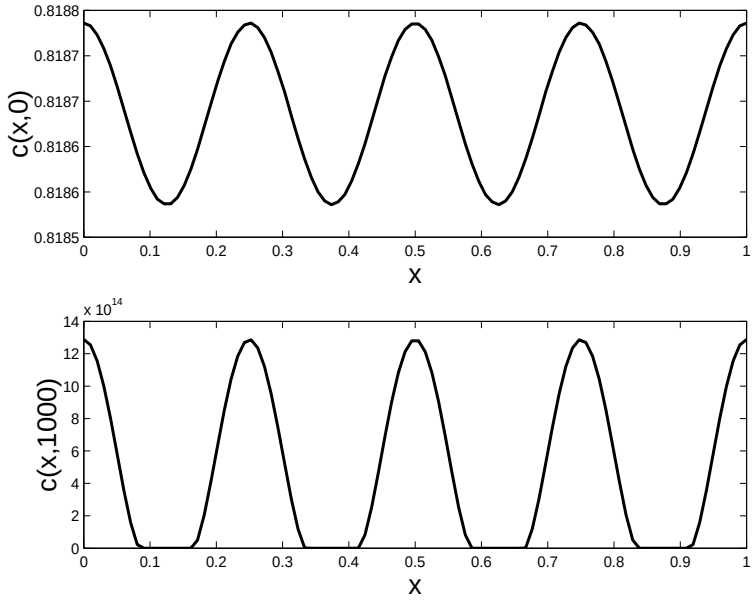

Figure 6.11. Spatial profile of the solution c with parameters and initial condition as in Fig. 6.6 and $\gamma = 1$. Initial perturbation with cosine function with frequency 8.

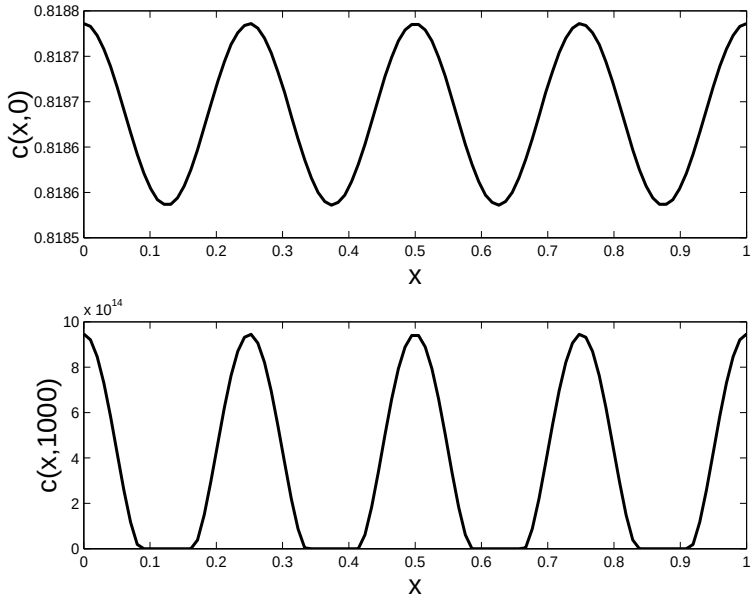

Figure 6.12. Spatial profile of the solution c with parameters and initial condition as in Fig. 6.6 and $\gamma = 10^2$.

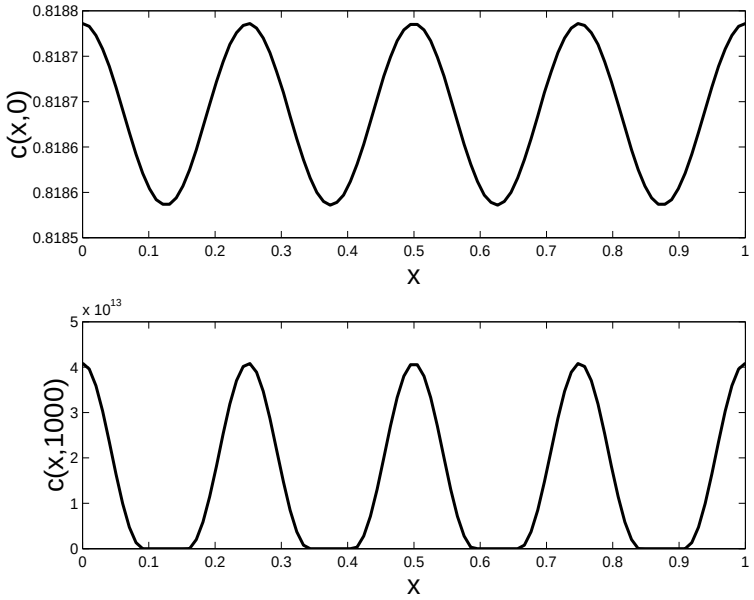

Figure 6.13. Spatial profile of the solution c with parameters and initial condition as in Fig. 6.6 and $\gamma = 10^3$.

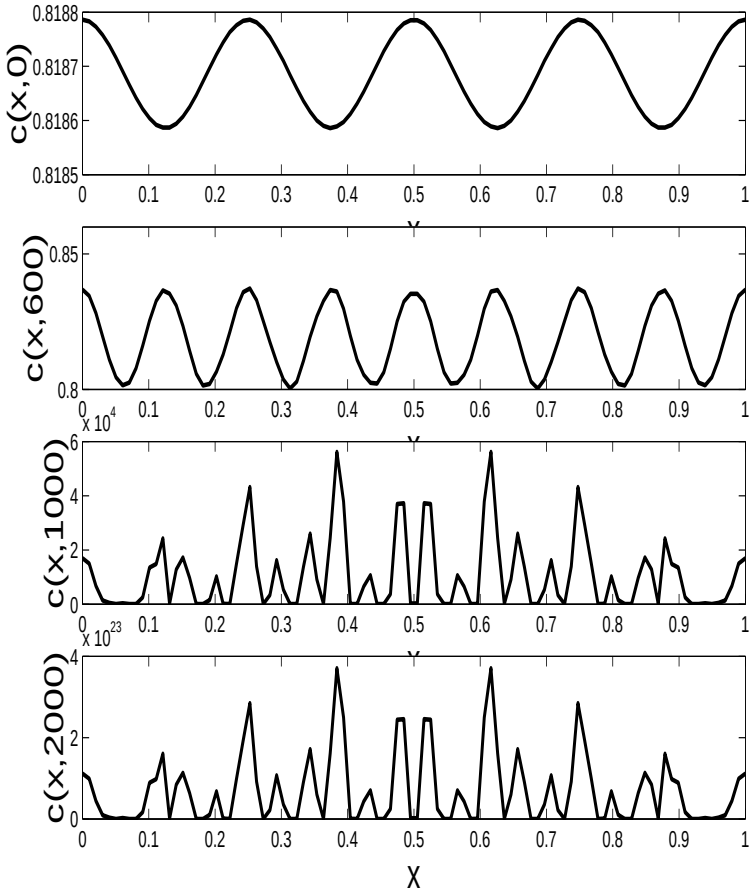

Figure 6.14. Spatial profile of the solution c with parameters and initial condition as in Fig. 6.6 and $\gamma = 10^4$.

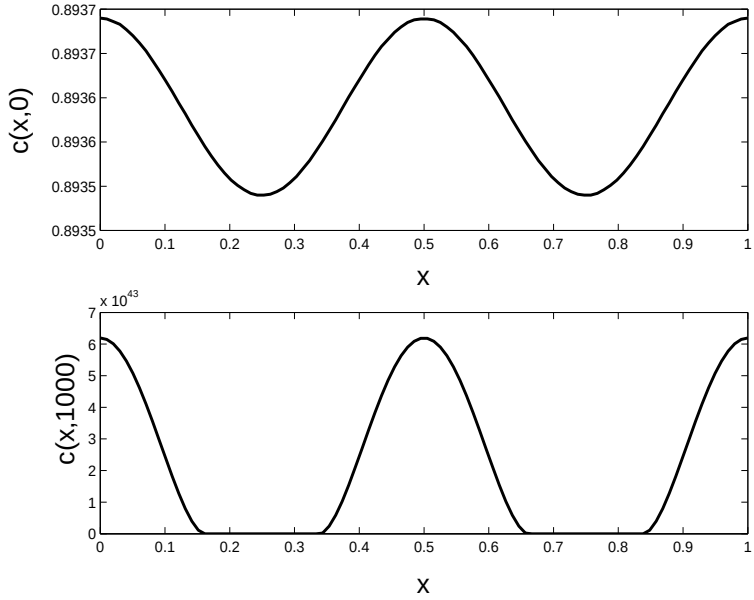

Figure 6.15. Spatial profile of the solution c with parameters, $a_1 = 0.2$, $h_0 = 1$, $r = 10$, $s = 2$, $b = 2$, $e = 1$, $d = 0.09$, $u = 0.1$, $\beta_1 = 1$ $\gamma = 1$. Initial perturbation with cosine function with frequency 4.

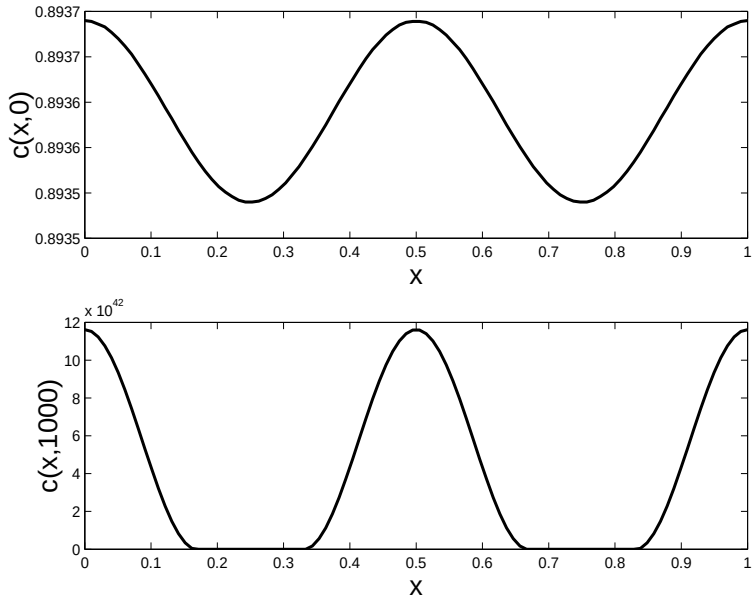

Figure 6.16. Spatial profile of the solution c with parameters and initial condition as in Fig. 6.15 and $\gamma = 10^2$.

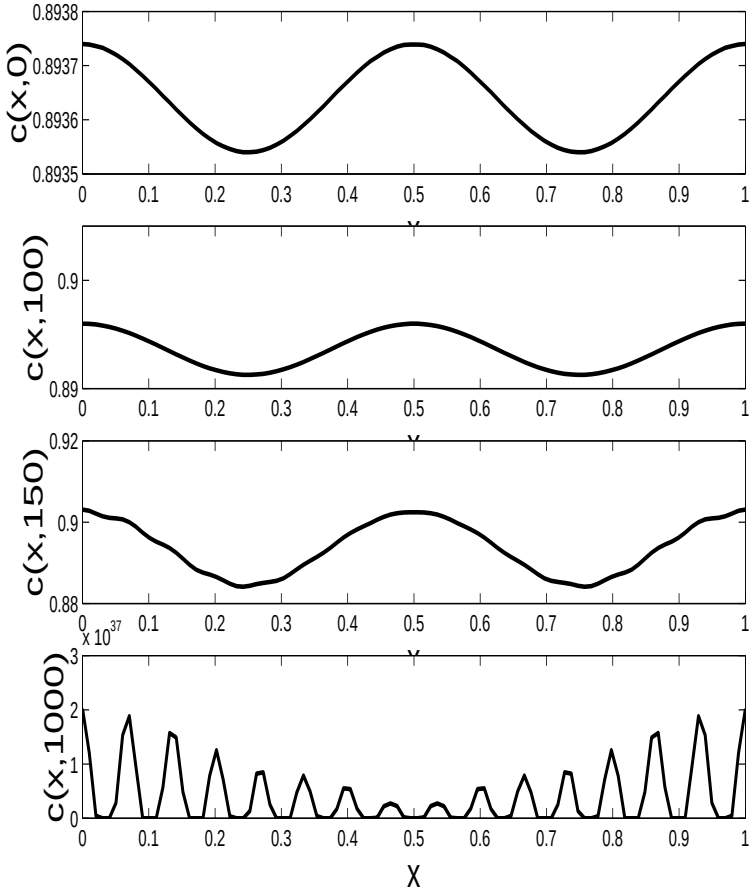

Figure 6.17. Spatial profile of the solution c with parameters and initial condition as in Fig. 6.15 and $\gamma = 10^3$.

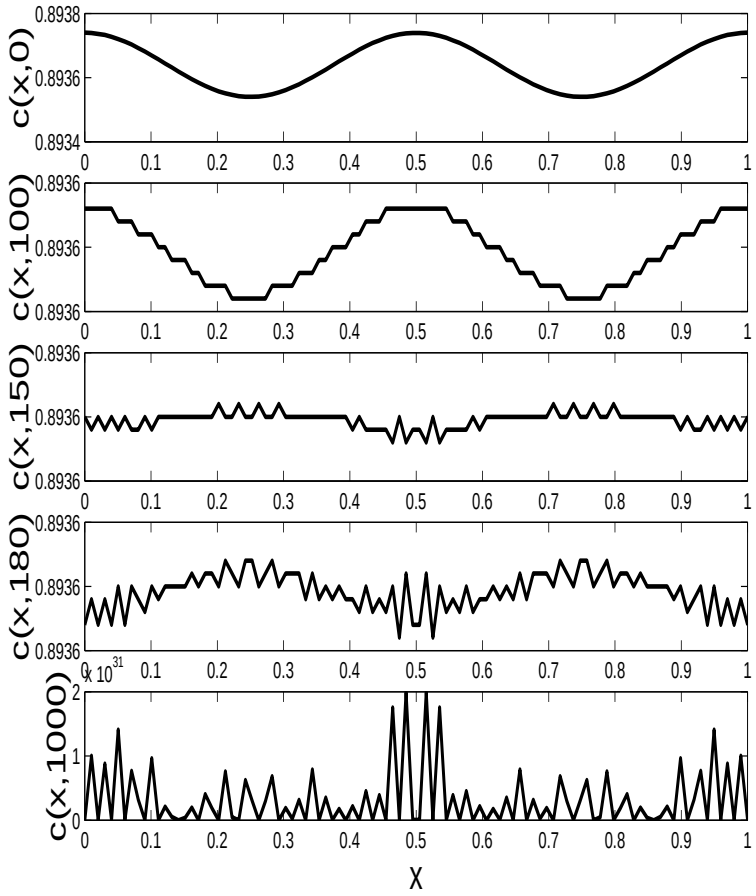

Figure 6.18. Spatial profile of the solution c with parameters and initial condition as in Fig. 6.15 and $\gamma = 10^4$.

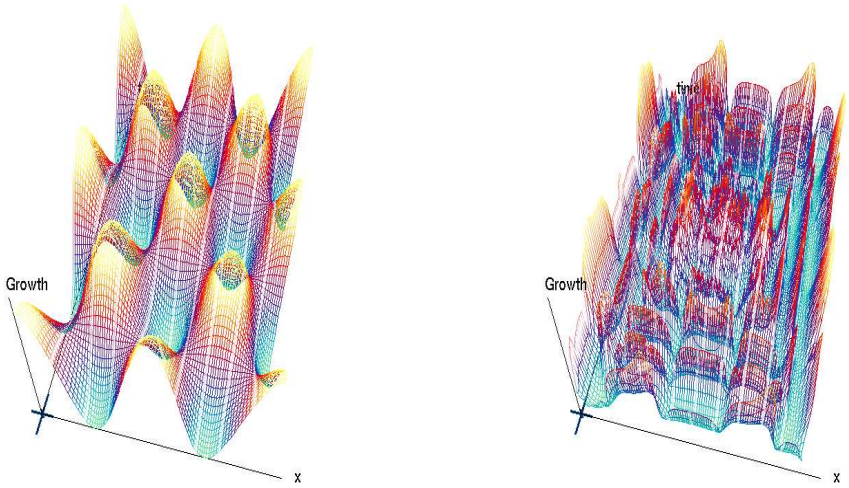

Figure 6.19. Spatial profile of the solution g of the model (6.2) in two dimensional space representing tubular geometry. On the left-hand side, we present the initial function $g(x, y, 0)$, on the right-hand side, the $g(x, y, 680)$. Simulations are performed for a regular perturbation (with function cosine) of the homogeneous steady state ($\bar{c} = 1.86,\ \bar{g} = 0.28,$) and γ equal to 10^4 with parameters: $a_0 = 0.2$, $h_0 = 1$, $r = 10$, $s = 2$, $b = 2$, $d = 0.09$, $k = 3$, $p = 1$, $u = 0.1$. We implemented the zero flux boundary conditions on the boundaries $(0, y)$ and $(1, y)$, $y \in [0, 1]$ and periodic conditions on the boundaries $(x, 0)$ and $(x, 1)$, $x \in [0, 1]$. We observe that regular initial conditions lead to the "chaotic" profile. Similarly like in the one-dimensional case the solution profile loses similarity to the initial condition and displays an increasing number of local maxima.

6.3.3 Simulations for the two-dimensional model

We discretise the system (6.2) on the unit square $[0, 1] \times [0, 1]$ with the zero flux boundary conditions on the boundaries $(0, y)$ and $(1, y)$, $y \in [0, 1]$ and periodic conditions on the boundaries $(x, 0)$ and $(x, 1)$, $x \in [0, 1]$.

We observe behaviour similar to the linear case, i.e. after some time patterns grow rapidly. For certain range of scaling parameter γ, the shape of the ultimate spatial pattern resembles the initial function. However, when γ is growing the solution looses this initial shape, solutions of the smaller wavelength appear and finally solution becomes "chaotic". An example of system's behaviour is depicted in Fig. 6.19.

6.4 Discussion

Behaviour of the model in the one-dimensional case can be interpreted as a period of tumour dormancy, followed by an "unexpected" onset of rapid growth. This is exactly the behaviour, which one finds puzzling in human tumours. However, since it has been obtained by purely numerical methods it should be further verified.

The growth observed is a purely nonlinear phenomenon. Indeed, its rate is much faster than in the linearised system. As evident from simulations in Fig. 6.9, the $c(x,t)$ profiles for higher values of t become irregular in shape. Whether this phenomenon should be considered chaotic, is an open question.

One other puzzling feature of the model is that, as illustrated by Figs. 6.6 - 6.9 and 6.11 - 6.14, the solution profiles become less regular as γ increases. However, if $\gamma^{-1} = 0$, the system becomes a continuum of decoupled ODE systems (indexed by x), each of which is asymptotically stable. This indicates that there might exist a discontinuity in system's behaviour at $\gamma^{-1} = 0$. Further investigation is needed.

Based on the limited number of simulations, it seems that the two-dimensional system qualitatively behaves similarly as the one-dimensional system. Again a complete verification is pending.

7

Conclusions

It has been our aim in the thesis to check under which conditions receptor-based models can describe formation and regulation of patterns in multicellular biological systems.

For the motivating biological example of hydra, we considered models of reaction-diffusion equations with zero flux boundary conditions coupled with ordinary differential equations. We studied two mechanisms of pattern formation: diffusion-driven instabilities and hysteresis-driven mechanism and demonstrated their possibilities and constraints in explanation of different aspects of pattern formation and regulation, such as self-organisation and regeneration.

For proposed models we considered the problems of existence of solutions, their positiveness and boundedness and also stability properties. We showed how the theoretical results concerning existence and uniqueness of solutions of evolution equations can be applied to such models. Existing qualitative theory of reaction-diffusion systems is mainly focused on stability conditions for homogeneous steady states (e.g. [7], [72]), which is only of supporting value for this work. The importance of such conditions is that they help exclude some regions of parameter space from consideration of diffusion-driven instability. Classical conditions for diffusion-driven instability use linearised stability conditions and give us only results regarding the destabilisation of the spatially homogeneous steady state. About asymptotic behaviour of the solutions we can decide only in some special cases when for example the Lyapunov function can be found for the FitzHugh-Nagumo system (e.g. [7], [72]).

For this reason, it is necessary to rely on numerical computations. These computations display complicated behaviour, particularly in the model of cancer progression, which is not covered by the existing theory (see further on).

We proposed two different approaches to model the pattern formation for fresh-water polyp hydra, both in the receptor-based framework. The first model uses special features of diffusion, which results in the destabilisation of the spatially homogeneous steady state and spatial patterns that are eigenfunctions of the Laplacian operator with zero flux boundary conditions. We showed that such diffusion-driven mechanism (Turing-type) for pattern formation can be involved in a receptor-based model, i.e. a model describing the dynamics of receptors and ligands and eventually also an enzyme which degrades ligands and is not of activator-inhibitor type. We investigated the performance of the simplest three-variable receptor-based model and showed what are the consequences of considering only one diffusing substance in such model.

We showed that already the simplest receptor-based model describing the dynamics of free and bound receptors and diffusing ligands allows, for some parameter space, the diffusion-driven instabilities (Turing-type patterns). However, analysis of the conditions for such pattern formation mechanism together with numerical simulations shows that such a model is not the best candidate for hydra patterning. The shape of the final pattern strongly depends on the initial conditions and since peaks are created just in one domain point, the biological interpretation is difficult. In this model diffusion-driven patterns can evolve only if we assume self-enhancement of free receptors, i.e. a positive feedback loop between the production of new free receptors and their present density.

This shows that such models can be applied only to some special biological systems (like proliferating cells). It is necessary to stress that such models lead to an infinite range of unstable wavenumbers, i.e. disturbances with very large and very small wavelenghts are all unstable. The final spatial pattern in this situation critically depends on the initial conditions. However, we observed different dependence of the solution on the initial perturbation in three-variable model for hydra and in the model of tumour growth. It shows again that the ultimate pattern is a strictly nonlinear phenomenon (compare [61]).

Introduction of a second diffusing biochemical species improved performance of the model. We showed that a four-variable model can produce diffusion-driven instabilities without any assumption of autocatalysis. In four-variable receptor-based model, similarly as in the activator-inhibitor model, the spatially homogeneous steady state bifurcates into the spatially inhomogeneous solution which has a maximum at the one end and a minimum at the other end for some range of the domain size. This model is robust and the final pattern does not depend on small perturbation of initial conditions.

The four-variable system with diffusion-driven instability models self-organisation of hydra cells and is able to simulate the cutting experiments.

We showed that such model can explain at least as much as activator-inhibitor model regarding *de novo* pattern formation and basic experiments. Numerical studies of the four-variable model developed as well as of the activator-inhibitor model proposed in [49] (see Appendix A) showed that the grafting experiments could not be explained within such approach without changing the size of domain (or diffusion coefficient), which does not reflect experimental conditions.

Since the diffusion-driven model fails to reproduce the grafting experiments, we proposed another model, based on the idea that, to explain the grafting experiments, cells should be equipped with memory. We introduce memory to the model adding two equations showing hysteresis, i.e. having multiple steady states and allowing the system to jump from one stable steady state to another, when the density of receptors and ligands is varied. Assuming small values of the diffusion coefficient we obtained spatial heterogeneity in the densities of substances considered. Due to the existence of multiple steady states such model can simulate the results of grafting experiments. We showed that in systems with hysteresis many inhomogeneous steady states can coexist. Such solutions depend on the initial conditions, which is in agreement with the outcome of grafting experiments. However, this model can simulate only some of the cutting experiments, in which the head or foot end of the body column is removed and it regenerates. The gradient-like solution recovers if the difference between values of the initial state on both ends of the domain is high enough. Thus, we can explain the kind of experiments, which show just the regeneration of head or foot (as in [70]). However, it is evident from experiments that hydra can also regenerate the whole organism from the half body column and from both halfs simultaneously. Proposed model with hysteresis is not able to reproduce such results.

Each model has shed light on different but overlapping aspects of the self-organisation and regeneration. Now, it is possible to state which conceptual elements have to be present in a complete model, although modelling hydra regeneration still involves quite a few unsolved problems. It is clear that the mechanism must involve some intracellular communication since the cells at the cut surface need to know what structures are in their vicinity in order to know whether to form a head or a foot. Grafting experiments suggest coexistence of different spatially inhomogeneous stationary patterns which grow up for different initial conditions. Experiments show that large perturbations (but within the range of the values of the solution itself) of the gradient-like solution should

lead to another solution. From the cutting experiments we conclude that gradient-like initial state should evolve into gradient like pattern.

Further biological discoveries are needed to gain insight into molecular nature of cell communication and of the positional value. To understand the morphogenesis in hydra it is necessary to bridge the gap between experimental observations at the cellular level and those at the genetic and biochemical levels. Also the role of cell division and very specific growth can be important in this process. It might be relevant to incorporate cell differentiation, coordination of cell movement and cell positioning. Also one should take under consideration that the communication over distance may involve cell-to-cell signalling mechanisms rather than simple diffusion. We tried to model this mechanism by building complicated kinetics system which describes interactions between receptors and diffusible molecules and includes also the dependence of the production of new molecules on the history of the whole system.

As mentioned by Kirkilionis in [38], the theoretical modelling should have a larger influence on the experimental work. " Models should be tested by the predictions they make, and predictions must be coupled to something measurable in laboratory" ([38]). While for some developmental problems the knowledge of the molecular and genetic mechanisms is already more detailed, for hydra almost all such information needed to design models, testable rather than conceptual, is still lacking [56]. Such models can only help to understand what could be the possible scenario and how complicated nonlinear interactions between biological molecules together with spatial signalling and movement result in the shape and properties of the ultimate pattern.

In models of hydra, as in many other classical papers on pattern formation, the ultimate goal is to achieve stability of the emerging pattern. It is clear that the shape of the organ developed during morphogenesis cannot be sensitive for the small perturbation of the system. It is also evident from experiments that in many systems there is a remarkable robustness of developmental mechanisms against perturbations, for example against variations of initial conditions or parameters. For example the number of pattern segments is crucial and should not depend on the domain size or geometry (as in the case of *Drosophila*, [32]).

The model of cancer progression addresses a phenomenon, which by its nature is unstable. Therefore, the model with single diffusion seems appropriate for this purpose, as the emerging pattern should strongly depend on slight changes in initial conditions. In a way, requirements for this model are complementary to those for the model of hydra.

The model's point of departure is a time-continuous Markov chain mechanism, describing proliferation of cells and propagation of a growth factor along tubular or linear structures. This setup is meant to represent observed instances of such growth, [23].

The model constitutes a metaphor of the physical and biological reality, in that it does not represent flows and transport phenomena in the surrounding tissue, but replaces them by a single diffusion mechanism. On the other hand, given the diffusion mechanism, classical and well-accepted models of cell proliferation are used, [36] and [37].

The most interesting feature of the model seems to be its ability to reproduce a long period of quasi-stability, followed by a rapid growth at saturation rate. This phenomenon closely mimics the transition from the in-situ phase of early tumour growth, followed by rapid invasion into surrounding tissues, [23]. At the same time, spatial-coordinate profiles become more and more complex. The complexity of the spatial pattern depends on the scaling parameter γ which includes the diffusion coefficient and the length of the domain. The ultimate pattern strongly depends on the initial condition. It is a model with an infinite range of unstable modes, and from the linear analysis we cannot decide which mode will grow to give the ultimate pattern. The simulations show that for certain range of γ the shape of the final pattern resembles the initial function. However, when γ is growing the solution looses this initial shape, more unstable modes appear and finally the pattern becomes apparently chaotic. It is an interesting feature that the complicated behaviour appears when diffusion coefficient becomes very small, while the system is stable when there is no diffusion at all. This seems to be an effect of the change in equation type

As shown in Appendix D, the wavenumbers corresponding to the discretised Laplacian with zero-flux boundary conditions are damped with respect to the wavenumbers of the original problem. This might eliminate some of the higher-frequency spatial oscillations.

To conclude, in the thesis, we addressed a range of issues concerning mechanisms of pattern formation inspired by two biological phenomena. In the case of hydra, we were looking for orderly patterns. In the case of cancer, we were looking for emerging unpredictability and growth. It is interesting that a set of related mathematical systems can lead to both types of behaviour. The problems we considered lead to many mathematical and modelling open problems, which will be subject of future research. Many uncertainties exist regarding the biological foundations of the models. Progress in cell biology and genetics will help resolve them in the future.

Appendix A

Existing models for pattern formation in hydra

Here we give mathematical formulation of the existing models of pattern formation in hydra which are discussed in Section 2.3.

A.1 Gierer-Meinhardt activator-inhibitor model

Gierer and Meinhardt proposed that biological pattern formation is based on local activation and long-range inhibition. They formulated the following system of reaction-diffusion equation [19].

$$\begin{aligned} \frac{\partial}{\partial t}a &= D_a\frac{\partial^2}{\partial x^2}a + \rho a\frac{a^2}{h} + \sigma_a - \mu_a a, \\ \frac{\partial}{\partial t}h &= D_h\frac{\partial^2}{\partial x^2}h + \rho_h a^2 + \sigma_h - \mu_h h. \end{aligned} \tag{A.1}$$

Here a and h are the concentrations of two substances, which are usually called activator and inhibitor.

The model and several its modifications were applied in the study of various topics from developmental biology (see e.g. [50]).

Meinhardt developed this idea further and proposed the model for pattern formation in hydra, in which head and foot formation are controlled by the density of different morphogens. Separate activator and inhibitor for head and foot are coupled by the influence of so called source density [49].

The model has the form

$$
\begin{aligned}
\frac{\partial}{\partial t}a_h &= D_{a_h}\frac{\partial^2}{\partial x^2}a_h + \mu_h\rho\frac{{a_h}^2+\rho_{0_h}}{h_h} - \mu_h a_h,\\
\frac{\partial}{\partial t}h_h &= D_{h_h}\frac{\partial^2}{\partial x^2}h_h + \mu_h\rho{a_h}^2 - \nu_{h_h}h_h + \rho_{1_h},\\
\frac{\partial}{\partial t}a_f &= D_{a_f}\frac{\partial^2}{\partial x^2}a_f + \mu_f\rho\frac{{a_f}^2+\rho_{0_f}}{h_f} - \mu_f a_f,\\
\frac{\partial}{\partial t}h_f &= D_{h_f}\frac{\partial^2}{\partial x^2}h_f + \mu_f\rho{a_f}^2 - \nu_{h_f}h_f + \rho_{1_f},\\
\frac{\partial}{\partial t}\rho &= D_\rho\frac{\partial^2}{\partial x^2}\rho + \mu_\rho a_h - \mu_\rho\rho - \gamma\rho a_f + \rho_0.
\end{aligned}
\tag{A.2}
$$

A.2 SMJM receptor-based model

The model proposed by Sherrat, Maini, Jäger an Müller in [70] has the following form,

$$
\begin{aligned}
\frac{\partial}{\partial t}a &= D_a\frac{\partial^2}{\partial x^2}a + s_a(x) - \mu_a a - k_e ae - k_a af + k_d b,\\
\frac{\partial}{\partial t}f &= k_d b - k_a af + k_i[\alpha(x) + \beta b - f],\\
\frac{\partial}{\partial t}b &= k_a af - (k_d + k_i)b,\\
\frac{\partial}{\partial t}e &= D_e\frac{\partial^2}{\partial x^2}e + s_e(x) - \mu_e e,
\end{aligned}
\tag{A.3}
$$

with zero-flux boundary conditions for a and e.

f, b, a and e denotes respectively the density of free receptors, bound receptors, biochemical (ligands) and enzyme.

It is crucial here that the production functions depend on the spatial variable $x \in [0, L]$ (the position along the body column) and also on $y(x)$, which denotes position from which the tissue at location x originates.

$$
\begin{aligned}
\alpha(x) &= \alpha_1[1 - y(x)/L] + \alpha_2 y(x)/L,\\
s_e(x) &= s_1[1 - y(x)/L] + s_2 y(x)/L.
\end{aligned}
$$

$s_a(x)$ is constant for $y(x) \in [0, \frac{4L}{5}]$ and decrease linearly to zero for $y(x) \in [\frac{4L}{5}, 1]$.

Appendix B

Mathematical settings for modelling of cutting and grafting experiments

In this chapter we give our mathematical formulation of the models corresponding to the experiments performed on hydra in laboratory. The two basic types of such experiments, i.e. cutting and grafting experiments, are connected with the changes of the initial state of hydra. Thus, we consider the models studied before for the normal development with different initial conditions. We formulate these conditions and explain how they are related to the experimental setting.

B.1 Cutting experiments

Assume that $v(x)$ is a vector of considered densities corresponding to the normal development and we cut a piece of the body column in x_1 and x_2. The initial conditions for the cutting experiment are,

$$u_0(x) = v(x_1 + x(x_2 - x_1)) \ \ for \ \ x \in [x_1, x_2], \tag{B.1}$$

$$0 \leq x_1 < x_2 \leq 1.$$

Since we assume that $x = 0$ corresponds to the upper end of the body column (head) and $x = 1$ to the lower end (foot), the case $x_1 = 0$, $x_2 < 1$ simulates a surgical removal of the foot, while the case $x_1 > 0$, $x_2 = 1$ – removal of the head.

Let us recall that for the dimensionless models the domain size equals 1 and $\gamma = \frac{L^2}{d_l}$ is a scaling coefficient depending on the domain size of the original problem. Cutting experiment changes the domain size of the problem. The "new" domain is smaller.

Thus, to get a model corresponding to the cutting experiments, one has to rescale also the coefficient γ. Since $\gamma = \frac{L^2}{d_l}$, we obtain $\gamma_{new} = \gamma|x_2 - x_1|^2$.

As we already mentioned in Section 2.2, the regeneration in hydra is morphallaxis (not involving the domain growth), thus, we model the cutting experiments with the constant domain size (constant γ).

For the numerical simulations as $v(x)$ we take the values obtained from the model in the simulations of normal development (gradient-like solutions).

B.2 Grafting experiments

Now we formulate the initial conditions describing grafting experiments. Assuming again that $v(x)$ is a solution corresponding to the normal development we put,

$$u_0(x) = \begin{array}{l} v(x) \ \ for \ \ x \in [0, x_1] \cup [x_2, 1], \\ v(x - x_1 + x_{graft}) \ \ for \ \ x \in [x_1, x_2]. \end{array} \tag{B.2}$$

It means that, instead of the tissue with coordinates $[x_1, x_2]$, we transplant the tissue of the same length from the position starting in x_{graft}.

Appendix C

Numerical tools

The computer algebra program MAPLE is used to solve the stationary problem, since in contrast to iterative methods, e.g. Newton method, it uses Gröbner bases for the description of the solution manifold and is able to find multiple zeros.

To solve numerically the considered systems we used the method of lines and thus the system of nonlinear partial differential equations was converted to a large system of ordinary differential equations by discretisation of Laplacian in three coordinates in one-dimensional case and five coordinates in two-dimensional case.

The discretised system of ordinary differential equations is numerically solved using the CVODE package and numerical estimates of the Jacobian matrix. This program offers an implicit method for time discretisation, originally developed for stiff problems of ODEs.

Space discretisation is a gridpoint on a unit interval. The size of the spatial grid is adjusted according to the value of the diffusion coefficient (value of the scaling parameter γ. Time discretisation is performed implicitly.

Homogeneous Neumann boundary conditions (zero flux) are implemented as a reflection at the boundary (see e.g. [1]).

The graphical visualisation of the numerical solutions in space and time is realized with the program Onom 2.0 and the space-profiles are shown using MATLAB.

Appendix D

Wavenumbers and wavefunctions for the discretised diffusion operator (one-dimensional model)

In the simulations, the Laplace operator has been replaced by a discrete difference scheme, incorporating the boundary conditions. Since discretisation may lead to destabilisation as it is the case, for example, for the logistic equation, it seems to make sense to investigate the spectrum of the discretised system.

Discretisation is equivalent to replacing the function $g(x,t)$ by a vector

$G(t) = (g_0(t), g_1(t), \ldots, g_{n-1}(t))$, and the continuous Laplacian Δ_x by a discrete Laplacian D,

$$\begin{aligned} [DG(t)]_0 &= a[2g_1(t) - 2g_0(t)], \\ [DG(t)]_1 &= a[g_{i+1}(t) - 2g_i(t) + g_{i-1}(t)],\ i = 1, \ldots, n-2, \\ [DG(t)]_{n-1} &= a[2g_{n-2}(t) - 2g_{n-1}(t)], \end{aligned} \tag{D.1}$$

where $a = (\gamma)^{-1} n^2$. The first and the last equation model the zero-flux boundary condition. The eigenproblem (6.10) is now replaced by the following matrix eigenproblem

$$\left[\begin{pmatrix} -2 & 2 & & & & & & \\ 1 & -2 & 1 & & & & & \\ & 1 & -2 & 1 & & & \mathbf{0} & \\ & & \ddots & \ddots & \ddots & & & \\ & & & \ddots & \ddots & \ddots & & \\ & \mathbf{0} & & & 1 & -2 & 1 & \\ & & & & & 1 & -2 & 1 \\ & & & & & & 2 & -2 \end{pmatrix} + wI \right] \Phi = 0,$$

where Φ is a column n-vector and $w = \mu^2 \gamma n^{-2}$, μ being the wavenumber corresponding to the now discrete wavefunction Φ. Tedious but straightforward computations prove

that the problem has n distinct eigenvalues

$$w_i = \frac{4(f_i^2+1) + \mathrm{sgn}(f_i)(4\sqrt{f_i^2+1})}{2(f_i^2+1)}, \tag{D.2}$$

where

$$f_i = \mathrm{tg}(\frac{i\pi}{n-1}),\ i = 0, 1, \ldots, n-1,$$

corresponding to discrete wavefunction

$$\Phi_i = [1, \cos(\beta_i), \cos(2\beta_i), \ldots, \cos((n-1)\beta_i)]',$$

where $\beta_i = \frac{i\pi}{n-1}$. Since the continuous wavenumbers and wavefunctions have the form

$$\mu_{(c)i}^2 = i^2\pi^2,\ \phi_i(x) = \cos(i\pi x),$$

we see that the discrete problem not only reduces the number of distinct wavefunctions from infinity to n, but the discrete wavenumbers are somewhat different from their continuous counterparts. Figure D.1 presents a graph comparing the discrete wavenumbers w_i to their continuous counterparts $v_i = \mu_{(c)}^2(\gamma n^{-2})$, for the case $\gamma = 1$. We see that the higher-order wavenumbers are damped in the discretised system.

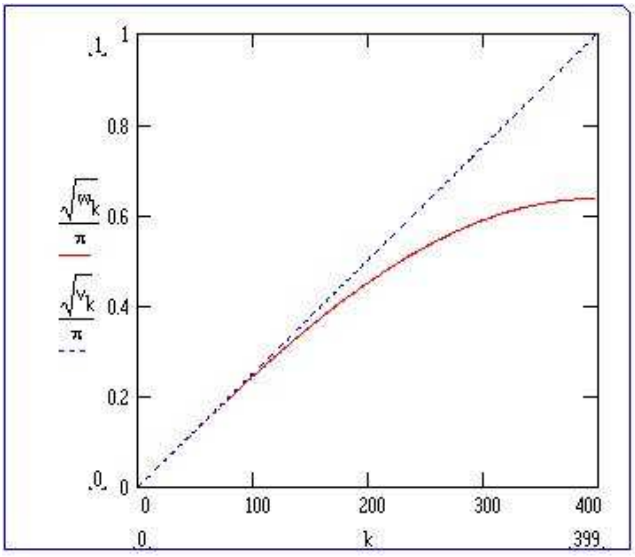

Figure D.1. Graph comparing the discrete wavenumbers $w_i = \mu_i^2(\gamma n^{-2})$ to their continuous counterparts $v_i = \mu_{(c)i}^2(\gamma n^{-2})$, for the case $\gamma = 1$. Initial condition (perturbation) is a cosinusoid with period 1/2.

References

[1] W.F. Ames. *Numerical Methods for Partial Differential Equations.* Academic Press, New York, 1977.

[2] W.J. Anderson. *Continuous Time Markov Chains: An Applications-Oriented Approach.* Springer-Verlag, New York, 1991.

[3] A. Babloyantz and J. Hiernaux. Models for cell differentiation and generation of polarity in diffusion-governed morphogenetic fields. *Bull. of Math. Biol.*, 37:637–657, 1975.

[4] A. Babloyantz and M. Sanglier. Chemical instabilities of "all-or-none" type in β-*galactosidase* induction and active transport. *FEBS Lett.*, 23:346–366, 1972.

[5] J.M. Ball. Strongly continuous semigroups, weak solutions and the variation of constants formula. *Proc. Amer. Math. Soc.*, 63:370–373, 1977.

[6] P.M. Bode and H.R. Bode. Patterning in hydra. In *Pattern Formation: A Primer in Developmental Biology*, pages 213–241, New York, 1984. MacMillan Publ. Co.

[7] N.F. Britton. *Reaction-Diffusion Equations and Their Applications to Biology.* Academic Press, 1986.

[8] R.G. Casten and C.J. Holland. Stability properties of solutions to systems of reaction-diffusion equations. *SIAM J. Appl. Math.*, 33:353–364, 1977.

[9] M.A.J. Chaplain, M. Ganesh, and I.G. Graham. Spatio-temporal pattern formation on spherical surfaces: numerical simulation and application to solid tumor growth. *J. Math. Biol.*, 42:387–423, 2001.

[10] C. Chiu and N. Walkington. Analysis of hysteretic reaction-diffusion systems. *Quart. of Appl. MAth.*, 16(1):89–106, 1998.

[11] M. Edgerton. Pagetoid spread in ductal carcinoma in situ: Characterization and computer simulation. In *Mathematical Models in Cancer*, http://www.math.vanderbilt.edu/ horn/biomath/abstracts.html, 2002. Abstracts, Vanderbilt University, May 3-5.

[12] K.J. Engel and R. Nagel. *One-Parameter Semigroups for Linear Evolution Equations.* Springer-Verlag, New York, 2000.

[13] A. Fasano. A mathematical model for tumor cords including the effects of radiation or chemical treatment. In *Mathematical Models in Cancer*, http://www.math.vanderbilt.edu/ horn/biomath/abstracts.html, 2002. Abstracts, Vanderbilt University, May 3-5.

[14] B. Fiedler and A. Scheel. Spatio-temporal dynamics of reaction-diffusion patterns. In Kirkilionis et al., editor, *Trends in Nonlinear Analysis*, Heidelberg, 2002. Springer-Verlag.

[15] P.C. Fife. *Mathematical aspects of reacting and diffusing systems.* Springer-Verlag, Berlin, 1979.

[16] A. Gandolfi. The response of tumor cords to therapeutic agents. In *Mathematical Models in Cancer*, http://www.math.vanderbilt.edu/ horn/biomath/abstracts.html, 2002. Abstracts, Vanderbilt University, May 3-5.

[17] F.R. Gantmacher. *Applications of the Theory of Matrices.* Interscience Publishers, New York, 1959.

[18] A. Gierer, S. Berking, H. Bode, C.N. David, K. Flick, G. Hansmann, H. Schaller, and E. Trenkner. Regeneration of hydra from reaggregated cells. *Nat.New Biol.*, 239:98–101, 1972.

[19] A. Gierer and H. Meinhardt. A theory of biological pattern formation. *Kybernetik*, 12:30–39, 1972.

[20] P. Grindrod. *Patterns and Waves.* Clarendon Press, Oxford, 1991.

[21] S. Heinze and B. Schweizer. Creeping fronts in degenerate reaction-diffusion systems. *in preparation*, 2003.

[22] D. Henry. *Geometric Theory of Semilinear Parabolic Equations.* Springer-Verlag, Berlin, 1981.

[23] C.I. Henschke, D.F. Yankelevitz, R. Mirtcheva, G. McGuinness, D. McCauley, and O.S. Miettinen. Ct screening for lung cancer: frequency and significance of part-solid and nonsolid nodules. *Am. J. Roentgenol.*, 178:1053–1057, 2002.

[24] T. Höfer, J.A. Sherrat, and P.K. Maini. *Dictyostelium discoideum*: cellular self-organisation in an excitable biological medium. *Proc. R. Soc. Lond. B*, 259:249–257, 1995.

[25] F. Hoppensteadt and W. Jäger. Pattern formation by bacteria. In S. Levin, editor, *Lecture Notes in Biomathematics: Biological Growth and Spread*, pages 69–81, Heidelberg, 1980. Springer-Verlag.

[26] F. Hoppensteadt, W. Jäger, and C. Pöppe. A hysteresis model for bacterial growth patterns. In S. Levin, editor, *Lecture Notes in Biomathematics: Modelling of Patterns in Space and Time*, pages 123–134, Heidelberg, 1983. Springer-Verlag.

[27] D. Horstmann. From 1970 until present: The keller-segel model in chemotaxis and its consequences. *Jahrebericht der DMV*, 105 (3):103–165, 2003.

[28] T.L. Jackson, S.R. Lubkin, and J.D Murray. Theoretical analysis of conjugate localization in two-step cancer treatment. *J. Math. Math.*, 39:335–376, 1999.

[29] T.L. Jackson, S.R. Lubkin, S.R. Siemens, N.O. Kerr, P.D Senter, and J.D. Murray. Mathematical and experimental analysis of localization of anti-tumor anti-body-enzyme conjugates. *Br. J. Cancer*, 80:1747–1753, 1999.

[30] T.L. Jackson, P.D Senter, and J.D. Murray. Development and validation of mathematical model to describe antibody enzyme conjugates. *J. Theor. Medic.*, 2:93–111, 1999.

[31] J. Jaros and T. Kusano. A picone type identity for second order half-linear differential equations. *Acta Math. Univ. Comenianae*, 68:137–151, 1999.

[32] S.A. Kauffman. Pattern formation in the *drosophila* embryo. *Phil. Trans. R. Soc. Lond.*, 295:567–594, 1981.

[33] E.F. Keller and L.A. Segel. Initiation of slime mold aggregation viewed as an instability. *J. Theor. Biol.*, 26:399–415, 1970.

[34] E.F. Keller and L.A. Segel. A model of chemotxis. *J. Theor. Biol.*, 30:225–234, 1971.

[35] M. Kerszberg. Morphogen propagation and action towards molecular models. *Semin. Cell. Dev. Biol.*, 10(3):297–302, 1999.

[36] M. Kimmel, A. Polanski, and A. Swierniak. Optimal control problem arising in cell-cycle-specific cancer chemotherapy. *Cell. Prolif.*, 29:117–139, 1996.

[37] M. Kimmel and F. Traganos. Estimation and prediction of cell cycle specific effects of anticancer drugs. *Math. Biosci.*, 80:187–208, 1986.

[38] M. Kirkilionis. On the modelling of cellular interactions in tissues. In A. Deutsch, editor, *Function and regulation of cellular systems: experiments and models.* Birkhäuser-Verlag, 2002.

[39] Ch.T. Klein. Hysteresis-driven structure formationin biochemical networks. *J. Theor. Biol.*, 194:263–274, 1998.

[40] S. Krömker. *Model and Analysis of Heterogeneous Catalysis with Phase Transition.* PhD thesis, University of Heidelberg, 1997.

[41] J.L. Lions. *Equations Differentielles Operationelles.* Springer-Verlag, New York, 1961.

[42] J.W. Macki, P. Nistri, and P. Zecca. Mathematical models for hysteresis. *SIAM Review*, 35:94–123, 1993.

[43] H.K. MacWilliams. Hydra transplantation phenomena and the mechanism of hydra head regeneration. 1 properties of the head inhibition. *Dev.Biol.*, 96:217–238, 1983.

[44] H.K. MacWilliams. Hydra transplantation phenomena and the mechanism of hydra head regeneration. 2 properties of the head activation. *Dev.Biol.*, 96:239–257, 1983.

[45] P.K. Maini. Some mathematical models for biological pattern formation. In M.A.J. Chaplain, G.D. Singh, and J.C. McLachlan, editors, *On Growth and Form. Spatio-temporal pattern formation in Biology*, pages 111–128, New York, 1999. Wiley.

[46] A. Marciniak-Czochra. Receptor-based models with diffusion-driven instability for pattern formation in hydra. *J. Biol. Sys.*, 11:293–324, 2003.

[47] A. Marciniak-Czochra and M. Kimmel. Mathematical model of tumor invasion along linear or tubular structures. *Mathematical and Computer Modelling*, 2003, accepted.

[48] J.-L. Martiel and A. Goldbeter. A model based on receptor desenitization for cyclic amp signalling in *disctyostelium* cells. *Biophys.J.*, 57:807–828, 1987.

[49] H. Meinhardt. A model for pattern formation of hypostome, tentacles, and foot in hydra: How to form structures close to each other, how to form them at a distance. *Dev.Biol.*, 157:321–333, 1993.

[50] H. Meinhardt. On pattern and growth. In M.A.J. Chaplain, G.D. Singh, and J.C. McLachlan, editors, *On Growth and Form. Spatio-temporal pattern formation in Biology*, pages 129–148, New York, 1999. Wiley.

[51] H. Meinhardt. The small freshwater polyp hydra as a model for axis formation in higher organisms. In A. Deutsch, editor, *Function and regulation of cellular systems: experiments and models.* Birkhäuser-Verlag, 2002.

[52] P.B. Monk and H.G. Othmer. Cyclic amp oscillations in suspensions of *dictyostelium discoideum. Phil. Trans. R. Soc. Lond. B*, 323:185–224, 1989.

[53] S.C. Müller and G. Venzl. Pattern formation in precipitation processes. In S. Levin, editor, *Lecture Notes in Biomathematics: Modelling of Patterns in Space and Time*, pages 254–278, Heidelberg, 1983. Springer-Verlag.

[54] W.A. Müller. Diacylglycerol-induced multihead formation in hydra. *Development*, 105:309–316, 1989.

[55] W.A. Müller. Ectopic head and foot formation in hydra. diacylglycerol induced increase in potential value and assistance of the head in foot formation. *Differentiation*, 42:131–143, 1990.

[56] W.A. Müller. Pattern control in hydra: basic experiments and concepts. In *Experimental and Theoretical Advances in Biological Pattern Formation*, New York, 1993. Plenum Press.

[57] W.A. Müller. Competition of factors and cellular resources as a principle of pattern formation in hydra. *Dev.Biol.*, 167:175–180, 1995.

[58] W.A. Müller. Head formation at the basal end and mirror-image pattern duplication in hydra vulgaris. *Int.J.Dev.Biol.*, 40:1119–1131, 1996.

[59] W.A. Müller. *Developmental Biology.* Springer-Verlag, New York, 1997.

[60] J.D. Murray. *Mathematical Biology.* Springer-Verlag, Berlin, 2nd edition, 1993.

[61] J.D. Murray. *Mathematical Biology. II: Spatial Models and Biological Applications.* Springer-Verlag, Berlin, 3rd edition, 2003.

[62] K. Noda. Reconstitution of dissociated cells of hydra. *Zool.Mag.*, 80:99–101, 1971.

[63] A. Pazy. *Semigroups of Linear Operators and Applications to Partial Differential Equations.* Springer-Verlag, New York, 1983.

[64] S. Piccolo, E. Agius, B. Lu, S. Goodman, L. Dale, and E.M. De Robertis. Cleavage of chordin by xolloid metalloproteaze suggests a role for proteolytic processing in the regulation of spemann organizer activity. *Cell*, 91:407–416, 1997.

[65] F. Rothe. *Global solutions of Reaction-Diffusion Systems.* Springer-Verlag, Berlin, 1984.

[66] R.A. Satnoianu, M. Menzinger, and P.K. Maini. Turing instabilities in general systems. *J.Math.Biol.*, 41:493–512, 2000.

[67] M. Sato, H. Tashiro, A. Oikawa, and Y. Sawada. Patterning of hydra cells aggregates without sorting of cells from different axial origins. *Dev.Biol.*, 151:111–116, 1992.

[68] S. Schnell, P.K. Maini, D. McInerney, D.J. Gavaghan, and P. Houston. Models for pattern formation in somitogenesis: a marriage of cellular and molecular biology. *C. R. Biologies*, 325:179–189, 2002.

[69] F.F. Seelig and B. Denzle. Hysteresis without autocatalysis in enzyme systems with substrate inhibition. *FEBS Lett.*, 24:283–287, 1972.

[70] J.A. Sherratt, P.K. Maini, W. Jäger, and W. Müller. A receptor based model for pattern formation in hydra. *Forma*, 10:77–95, 1995.

[71] H. Shimizu, Y. Sawada, and T. Sugiyama. Minimum tissue size required for hydra regeneration. *Dev. Biol.*, 155:287–296, 1993.

[72] J. Smoller. *Shock-Waves and Reaction-Diffusion Equations.* Springer-Verlag, New York, 2nd edition, 1994.

[73] A. Stevens. The derivation of chemotaxis equations as limit dynamic of moderately interacting stochastic many-particle systems. *SIAM J. Appl. Math.*, 61:183–212, 2000.

[74] J.R. Tata. Autoinduction of nuclear hormon receptors during metamorphosis and its significance. *Insect. Biochem. Mol. Biol.*, 30(8-9):645–651, 2000.

[75] U. Technau, B. Hobmayer, F. Rentzsch, and T. Holstein. Molecular and cellular analysis of de novo pattern formation in hydra. In A. Deutsch, editor, *Function and regulation of cellular systems: experiments and models.* Birkhäuser-Verlag, 2002.

[76] U. Technau and T. Holstein. Cell sorting during the regeneration of hydra from reaggregated cells. *Dev.Biol*, 151:117–127, 1992.

[77] A.M. Turing. The chemical basis of morphogenesis. *Phil.Trans.Roy.Soc.B*, 237:37–72, 1952.

[78] G. Webster and L. Wolpert. Studies on pattern regulation in hydra. 1. regional differences in time required for hypostome determination. *J.Embryol.Exp.Morph.*, 16:91–104, 1966.

[79] L. Wolpert. Positional information and the spatial pattern of cellular differentiation. *J.Theor.Biol.*, 25:1–47, 1969.

[80] L. Wolpert. *Principles of Development.* Oxford Univeristy Press, Oxford, 1998.